How Auction Houses Have Reshaped the Gem Market

The Spectroscopic Properties of Filled Moonstone

Distinguishing Mammoth and Modern Elephant Ivory

THE 4Cs APP THAT ALSO PUTS YOU ON THE MAP.

List your retail location on GIA's free 4Cs app for consumers. In addition to learning more about diamonds and the 4Cs through videos and fun interactive tools, consumers will soon be able to use the app to locate registered retailers who carry GIA-graded diamonds or have GIA-trained staff. The feature is currently available at www.gia.edu and will be available soon on the Android™ and Apple® apps. Register for the Retailer Locator today at **www.retailer.gia.edu.**

The Retailer Locator feature is coming soon to the GIA 4Cs App.

You can also visit **www.retailer.gia.edu** to download a free retailer version of the 4Cs app for use at point of sale. Available for iPad and Android.

GIA

gia.edu/gems-gemology

About the Cover

In recent years, auction prices for luxury gems and jewelry have reached breathtaking heights. The lead article in this issue recaps the emergence of the two largest auction houses, Christie's and Sotheby's, as market forces influencing price and consumer demand. The Bulgari Blue, a distinctive two-stone ring featuring a 10.95 ct Fancy Vivid blue diamond and a 9.87 ct G-color diamond, fetched $15.76 million at Christie's New York on October 20, 2010. Jewelry courtesy of Christie's; photo by Jian Xin (Jae) Liao.

FSC
www.fsc.org
MIX
Paper from responsible sources
FSC® C006300

ENRICHING A TRADITION

As the new editor-in-chief of *Gems & Gemology*, I thank Jan Iverson for her recent stewardship of the journal. Jan will be taking over as GIA's director of Education Content Development. I wish her every success in this new role. Let me also thank GIA president and CEO Donna Baker and vice president of Education Bev Hori for giving me this opportunity.

Allow me to introduce myself. My background is in the colored stone industry. I also have extensive experience in jewelry manufacture and retail. Besides being a Graduate Gemologist, I am a Fellow of the Gemological Association of Great Britain (Gem-A). At GIA, I've been director of Course Development for over a decade. One of my proudest accomplishments is the recent transformation of our distance-education gemology courses from print to eLearning.

I join *G&G* at a tremendously exciting time. GIA has the largest cadre of talented research scientists and the most extensive network of labs and research centers in its history. The topics of their investigations have never been wider—or more challenging. And *G&G* is your window into this exciting world of research.

We're placing a remarkable resource—almost 80 years of groundbreaking gemological knowledge—at your fingertips.

G&G will be at the center of the Research & News section of the new GIA website, which launches April 30, so please keep this date in mind. The new website provides an unparalleled online knowledge base that will serve your professional needs better than we've ever done before.

We're placing a remarkable resource—almost 80 years of groundbreaking gemological knowledge—at your fingertips. As a visitor to www.gia.edu, you'll have unrestricted access to every *G&G* issue back to the journal's inception in January 1934—full articles, Gem News International, Lab Notes, and all the regular features. And we pledge to continue to provide the highest levels of gemological research in the exacting tradition of *G&G*'s rich legacy.

G&G has never been more necessary. Let no one be in any doubt over GIA's commitment to our journal. We see it as a vital part of a wider system, one that links GIA's education with its ongoing research, and delivers that essential knowledge to our readers.

Duncan Pay | Editor-in-Chief | dpay@gia.edu

AUCTION HOUSES: A POWERFUL MARKET INFLUENCE ON MAJOR DIAMONDS AND COLORED GEMSTONES

Russell Shor

The world's two largest auction houses, Sotheby's and Christie's, began regular sales devoted to important diamonds and colored stones in the 1970s. Through their ability to generate publicity, they have become a significant force in price and demand throughout the world, while also generating interest in fancy-color diamonds and the geographic origin of top gemstones. In the process, they have become both supplier and competitor to the world's top jewelry houses.

I n December 2008, as most of the world plunged into an economic crisis, a historic Fancy Deep grayish blue diamond achieved the highest price ever paid for a single gemstone: $24.3 million. The sale of the Wittelsbach Blue made international head-lines because it was conducted not in the privacy of a showroom but in public at an auction house in London, with the news media and dealers from around the world in attendance. The results were broadcast within seconds of the hammer fall.

Today, the highest-profile sellers of major diamonds—larger than 10 carats, both colorless and fancy-color—and top gemstones are the world's two largest auction houses, Sotheby's and Christie's. In 2011, their combined jewelry sales reached $990.1 million ("Christie's jewelry, watch sales up 40%," 2012; "Sotheby's 2011 revenues rise 7%," 2012). And while there are no reliable figures of their share of large stone sales, for more than two decades the auctions have been a major competitor to the world's leading jewelry houses such as Cartier, Harry Winston, and Van Cleef & Arpels.

Auction sales have also had a profound effect on the diamond and gem markets, influencing both prices and consumer sentiment (Rapaport, 2008). In doing so, they have promoted awareness of fancy-color diamonds and country of origin for colored stones among buyers and dealers worldwide (King, 2006; R. Drucker, pers. comm., 2012).

In the four years since the sale of the Wittelsbach Blue diamond, which was immediately renamed the Wittelsbach-Graff, a number of price records have been broken. Less than a year later, a 24.78 ct pink diamond commanded $46 million. And the media at-tention paid to the Wittelsbach-Graff (figure 1) was dwarfed by the coverage lavished on the December 2011 sale of actress Elizabeth Taylor's jewels.

BACKGROUND

The two auction houses have histories dating back to the 18th century. Sotheby's began in 1744 when London bookseller Samuel Baker auctioned the rare book collection of a British aristocrat. After Baker's death in 1778, his business partner George Leigh and his nephew, John Sotheby, assumed control (Live Auctioneers, 2010). Sotheby's expanded beyond books to include prints, medals, and coins, and by the mid-19th century it had begun to rival Christie's in the fine art world.

James Christie was a London art dealer who in 1766 established an auction business to trade art-works. Both Baker and Christie understood that the key to success in the auction trade was establishing

Figure 1. The Wittelsbach Blue diamond sold for $24.3 million, at the time the highest price ever paid for a diamond, in December 2008, when the world was in the midst of a financial crisis. The sale of the 35.56 ct Fancy Deep grayish blue VS$_2$ diamond, with its combination of rarity and royal provenance, made headlines around the world. The renamed Wittelsbach-Graff diamond was recut to 31.06 ct to make it Fancy Deep blue and internally flawless. Photo by Robert Weldon.

strong connections with titled society. But Christie established the importance of *provenance*—an item's prestigious history or connection to an important person—as a value-adding proposition (Baptist, 2011). Christie's first sale of fine jewelry came in the aftermath of the French Revolution. In 1795, it auctioned the many jewels of Madame du Barry, King Louis XV's mistress, who had been executed two years earlier. That sale realized £8,791, the equivalent of $1.3 million today (F. Curiel, pers. comm., 2012).

Fine art was the mainstay of both houses through the 19th and early 20th centuries. Indeed, it remains their largest category. The auction houses occasionally handled top jewelry pieces, when nobility were obliged to sell some of their treasures—for example, Christie's 1875 sale from the gem collection of the Duke of Marlborough, which brought £36,750, equivalent to about $4.5 million today (F. Curiel, pers. comm., 2012).

A review of pre-1965 catalogs shows that most major jewelry auctions up to that time were conducted at Christie's and Sotheby's headquarters, both in London. Jewelry items were usually included as part of larger auctions of wealthy estates, in tandem with *objets d'art*, furs, and other luxury goods (Bap-

tist, 2011). In the late 1960s, the houses began holding separate sales for large gems and major jewelry pieces. These were conducted in Geneva, which became the main venue for both houses until they established similar events in New York. Yet most top jewels of the royalty were still sold through established jewelers such as Cartier, Harry Winston, and Van Cleef & Arpels, which had connections to European royal families, and later to wealthy families and celebrities in the United States and Latin America.

Parke-Bernet, a New York auction house founded in 1937 by noted art dealers Hiram Parke and Otto Bernet, was the first to hold regularly scheduled sales dedicated to jewelry. In its first "Precious-Stone Jewelry" sale, held in 1938, all 60 of the lots on offer came from an estate. The auction catalog (figure 2) shows the finished pieces described in some detail, including cut styles and approximate carat weights. But none of the lots carried price estimates, and little

Figure 2. This Parke-Bernet catalog is from one of the first jewelry-specific auctions, held in October 1938. The catalog offered few gemological details except for estimated carat weight. Photo by Robert Weldon.
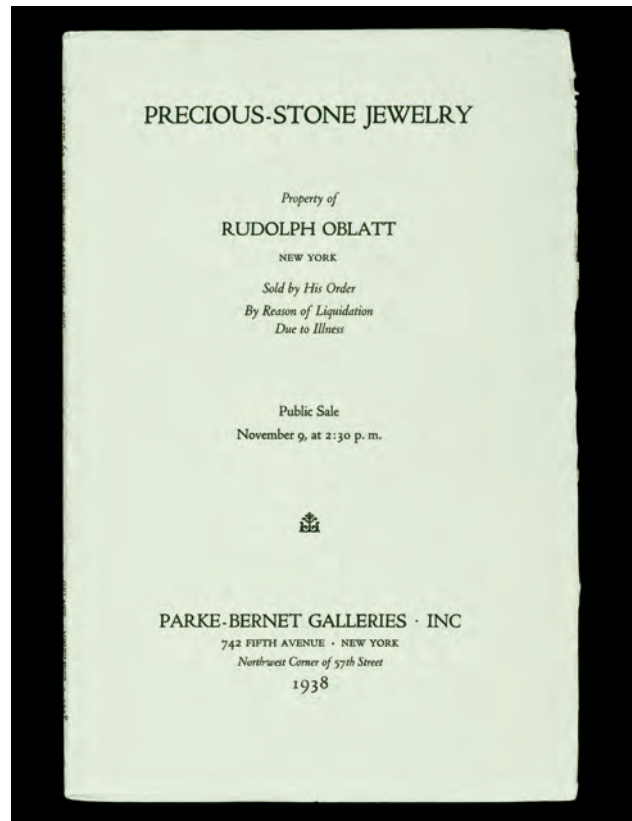
gemological information was offered, beyond grouping sapphires as "Ceylon" or "Oriental" (Parke-Bernet, 1938).

AUCTIONS AS MARKET INFLUENCER

The first "celebrity" gem auction occurred 31 years later. A 69.42 ct diamond sold by Parke-Bernet made worldwide headlines in October 1969, when it became the first gemstone to break the million-dollar barrier at public auction. It was also one of the first significant diamonds graded by a gemological laboratory, carrying a GIA report with a grade of E-F Flawless (Parke-Bernet, 1969). The diamond had already gained some notoriety, if not a name, by having been cut from a 240.8 ct rough by Harry Winston in 1966. The first cleaving of the diamond was done before television cameras. After Winston's cutters completed their work, the company sold the 69.42 ct pear-shaped diamond to Harriet Annenberg Ames the following year. Ames put the gem up for auction in 1969, saying she did not like it languishing in a bank vault. After a round of spirited bidding, Cartier bought the diamond for $1,050,000 (Balfour, 2009; figure 3).

The underbidder for this diamond was a representative for actor Richard Burton, who had dropped out after the bidding surpassed the million-dollar mark. Burton instead bought the stone from Cartier the following day, but gave the retailer permission to display the diamond in its showroom for one week. Publicity surrounding the diamond's auction price, and the celebrity aura of the renamed Taylor-Burton diamond, brought out the crowds. An estimated 6,000 people lined up daily at Cartier's New York and Chicago stores, to view the stone.

That same year, Christie's New York created a specialty jewelry department and held its first sale in May. Like Parke-Bernet's jewelry auctions, the offerings came exclusively from estates. The catalogs contained only a few photos, mostly black-and–white, with no price estimates and only terse descriptions. The sales were as basic as the catalogs, attended by a small coterie of local dealers (Shor et al., 1997). Sotheby's, which had acquired Parke-Bernet in 1964, continued its jewelry auctions under the latter banner into the 1970s, when the house became Sotheby Parke-Bernet.

In the 1970s, the world economy was beset by inflation and languishing stock prices, which prompted investors to turn to hard assets—starting with exchange-traded commodities such as gold and silver, followed by gemstones. Private buyers began bidding

Figure 3. In October 1969, Parke-Bernet offered the first "celebrity" gem sold at auction, a 69.42 ct pear-shaped E-F Flawless diamond that topped $1 million. After Richard Burton purchased the diamond for Elizabeth Taylor, it became known as the Taylor-Burton diamond.

on important stones at auctions as investments (Edelstein, 1989), and prices for top gemstones were soaring by the late 1970s. Yet the auction houses, which dealt only in estate pieces with very restricted supply, remained at the fringe of this bubble. The vast majority of their clientele still consisted of local dealers, major jewelry houses buying back their own pieces for inventory, and important estate jewelry dealers such as A La Vieille Russie and J. & S.S. DeYoung. Still, business was booming for the auction houses. Christie's New York branch sold $2 million in 1977, a total that jumped to $8 million in 1978 and $10.6 million the following year. In Geneva, which was still the primary venue for jewelry auctions, Christie's

recorded a total of $57.2 million in 1979, nearly three times its 1978 total (Donohue, 1980b; F. Curiel, pers. comm., 2012). Meanwhile, Sotheby's New York achieved jewelry sales of $18 million in 1979—a new record—while Christie's New York reported sales of $10.6 million and another competitor, William Doyle Galleries, sold an estimated $3 million.

As the amount of jewelry consigned to auctions increased, Christie's and Sotheby's segmented their sales into a value hierarchy. These categories, from lowest to highest value, were Fine, Important, Highly Important, and Magnificent jewelry. The two houses set a regular schedule for their most important sales in New York and Geneva, where they had the largest international following. Each would offer one Magnificent Jewels sale, generally featuring some pieces expected to bring $500,000 or more, in the spring and fall seasons. Just before the close of each season, they would follow up with a Fine Jewelry sale.

In October 1979, a two-day Magnificent Jewelry sale at Sotheby Parke-Bernet in New York garnered network news coverage for a 22.30 ct emerald-cut diamond that was expected to bring $1 million. The hammer price fell just short of that mark, but with the house commission, the final price was $1,072,500 ("Auction fever," 1979). The sale also included a 6.75 ct marquise-cut diamond that went for $319,000, or $47,260 per carat—an extraordinary price for that time.

As jewelry auctions grew substantially, mainly in finished pieces, the heightened media attention led many dealers to recognize that these sales represented a new market channel—both source and competitor (Donohue, 1980b). Dealers of estate and antique jewelry feared that the auction houses, with their ability to generate national publicity, could take over the high-end segment of the industry. By now at least half of the bidders on estate pieces were private rather than trade buyers. Retail jewelers who handled such goods claimed they could not pay auction prices, especially for highly desirable pieces that resulted in a bidding war (Donohue, 1980b).

Gem dealers also described the "auction effect": price bumps for top-quality diamonds and gemstones after similar goods had achieved high prices at a publicized auction, particularly as diamonds and gemstones were being touted as investment pieces during this inflationary period (Donohue, 1980a). A record-setting Christie's sale in Geneva in 1979 illustrates this effect. At the event, a 4.12 ct Burmese ruby sold for $414,832—the first time a colored gemstone attained more than $100,000 per carat at auction (and

three times the previous record, set a year earlier). A 12.46 ct Colombian emerald brought $48,000 per carat, while an 11.81 ct Kashmir sapphire sold for $25,815 per carat, both record prices. Afterward, one New York dealer noted that a ruby, which had been offered to him for $25,000 per carat on the open market, sold for $40,000 per carat at the Christie's auction (Donohue, 1980a).

In 1981, a sharp recession in the U.S. caused the gem investment bubble to collapse. Diamond prices

In Brief

- Over the last 30 years, the jewelry auction market has grown from less than $50 million to nearly $1 billion a year.
- Burgeoning global wealth and price speculation have led to record prices for gems and jewelry at auction.
- The publicity surrounding high-profile auction sales has sparked consumer interest in provenance, country of origin, and fancy-color diamonds.
- Sotheby's and Christie's have become formidable competitors to long-established luxury jewelers such as Cartier, Tiffany, and Van Cleef & Arpels.

fell nearly 50% within a few months, especially for top qualities. The slowdown hit the auction houses as well. Auction sales barely made their pre-sale estimates, and the percentage of unsold lots rose sharply (Blauer, 1981). Buyers began seeking only the "very special" pieces signed by prestigious houses such as Cartier, Van Cleef & Arpels, and Bulgari, and shied away from loose stones altogether as prices declined. During the recession, the auction houses focused on their mainstays of classic period jewelry, particularly Art Deco and Art Nouveau pieces from the top jewelry houses (Blauer, 1983).

By the end of 1983, the market for top gemstones had stabilized. These goods began to resurface at the auctions, but now there were two important differences. Fancy-color diamonds, which had once only interested collectors and connoisseurs, were being offered. And the buyers were a new breed of players, luxury jewelry houses such as Laurence Graff, Moussaieff Jewellers, and Robert Mouawad. These jewelers found the auctions helpful in two ways: as a source of important stones, and as a way to focus publicity on their own growing businesses.

Sotheby's October 1983 New York sale of $8.5 mil-

lion matched a 1979 record. Meanwhile, Christie's reported overall record sales for the first half of 1983—40% over the previous year (Shor, 1983). In 1984, Sotheby's and Christie's sold a total of $70 million in gems and jewelry in New York alone, nearly doubling their volume within two years (Gertz, 1985).

The transformation of the jewelry auction business into the market-leading role came in 1986–1987, when two things happened.

First, Christie's and Sotheby's, which had by now dropped Parke-Bernet from its name, recognized that the key to growth was moving beyond estate goods and into newly mined and cut stones—diamonds over 10 carats and major diamond necklaces containing 50 carats or more of high-quality stones. To a lesser extent, they also commissioned jewelry houses to create major ruby, sapphire, and emerald pieces (Shor et al., 1997).

In 1986, Christie's began aggressively soliciting dealers to list important stones in its major sales, as a supplement to the estate pieces. Sotheby's, which had accepted dealer consignments on a limited basis, redoubled its efforts to secure trade goods, a move that enabled their combined sales to grow from about $100 million that year to $500 million within a decade (Shor et al., 1997). In short, the auction houses became retailers of newly cut stones.

The immediate effect was that the 1986–87 auctions brought an influx of very large diamonds—all from dealers rather than estates (Shor, 1988). Four D-Flawless diamonds over 50 carats came up for auction during those two seasons, whereas previously only one or two such stones would appear in the course of a decade. The reason behind this influx was that De Beers had resumed selling the very large diamonds it had stockpiled during the early 1980s, when prices were depressed. The company also changed its mining and rough sorting procedures to reduce breakage of large stones (Shor, 1988). Dealers started putting these stones up for auction, claiming they could get higher prices there. The catalyst for this was a 64.83 ct D-IF diamond that brought $6.3 million at Christie's October 1986 New York sale. It was a record price (soon broken) and attracted more large stones at subsequent sales.

By now, extremely wealthy private buyers were returning to the auction houses to buy jewelry. Many of these private buyers engaged in bidding competition, often becoming emotional, while dealers tended to be much cooler and stay within their spending limits so they could realize a profit (Shor, 1988). But in a bullish market, even seasoned dealers can get caught up in the competitive spirit and surpass their own limit, especially when bidding against another dealer (Rapaport, 2012).

Finally, dealers rushed to consign major stones because they felt they could insist on setting reserve prices high—generally at the price they would set in their own office, making the transaction ostensibly risk-free. Yet some dealers found that if their stones failed to sell, the failure received almost as much media attention as the successes, putting a stigma on those goods (Shor, 1988).

The second turning point that established auction houses as a major force was the most publicized jewelry event up to that point: the April 1987 sale of the jewels of the Duchess of Windsor (Schupak, 2011).

The Duchess, formerly Wallis Simpson, had been an international celebrity since 1937, when King Edward of England abdicated his throne to marry her. In their 35 years of marriage, she amassed a large collection of jewels from the major jewelry houses, many of them immortalized in photographs (figure 4). Edward, the Duke of Windsor, died in 1972, and after the Duchess's death in 1986, her jewelry collec-

Figure 4. The Duke and Duchess of Windsor, seen in 1959. Their headline lives made for a headline-making jewelry auction by Sotheby's in April 1987, which permanently established auction houses as major players in the top jewelry market. Photo by Maurice Tabard, Camera Press Ltd., London.

Figure 5. The "Panther" brooch, featuring a 152.35 ct cabochon sapphire, was the most famous piece in the Duchess of Windsor collection. Cartier, which originally sold the brooch to the Duchess in 1949, purchased the piece at the April 1987 auction for its historical collection. Photo by Nick Welsh; courtesy of the Cartier Collection.

tion was sent to Sotheby's in Geneva for auction.

The Duchess of Windsor sale was scheduled for April 2–3, 1987. The pre-sale estimate for the collection was $7 to $8 million. Sotheby's divided the collection into 305 lots, including 87 pieces signed by Cartier (the Duke and Duchess's favorite jeweler) and 23 items by Van Cleef & Arpels. Media coverage was heavy, with most major networks around the world airing preview features about the legendary jewelry collection and reporting from the sale. A *New York Times Magazine* piece from February 1987 reported the history of the major pieces. The notoriety of some of the buyers, which included Elizabeth Taylor and Laurence Graff, also attracted media attention (Vogel, 1987).

After the bidding was over, the total came out to $50.3 million—seven times the pre-sale estimate. Iconic pieces such as Cartier's sapphire "Panther"

brooch (figure 5) and "Flamingo" brooch (figure 6) achieved 15 times their pre-sale estimates. Twenty-three years later, Sotheby's grouped 20 items from the sale into a second auction that realized $12.5 million and garnered another round of international press coverage. The record prices stemmed from the Windsor jewels' extraordinary provenance, which generated bids worth many times the intrinsic market value of the pieces (Schupak, 2011).

The reverberations from the Windsor sale boosted prices and demand and "got the world emotionally involved in jewelry," according to one major diamond dealer (Shor, 1988). One auction executive said the sale put jewelry in the same league with Impres-

Figure 6. Cartier's 1940 "Flamingo" brooch, fashioned with diamonds, sapphires, emeralds, rubies, and citrine, was another iconic piece from the Windsor collection. The brooch went for $806,000 in 1987, and Sotheby's resold it in 2010 for $2.67 million. Photo courtesy of Sotheby's New York.

sionist paintings, historically the top-selling category. The auction houses put their considerable public relations abilities to use, generating the type of mystique Harry Winston had evoked a generation earlier (Shor et al., 1997). They also began proactively reaching out to potential buyers: dealers of significant gems and the wealthy clientele who also collected art, antique furniture, rare wines, and watches from their other departments.

The immense publicity generated by the Duchess of Windsor sale, and the auction houses' aggressive moves to capture a greater share of the top jewelry market, attracted numerous private clients. By the mid-1990s, at least half the buyers at major auctions were purchasing for themselves. At the same time, Sotheby's and Christie's determined efforts to obtain consignments gave them a clear market dominance in top jewelry over competing firms such as William Doyle Galleries, Butterfields, and Skinner Galleries (Shor et al., 1997).

Although auction sales grew substantially though the 1970s and 1980s, auction executives point to the Windsor sale as the watershed event that permanently established auction houses as major players in the top jewelry market (Schuler, 2011). The event demonstrated the auction houses' global reach in attracting bidders and promoting sales. From a total of about $300 million in jewelry auction sales in 1988, Christie's and Sotheby's combined to reach $500 million within seven years.

After the Windsor sale, emotions continued to soar as bidders pushed prices of top goods to record prices. Within weeks, the 0.95 ct Hancock Red diamond (figure 7) became the most expensive per-carat gemstone ever sold at auction. The hammer came down at $880,000—a remarkable $926,315 per carat, eight times its pre-sale estimate. In 1989, a 32.08 ct Burmese ruby brought $4.62 million, five times its pre-sale estimate (Blauer, 2012).

Aside from pushing up prices, selling at auction held another attraction for dealers of top colored stones and diamonds: The auction houses paid quickly during a time when retailers were demanding longer and longer memo terms (Shor, 1998).

The jewelry auction catalogs, once very basic, were now being given the fine art treatment, with full-color illustrations and more detailed descriptions. The following year brought another addition to the catalogs. In 1988, both houses began listing country of origin reports on many of the major untreated rubies and sapphires (emeralds followed

later), along with background on the rich histories of Burmese rubies (see Enriquez, 1930) and sapphires from Kashmir and Ceylon. Before then, geographic origin notations were very sporadic. As auction houses recognized the historic premium on gemstones from certain localities, they sought to envelop these top stones in a historical mystique that mimicked the provenance of an estate jewel. A 15.97 ct ruby, offered by Sotheby's at its October 1988 New York auction (figure 8), carried the following description:

> The source is the Mogok region of Burma…an area forbidden to foreigners since 1963…The ancient alluvial deposits are being worked by native Burmese by the same primitive methods used since the 16th Century, resulting in a small production. Rarely is a stone of importance found….and little mention of them is made throughout history… (Sotheby's, 1988)

The ruby sold to Graff for a record per-carat price of $227,301, or $3.63 million total.

Publicity surrounding the sale of this and other important gemstones at auction has broadened the awareness of geographic origin among buyers and re-

Figure 7. Auctioned at Christie's in New York a few weeks after the Windsor sale, the 0.95 ct Hancock Red diamond brought more than $926,000 per carat, a record that stood for 20 years. Photo by Tino Hammid.
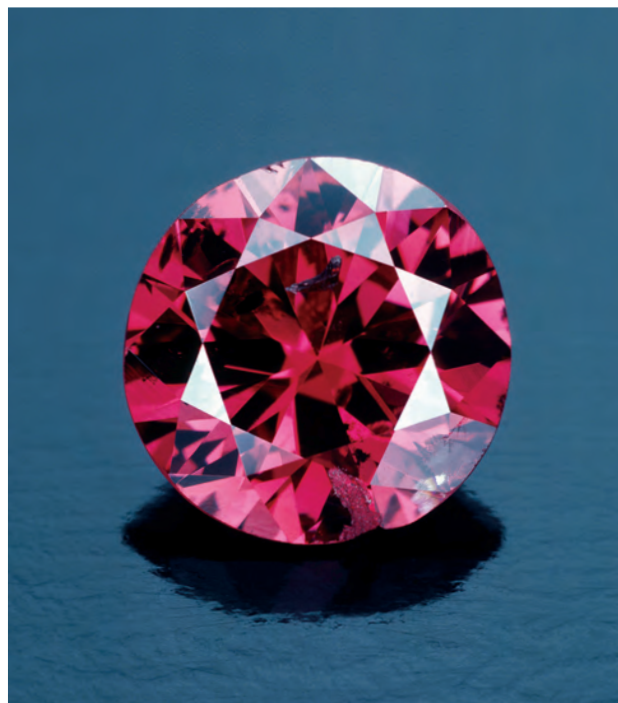
Figure 8. This page from a 1988 Sotheby's catalog shows a 15.97 ct Burmese ruby. This geographic origin helped it achieve $227,301 per carat, a record at the time. Photo by Robert Weldon.

tailers, increasing the premiums for stones such as untreated Burmese rubies, Kashmir and Burmese sapphires, and Colombian emeralds. Christie's and Sotheby's auction results are always public, so record prices generate big headlines and promote consumer awareness of these special gems. Auctions would not have the same market influence if the results were private. The auction influence was not all in one direction, however. As ruby and sapphire treatments proliferated during the 1980s, the auction houses responded to trade demand by adding more treatment information for the important gems offered in their sales (Shor et al., 1997; R. Drucker, pers. comm., 2012).

Historically, diamonds larger than 50 carats have been exceptional rarities. Between 1990 and 1995, however, the market saw more 50-plus ct diamonds than the known total since Jean-Baptiste Tavernier began cataloging large diamonds in the mid-17th century (Shor, 1998). Many of them began appearing at auction, and some achieved strong prices. But after a 101 ct D-Flawless heart shape failed to draw the seller's $10 million reserve price at a 1996 Christie's New York auction, it became apparent that neither dealers nor private buyers would keep paying such lofty prices. Laurence Graff, the likely buyer for such a stone, noted that dealers had gone too far in their asking prices (Shor, 1998).

CONTROVERSY OVER PRICING

Fine jewelry houses, which used the auctions as a source for large stones as well as some of their own historic pieces, began feeling the competition. Several complained that dealers who had previously supplied them now wanted to put their best pieces at auction. In addition, Sotheby's and Christie's began engaging in more direct competition with retailers by setting up departments to sell large diamonds and major jewelry pieces directly to clients, outside of the auction process (Shor et al., 1997). The auction houses' critics added a more serious charge, alleging that many of the pieces signed by famous jewelry houses or designers (Schlumberger, Webb, and the like) were actually forgeries made by consignors, or "reconstructions" where a large piece was built around a much smaller one with an authentic signature. Some retailers also claimed that auction houses sold treated gemstones without proper disclosure (Shor et al., 1997).

As the houses moved to address these complaints—auction catalogs showed a substantial increase in the number of diamonds and colored stones with reports from gemological labs—more serious issues emerged. The near-total dominance of Sotheby's and Christie's in the fine art and jewelry worlds, combined with their similar sale dates, consignment fees, and sales commissions, eventually attracted the attention of European and U.S. regulatory agencies.

BOX A: AUCTION RECORD PRICES

Prices for major diamonds and colored stones sold at auction can vary widely, even among gems of similar quality. Influencing factors include provenance, buyer competition, and market mood. The highest per-carat price for a colorless diamond sold at auction is from the Elizabeth Taylor sale in 2011. It sold for more than double the per-carat price ($265,697 vs. $138,526) of a diamond with similar size and quality auctioned a year earlier. The most expensive gem ever sold at auction, a 24.78 ct Fancy Intense pink diamond, had no historical ties. But it was exceptionally rare, being one of the largest pink diamonds ever offered for sale. Below is a list of the record-breaking prices for gemstones sold at auction.

Total price for any gem: $46,158,674
24.78 ct Fancy Intense pink diamond, Sotheby's Geneva, November 16, 2010

Per-carat price for any gem: $2,155,332
5 ct Fancy Vivid pink diamond, Christie's Hong Kong, December 1, 2010 (the "Vivid Pink")

Total price for a colorless diamond: $21,506,914
76.02 ct D-IF, Christie's Geneva, November 13, 2012 (the "Archduke Joseph")

Per-carat price for a colorless diamond: $282,545
76.02 ct D-IF, Christie's Geneva, November 13, 2012 (the "Archduke Joseph")

Total price for a pink diamond: $46,158,674
24.78 ct Fancy Intense pink, Sotheby's Geneva, November 16, 2010

Per-carat price for a pink diamond: $2,155,332
5 ct Fancy Vivid pink, Christie's Hong Kong, December 1, 2010 (the "Vivid Pink")

Total price for a blue diamond: $24,311,190
35.56 ct Fancy Deep grayish blue VS_2, Christie's London, December 10, 2008 (the "Wittelsbach Blue")

Per-carat price for a blue diamond: $1,439,497
10.95 ct Fancy Vivid blue, Christie's New York, October 20, 2010 (the "Bulgari Blue")

Total price for a yellow diamond: $12,361,558
110.03 ct Fancy Vivid yellow VVS_1, Sotheby's Geneva, November 15, 2011 (the "Sun Drop")

Per-carat price for a yellow diamond: $367,366
2.62 ct Fancy Vivid yellow, VVS_1, Christie's New York, December 13, 2011

Total price for a ruby: $4,620,000
6.04 ct Burmese, Christie's Hong Kong, May 29, 2012

Per-carat price for a ruby: $551,000
6.04 ct Burmese, Christie's Hong Kong, May 29, 2012

Total price for a sapphire: $7,122,742
130.50 ct, Christie's Geneva, May 18, 2011

Per-carat price for a sapphire: $145,339
A pair, 14.84 ct and 13.47 ct Kashmir, Christie's Hong Kong, May 31, 2011
(Note: A 26.41 ct Kashmir sapphire achieved virtually the same per-carat price at Christie's Hong Kong on November 29, 2011.)

Price for an emerald: $6,578,500
23.46 ct Colombian, Christie's New York, December 13, 2011 (Elizabeth Taylor sale)

Per-carat price for an emerald: $280,000
23.46 ct Colombian, Christie's New York, December 13, 2011 (Elizabeth Taylor sale)

Allegations of fee-fixing actually went back to 1975, when Christie's imposed a 10% buyers' premium and Sotheby's immediately followed, which brought lawsuits from the Society of London Art Dealers and British Antique Dealers' Association (Ashenfelter and Graddy, 2005). But the collapse of the fine art market in the early 1990s brought an era of cutthroat competition between the two houses in the form of slashed buyers' fees, donations to consignors' favorite charities, and even loans to potential consigners. During this period, CEOs Christopher Davidge of Christie's and Diana Brooks of Sotheby's met to discuss a truce. Sotheby's subsequently abandoned its loans and charitable donations to consignors. In March 1995, Christie's imposed a non-negotiable sell-ers' commission, ranging from 10% for items under $100,000 down to 2% for items that sold for more than $5 million. Sotheby's delayed following suit and won a $10 million jewelry consignment before instituting a similar commission.

In 1996, the UK's Office of Fair Trading announced an inquiry into possible anti-competitive practices, which ultimately led to Davidge's resignation from Christie's in December 1999 (Ashenfelter and Graddy, 2005). News reports soon began circulating that Davidge had made a deal with the U.S. Department of Justice to testify in a four-year investigation into charges of price-fixing. The Justice Department's report (2001) noted that the two houses controlled more than 90% of the auction market for fine art and jewelry.

Davidge's cooperation brought immunity from prosecution for himself and other Christie's executives, with the exception of board chairman Anthony Tennant. But Tennant could not be extradited to the United States, because price-fixing is a civil rather than a criminal matter in the UK ("Sir Anthony Tennant," 2011). Meanwhile, the Justice Department pursued Sotheby's majority owner and chairman, A. Alfred Taubman, and CEO Diana Brooks. Brooks, who agreed to testify against Taubman, pleaded guilty and was sentenced to three months' probation, six months' house arrest, 1,000 hours of community service, and a $350,000 fine (Ackman, 2002). Taubman was sentenced to a year in federal prison but was released after nine months (Johnson, 2007).

Yet these legal problems did not topple Sotheby's and Christie's dominance of the jewelry and fine arts auction markets, as evidenced by their sales over the following decade. The houses did change commission rates and separate their sales dates, which had been closely intertwined (Ashenfelter and Graddy, 2005). Sotheby's eventually moved its major fall auctions from October to November and December to better accommodate the wishes of private buyers (Schupak, 2011).

THE 21ST CENTURY

At the dawn of the new millennium, the number of ultra-wealthy people increased worldwide, especially in emerging parts of the world. The newly rich in Russia and several former Soviet states, China, and Middle East trade centers such as Dubai, Bahrain, Qatar, and Abu Dhabi joined a growing list in Europe and the U.S., where the number of high net worth individuals increased 48% during the 2000s. This burgeoning wealth, combined with price speculation, created a "perfect storm" for luxury jewelry sales at auction (Rapaport, 2008; Shor, 2008).

Asia in particular enjoyed rising wealth. During the 1980s, Asian economies, following the lead of Japan, began a period of strong growth in South Korea, Thailand, Taiwan, Singapore, and Hong Kong, which remains the major regional trading center. Taken as a whole, their economies grew an average of 5.5% annually between 1965 and 1990, one of the longest sustained growth periods of any region in history (Radelet et al., 1997). With the developing wealth in Asia, where there is an extremely high savings rate and jewelry is traditionally viewed as an asset rather than a consumable, demand for fine jewelry surged (Shor, 1997; Shor et al., 1997). As a result, Asian buyers were becoming major buyers of jewelry across the board, including the major jewelry auctions.

Christie's held its first major jewelry auction in Hong Kong in 1992. Sotheby's, which had opened a Hong Kong sales room devoted mainly to Asian art in 1973, began holding major jewelry auctions there shortly after Christie's. By the 2000s, Hong Kong stood alongside Geneva and New York as a venue for the Magnificent Jewelry sales, where the costliest lots are offered. By 2010, Hong Kong was Christie's leading jewelry venue, with annual sales totaling $163 million (Christie's, 2010). According to its Sotheby's 2011 annual report, Hong Kong accounted for 18% of the company's total sales in 2011, triple the share from 2007. Asia, including mainland China, has become a leading buyer of fancy-color diamonds, large colorless diamonds, and top gemstones, along with traditional favorite jadeite (Christie's, 2010).

Many of the auction headliners of the past 15 years have been fancy-color diamonds, which captured the market's attention and bidders' funds. The watershed for fancies was the record price achieved by the Hancock Red in 1987, which heightened global interest in colored diamonds. Following the sale, auction houses increased their offerings of colored diamonds with top grades. These quickly commanded the highest per-carat prices of any gemstones offered for sale (King, 2006). Indeed, during the past decade, nearly every major auction in the three main venues—Geneva, New York, and Hong Kong—has featured at least one significant fancy-color diamond.

Prices at auction soared through the 1990s and into the 2000s, fed by the burgeoning number of ultra-high net worth individuals. Prices for colored diamonds doubled and kept rising. The $1 million per-carat barrier was crossed in 2007, when Christie's sold a 2.26 ct Fancy purplish red diamond for $2.67 million, or $1.18 million per carat. Nor were record prices limited to colored diamonds. Burmese rubies and large colorless diamonds also saw substantial increases. In 2006, an 8.62 ct Burmese ruby sold for $3.64 million, or $422,000 per carat. Colorless diamond broke the $100,000 per-carat mark in 2005, and nearly doubled that by 2011. Indeed, while the financial crisis of September 2008 slowed economic activity around the world, it seemed to have little effect on auctions. Just three months after the collapse of Lehman Brothers, the Wittelsbach Blue diamond achieved the highest price ever paid for any gemstone when Christie's auctioned it in London.

Figure 9. Christie's New York salesroom was the scene of another celebrity jewels auction in December 2011. The sale of Elizabeth Taylor's collection, covered by the global media, realized a record $156.8 million. Photo courtesy of Christie's.

While the Wittelsbach diamond enjoys a rich history and a royal provenance, unpedigreed diamonds such as a 5.00 ct Fancy Vivid pink diamond doubled the $1 million per-carat mark to sell for $10.8 million at Christie's Hong Kong. The newly named Star of Josephine, a 7.03 ct Fancy Vivid blue, went for $9.49 million in May 2009 at Sotheby's Geneva (Burwell, 2011).

If 2009 was an unexpected banner year for jewelry auctions, 2010 shattered records. In November of that year, Sotheby's Geneva saw the first single-day auction to top $100 million. Nearly half of the total came from a 24.78 ct Fancy Intense pink diamond that Graff won with a top bid of $46.16 million, topping the Wittelsbach for the highest price ever paid for a gemstone at auction. And just before that sale, a 10.95 ct Fancy Vivid blue diamond, the Bulgari Blue, became the third-highest-priced gemstone to sell at auction, with a $15.76 million hammer price (Blauer, 2010).

The sales records set in 2010 did not last long. On December 13 and 14 of the following year, Christie's auctioned the jewelry of famed actress Elizabeth Taylor, who lived virtually her entire life in the headlines. The two-day sale (figure 9) saw 270 lots bring a total of $156.8 million. One of the top lots, the 33.19 ct D-VS$_1$ Elizabeth Taylor diamond, shattered the per-carat price record for a colorless diamond—$265,697 for a total of $8.8 million. A Bulgari brooch set with a 23.46 ct Colombian emerald (figure 10) sold for nearly $6.58 million, the highest price paid for an emerald at auction (The Collection of Eliza-

Figure 10. Elizabeth Taylor's Bulgari brooch holding a 23.46 ct Colombian emerald brought nearly $6.6 million at the auction of her jewelry collection. Photo courtesy of Christie's.

Figure 11. La Peregrina, a 203-grain natural pearl that belonged to European royalty for centuries, sold for a record $11.8 million at the Elizabeth Taylor auction. Photo courtesy of Christie's.

by Harry Winston in 1976, sell for $17.4 million, or $1.44 million per carat (Christie's, 2012).

In November 2012, even Elizabeth Taylor was upstaged, when a 76.02 ct colorless diamond that once belonged to Austrian royalty brought $21.5 million at Christie's Geneva. This was an all-time high for a colorless diamond, as well as a record per-carat price of $282,545. Sold to a private, anonymous buyer, the Archduke Joseph diamond (figure 12) was believed to have been mined centuries ago at India's famed Golconda mines (Shor, 2012).

Auction house executives offer three primary reasons why prices keep rising past record levels, even while the world economy has stagnated. The first is international reach. Whether conducted in Geneva, New York, or Hong Kong, the auctions now attract a worldwide clientele. Hong Kong, once a niche venue that specialized in jade and Chinese art, was Christie's leader in jewelry sales for 2009 and 2010. Many of the top lot buyers were Chinese businesspeople venturing internationally for the first time. Geneva and New York also turned in record numbers

Figure 12. The 76.02 ct Archduke Joseph diamond set a per-carat price record for a colorless diamond of $285,545 in November 2012, surpassing even the Elizabeth Taylor diamond auctioned the previous year. Photo by Tony Falcone; courtesy of Christie's.

beth Taylor, 2011). That auction also saw the most expensive natural pearl ever sold at auction, the 500-year-old La Peregrina (figure 11), which earned $11.8 million.

Like the Windsor auction, the Elizabeth Taylor sale received worldwide media coverage. The headlines and the record prices were broadcast around the world by television and print media, along with numerous Internet reports and blog posts.

The spring of 2012 saw more records fall. On May 29 at Christie's Hong Kong, a private buyer paid $3.33 million for a 6.04 ct Burmese ruby. At $551,000, this was the highest per-carat price ever paid for a ruby at auction. That same auction saw the Martian Pink, a 12.04 ct Fancy Intense pink named

as lots went to buyers from 30 countries during 2011.

Another reason is the rarity of top diamonds, especially blues and pinks. Of the millions of diamonds mined each year, only .001% qualify as fancy colors, and only a handful of those can achieve the top grades of intense and vivid. An even smaller percent are larger than a carat, let alone 5 carats. This exceptional rarity appeals to the growing number of collectors and investors.

A third factor is the shift toward the private buyer. In the past, dealers represented the majority of top-lot buyers at jewelry auctions. Today, individuals account for more than half of such sales. Auction house executives say these buyers range from collector-connoisseurs who seek the very best to investors who believe the jewels' extreme rarity, coupled with rising demand, will continue to push the value higher (Shor, 2011).

Meanwhile, both auction houses continue to compete with retail jewelers by selling diamonds and jewels privately. Christie's matches its clients' buying requests to a network of dealers. Sotheby's, in conjunction with the Steinmetz Group, a global diamond company, offers single stones or jewelry collections (Schupak, 2011).

CONCLUSION

During the past 30 years, the two largest auction houses have exerted a significant influence on the market prices for major diamonds and colored stones, while heightening interest in fancy-color diamonds and gemstones from historically prized countries of origin. The international reach and headline power of Sotheby's and Christie's have made them a formidable competitor to long-established jewelry houses such as Cartier, Tiffany, and Van Cleef & Arpels, while widening access to major stones for private buyers and newer high-end jewelry retailers such as Laurence Graff. Like many upscale retailers, the auction houses have adapted to technology, offering diamonds and jewelry to online buyers and displaying highlights from upcoming sales on Facebook and other social media sites. While annual auction sales have grown from less than $50 million to nearly $1 billion in those 30 years, such growth has not been accomplished without controversy and legal problems. But as the headlines surrounding the 2011 sale of the Elizabeth Taylor collection demonstrate, the auction market has become an influential force—in both demand and price—in the jewelry world today.

REFERENCES

Ackman D. (2002) Sotheby's Brooks sent to her room. *Forbes*, April 29, http://www.forbes.com/2002/04/29/0429brooks.html [date accessed: Jan. 30, 2013].

Ashenfelter O., Graddy K. (2005) Anatomy of the rise and fall of a price-fixing conspiracy: Auctions at Sotheby's and Christie's. *Journal of Competition Law and Economics*, Vol. 1, No. 1, pp. 3–20, http://dx.doi.org/10.1093/joclec/nhi003.

Auction fever (1979) *JCK*, Vol. 150, No. 12, p. G.

Balfour I. (2009) *Famous Diamonds*, 5th ed. Antique Collectors Club, Woodbridge, Suffolk, UK, p. 277.

Baptist M. (2011) Gem and jewelry auctions—A high flying business. *InColor*, No. 18, Winter, pp. 18–24.

Blauer (Lauré) E. (1981) Will auctioneers outbid jewelers? *JCK*, Vol. 152, No. 1, pp. 128–132.

——— (1981) Auctions, a market in transition. *JCK*, Vol. 152, No. 8, pp. 206–207.

——— (1983) A retailers' guide to estate jewelry. *JCK*, Vol. 154, No. 1, pp. 81, 84–85.

Blauer E. (2010) Pink power. *Rapaport Diamond Report*, Vol. 33,
No. 12, pp. 62–63.

——— (2012) Record setters. *Rapaport Diamond Report*, Vol. 35, No. 2, pp. 46–60.

Burwell A. (2011) Colored diamonds: An insider's guide. *Departures*, May/June 2011 http://www.departures.com/articles/colored-diamonds-an-insiders-guide [date accessed: Jan. 30, 2013].

Christie's (2010) 2010 global jewelry sales exceed $426 million. Press release, February 3.

Christie's (2011) The collection of Elizabeth Taylor. http://www.christies.com/elizabethtaylor/saleroom.aspx [date accessed: Jan. 30, 2013].

Christie's Hong Kong (2012) Magnificent Jewels sale. Press release, May 29.

Christie's jewelry, watch sales up 40% (2012) *National Jeweler*, February 3. http://www.nationaljeweler.com/nj/fashion/a/~27770-Christies-jewelry-watch-sales-up [date accessed: Jan. 30, 2013].

Donohue P. (1980a) Do auction gems ruffle market? *JCK*, Vol. 151, No. 2, pp. 227–228.

——— (1980b) Estate jewelry: Will auction houses corner the mar-

ket? *JCK*, Vol. 151, No. 7, pp. 192–196.

Edelstein C. (1989) Auctions: Everything old is new again. *JCK*, Vol. 160, No. 9, Part 2, pp. 44, 46, 48, 50–51.

Enriquez C.M. (1930) Fire-hearted pebbles from Burma. *Asia*, Vol. 30, No. 10, pp. 722–725, 733, http://www.palagems.com/burma_ruby.htm [date accessed: Jan. 30, 2013].

Gertz L. (1985) $70 million in second hand jewelry. *JCK*, Vol. 156, No. 4, pp. 60–62, 64, 68.

Johnson C.A. (2007) For billionaire there's life after jail. *CBS Sunday Morning*, April 15, http://www.cbsnews.com/2100-3445_162-2684957.html.

King J. (2006) The allure of colored diamonds. In J. King, Ed., *Gems & Gemology in Review: Colored Diamonds*. Gemological Institute of America, Carlsbad, CA, pp. xiv–xix.

Live Auctioneers (2010) Sotheby's New York. http://www.liveauctioneers.com/auctioneer/246-sothebys-new-york [date accessed: Jan. 30, 2013].

Parke-Bernet (1938) *Precious-Stone Jewelry*. Auction catalog, November 9.

Parke-Bernet (1969) *Magnificent Jewelry*. Auction catalog, October 23.

Radelet S., Sachs J., Lee J.-W. (1997) Economic growth in Asia. Harvard Institute for International Development, http://www.cid.harvard.edu/archive/hiid/papers/ecgasia.pdf [date accessed: Jan. 30, 2013].

Rapaport M. (2008) Inside the auction market. Diamonds.net, November 7, http://www.diamonds.net/news/NewsItem.aspx?ArticleID=24052 [date accessed: Jan. 30, 2013].

Schuler G. (2011) Everything old is new again. *G&G*, Vol. 47, No. 2, pp. 100–101.

Schupak H. (2011) Auction houses: A formidable competitor sneaks up. *Centurion News*, September 13, http://news.centurionjewelry.com/articles/view/auction-houses-a-formidable-competitor-sneaks-up [date accessed: Jan. 30, 2013].

Shor R. (1983) Fall auction report: Colored diamonds, important jewels sparkle. *JCK*, Vol. 154, No. 12, pp. 46–48, 50, 52.

——— (1988) Auction fever fuels gem market. *JCK*, Vol. 158, No. 12, pp. 132–135.

——— (1997) Will there be enough good diamonds to go around? *New York Diamonds*, Vol. 39, pp. 40–44, 46, 58.

——— (1998) Mega diamonds still on ice. *New York Diamonds*, No. 46, pp. 42–44.

——— (2008) GIA GemFest Basel charts luxury growth. *The Loupe*. Summer. Vol. 17, No. 3, p. 13.

——— (2011) Why are auction house diamond sales breaking records? GIA news release, April 5, http://www.gia.edu/nav/toolbar/newsroom/news-releases/2011-news-releases/Auction%20House%20Analysis_04%2005%2011_FINAL.pdf [date accessed: Jan. 30, 2013].

——— (2012) Industry Analysis: Archduke diamond sets price record. *GIA Insider*, Nov. 19.

Shor R., King S., Weldon R. (1997) Auction houses vs. luxury retailers: Myth vs. reality. *JCK*, Vol. 168, No. 1, pp. 134–138, 140.

Sir Anthony Tennant (2011) *Daily Telegraph*, obituaries, August 6, http://www.telegraph.co.uk/news/obituaries/finance-obituaries/8687415/Sir-Anthony-Tennant.html [date accessed: Jan. 30, 2013].

Sotheby's (1988) *Magnificent Jewels*. Auction catalog, October 17.

Sotheby's 2011 revenues rise 7% (2012) *National Jeweler*, March 2, http://www.nationaljeweler.com/nj/fashion/a/~27983-Sothebys-2011-revenues-rise-7 [date accessed: Jan. 30, 2013].

U.S. Department of Justice (2001) Former chairmen of Sotheby's and Christie's auction houses indicted in international price-fixing conspiracy. Press release, May 2.

Vogel C. (1987) Jewels of Windsor. *New York Times Magazine*, February 8, http://www.nytimes.com/1987/02/08/magazine/jewels-of-windsor.html?pagewanted=all&src=pm [date accessed: Jan. 30, 2013].

For online access to all issues of GEMS & GEMOLOGY, visit:

gia.edu/gems-gemology

A Comparison of Modern and Fossil Ivories Using Multiple Techniques

Zuowei Yin, Pengfei Zhang, Quanli Chen, Qinfeng Luo, Chen Zheng, and Yuling Li

To distinguish between modern and fossil (mammoth) elephant ivory, samples of both were analyzed by petrographic microscopy, scanning electron microscopy, infrared spectroscopy, and laser-induced breakdown spectroscopy. In addition to the differences observed under low magnification, SEM demonstrated each variety's structure in greater detail. While modern ivory appeared very compact under high magnification, fossil ivory showed a loose structure with many long channels and splintery cracks. IR spectroscopy revealed differences in water and collagen contents. Modern ivory exhibits a broad IR absorption band around the 3320 cm^{-1} peak, while the sharp bands between 3300 and 3500 cm^{-1} in fossil ivory indicate a much lower water content. Modern ivory's IR peaks at 2927 and 2855 cm^{-1}, compared to fossil ivory's weak peak near 3000 cm^{-1}, suggest a significant loss of collagen after burial for tens of thousands of years. LIBS chemical analysis showed different amounts of various trace elements. Weakly weathered fossil ivory contains Fe, Ti, Mn, and Al, while the similar-looking modern ivory contains Hg, Cr, and Si, indicating that trace elements could be used to distinguish them.

T he modern elephant, threatened by extinction, is protected by international agreements banning the sale of ivory from tusks. This trade ban does not apply to ornaments made of mammoth fossil ivory, which is still legally sold in the gem market. The two materials look similar, and it is difficult to distinguish them with the unaided eye, especially when the fossil ivory is relatively unweathered. There is such a need to identify the modern and mammoth ivory in the Chinese jewelry market because the jewelry prices of modern ivory and fossil ivory vary greatly. For example, the price of modern ivory bangles range from US$400–$500 per piece, while the price of mammoth fossil ivory bangles ranges from US$200–$300 per piece.

Mammoth is an extinct mammal species belonging to the Elephantidae family, which lived during the late Pleistocene in Europe, northern Asia, and North America. Their fossils are commonly found in frozen ground in Alaska and Siberia. Reports on mammoth have mainly dealt with the species' life, extinction, and prospects for regeneration (Iacumin et al., 2005; Basilyan et al., 2011). Gemological studies on mammoth ivory are virtually nonexistent, while the literature on elephant ivory is also quite limited (Edwards and Farwell, 1995; Edwards et al., 1997; Raubenheimer et al., 1998; Su and Cui, 1999; Reiche et al., 2001; Sakae et al., 2005; Edwards et al., 2006; Singh et al., 2006; Müller and Reiche, 2011). This study examines the two ivories' structure and chemical composition to better explore their identification characteristics.

MATERIALS AND METHODS
The modern elephant ivory samples consist of beads provided by the Museum of China University of Geosciences (figure 1). They are originally from Thailand and belong to the Asian elephant species. The authors were allowed to cut one bead in half for scanning electron microscopy (SEM) testing.

Figure 1. Modern elephant ivory samples were taken from a necklace, including the bead in the inset photo (magnified 20×). The red line indicates where the bead was cut for SEM analysis. Schreger lines can be observed on the bead. Photos by Zuowei Yin.

The authors obtained fossil ivory specimens from mammoth tusks sold in the gift shop at the Geological Museum of Guangdong Province, China. All three samples (figure 2) were cut perpendicular to the length of the tusk. Sample M1 contained three layers: a strongly weathered black surface, a semi-weathered brown middle layer, and a weakly weathered white inner layer. This sample was sliced into four pieces for analysis, and each piece contained all three layers. Sample M2 contained only the semi-weathered brown middle layer, and M3 only the weakly weathered white inner layer.

The samples underwent standard gemological testing to determine their spot refractive index, specific gravity, and UV fluorescence reaction. To study the structure at various resolutions, the samples were observed using both a petrographic microscope and SEM. Samples or sample portions from both ivory types were carefully ground with carborundum until they became nearly transparent thin sections for examination with the petrographic microscope. A Quanta 200 scanning electron microscope at the China University of Geosciences in Wuhan was used for this study. Samples with Schreger lines were chosen, and they were cleaned with alcohol and dried in air. The specimens were fractured by the authors, and the fracture surfaces were sputter-coated with gold powders using a SCD-005 ion sputtering coater. Then they were fastened to a round metal board for observation. The resolution of the Quanta 200 is 3.5 nm under 30 KV voltage in both high- and low-vac-

Figure 2. These three fossil ivory specimens are from mammoth tusks (bottom right). On the top row, sample M1 is composed of the weakly weathered white layer, the semi-weathered brown middle layer, and the strongly weathered black surface layer. Sample M2 (bottom left) shows the semi-weathered brown middle layer of fossil ivory. M3 (botom middle) is only of the weakly weathered white inner layer. Photos by Zuowei Yin.
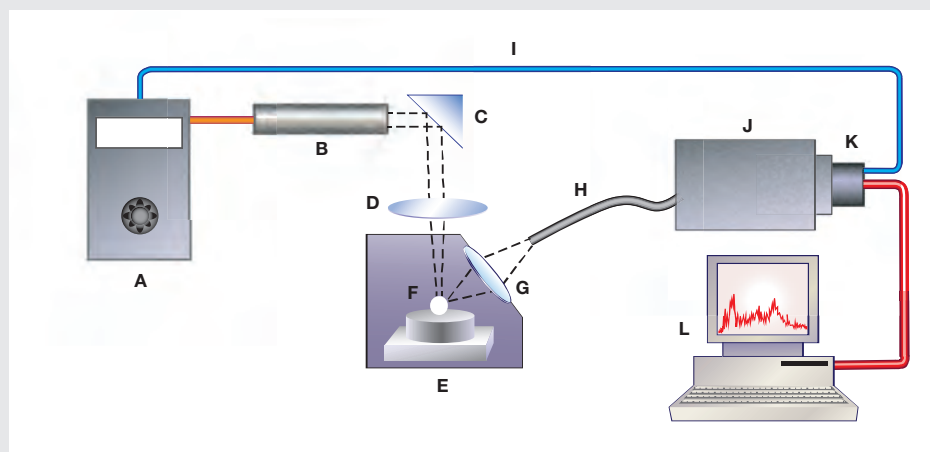
BOX A: WHAT IS LIBS?

Figure A-1. This diagram shows the main components of a modern LIBS system: (a) laser source and cooler; (b) pulsed laser head; (c) mirror; (d) focusing lens; (e) excitation chamber; (f) sample; (g) collecting optics; (h) optical fiber; (i) detector trigger signal; (j) wavelength selector; (k) detector array; and (l) microcomputer. From Pasquini et al. (2007).

Laser-induced breakdown spectroscopy is a rapid chemical analysis technique. A modern LIBS system includes a laser source, delivery optics, collecting optics, a spectrometer, and an attached computer (figure A-1). This technology requires no sample preparation. Broad elemental coverage and extremely short measurement time for each spot are additional advantages that make this one of the most practical and efficient micro-beam technologies available to gemologists.

Short, powerful laser pulses are focused on the target to vaporize and atomize a small amount of sample (0.1μg–0.1 mg) in a process known as laser ablation. The vaporized portion then further interacts with a second laser pulse to form the high-temperature plasma. This excited material (electrons, ions, molecules, etc.) produces an electromagnetic emission during the cooling process. High-resolution optics detect and record the intensity of this emission, which allows not only the identification of the elements via their unique spectral signatures but also the measurement of their concentrations above the detection limits. Typical detection limits of LIBS are in the ppm (parts per million) range. Both qualitative and quantitative analyses can be performed, but for quantitative measurements the system needs to be calibrated for each elemental species (Pasquini et al., 2007).

The crater formed by laser ablation usually has a diameter of 10–100 μm and a depth of 100 nm. With 0.1 nm (1 Å) widths, the emission peaks of LIBS spectra are narrower than those from passive emission or reflectance spectroscopy. The spectral region of interest, typically from about 180 to 850 nm, generally includes numerous peaks per element, allowing cross-checking for interferences. The analyses of our samples were very rapid, with each spot measured for less than 1 second.

uum modes, 3.5 nm in ESEM vacuum mode under 30 KV, and 15 nm in a low vacuum under 3 KV. We used 7×–1,000,000× magnification and an accelerating voltage of 200 V to 30 KV with a tungsten filament and a maximum beam current of 2 μA. The SEM images are from secondary electrons.

Infrared spectral analysis was carried out using a Nicolet 550 Fourier transform infrared (FTIR) spectrometer with a resolution of 0.5 cm^{-1}, a scanning range of 4000–400 cm^{-1}, and 32 scans per second at room temperature (25ºC). Half of a modern ivory bead and one fossil specimen with black, brown, and white layers (sample M1) were analyzed in transmission mode with a KBr pellet. Only the white layers of sample M1 were tested by FTIR, because their color was close to that of modern ivory.

Laser-induced breakdown spectroscopy (LIBS) analysis was carried out using a LIBS2005 with Nd:YAG solid state laser (1064 nm wavelength) at the China University of Geosciences to measure trace elements semi-quantitatively. (See box A for more on this technique.) The test used a voltage of 500–650V and a frequency of 10 Hz.

RESULTS AND DISCUSSION

Gemological Properties. Both ivory types showed overlapping spot RI (1.52–1.54) and SG (1.69–1.81), so they cannot be distinguished by these properties. The

Figure 3. Modern elephant ivory fluoresced bluish white in long-wave UV (left) and very weak bluish white in short-wave UV (right). Photos by Zuowei Yin.

modern ivory beads fluoresced bluish white to long-wave UV radiation and very weak bluish white to short-wave UV (figure 3).

The weakly weathered white layer of fossil ivory (M1) showed stronger fluorescence to long-wave than short-wave UV, while the semi-weathered brown layer (M2) displayed weaker fluorescence than the white layer under both long- and short-wave UV (figure 4, top). The strongly weathered black layer from sample M1 was inert to both wavelengths. These observations suggest that the degree of weathering is inversely proportional to the strength of fluorescence reaction.

Both ivories are composed mainly of the mineral

Figure 4. These photos show the fluorescence reaction of mammoth ivory samples M1 and M2 to long- and short-wave UV. The front side of sample M1 is the weakly weathered white layer, which fluoresces stronger bluish white color in long-wave UV (A) and weak bluish white color in short-wave (B). The strongly weathered black layer of sample M1 is inert to both wavelengths (C and D). Sample M2, the semi-weathered brown layer, fluoresces weak bluish white in long-wave UV (A and C) and is inert to short-wave (B and D). Photos by Qinfeng Luo.

hydroxyapatite and organic materials. Because hydroxyapatite usually does not display characteristic fluorescence while the organic material typically does, ivory with more organic material displays a more intense fluorescence. This implies that weathering is more destructive for organic than inorganic material.

Structural Analysis. Both modern and mammoth elephant ivories display intersecting chevron patterns known as Schreger lines (Singh et al., 2006; Palombo et al., 2012). The Schreger angle of the modern elephant ivory sample is about 115° or 65° (see figure 1, inset). According to Singh et al. (2006), the mean Schreger angle value taken at all three portions in Asian elephant ivories is (91.1 ± 0.70)°.

Figure 5. In modern elephant ivory, Schreger lines and thin polishing lines are visible under plane polarized light. Photo by Qinfeng Luo; magnified 200×.

In Brief

- Ivory from mammoth and modern elephant ivory look quite similar. Distinguishing between the two is important in protecting endangered elephant species.
- Petrographic microscopy and scanning electron microscopy (SEM) were used to reveal structural differences between the two materials.
- Infrared spectroscopy was effective in identifying the two ivory types, while laser-induced breakdown spectroscopy (LIBS) showed significant differences in trace-element concentrations.

Fossil Ivory. The thin section is made of semi-weathered sample M2. At 200× magnification, the Schreger lines are not apparent; only polishing lines and cracks can be observed (figure 6). The thin section fashioned from only the white layer of sample M1 showed no obvious differences with modern ivory under the petrographic microscope, because the white layers are less weathered and both look similar at less than 500× magnification.

Schreger lines of both ivory types are visible at lower magnification (less than 100×) through the thin

Figure 6. In semi-weathered fossil ivory, only dark polishing lines and cracks can be observed under plane polarized light. Photo by Qinfeng Luo; magnified 200×.

Fossil ivory sample M3 (again, see figure 2) has a Schreger angle of approximately 100°. According to Fisher et al. (1998), the Schreger angles in mammoth tusks range from 62° to 105° within the various layers, with a mean of 87.1°. The Schreger angles from the outermost layer of mammoth tusks, measured by Trapani and Fisher (2003) at the dentine-cementum junction, range from about 70° to 100° (Palombo et al., 2012). Therefore, identification of fossil and modern ivories based on Schreger angles requires caution. Ivory ornaments cut from different layers of the tusk, or cut at a slightly different angle relative to the length of the tusk, can have varying Schreger angles.

Microstructure. *Modern Elephant Ivory.* A photomicrograph of modern ivory at 200× magnification shows that the Schreger pattern lines (the sparse vertical lines) occur along one direction (figure 5). The thin horizontal lines closely parallel to each other are polishing lines.
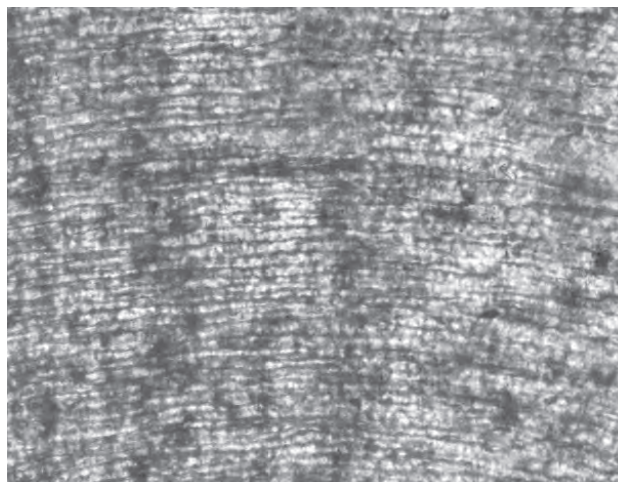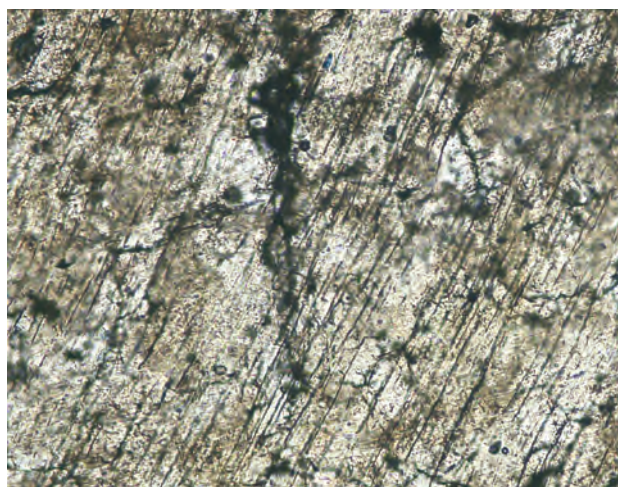
Figure 7. The laminar structure of a modern elephant ivory sample is shown at 800× magnification (left). The sample was halved along the hole of the bead, indicating that the cracks were manmade. The structure of the elephant ivory sample looks compact. The layers of the fracture show the splintery structure of modern elephant ivory (where the arrow points) at 3000× magnification (center). At 24,000× magnification (right), the platy crystals of hydroxyapatite in modern elephant ivory exhibit a laminar structure. Photos by Qinfeng Luo.

section. At higher magnification, the Schreger lines are less likely to be seen. Cracks and holes cannot be observed in a modern ivory thin section, but they are obvious in fossil ivory sample M2.

SEM Analysis. *Modern Ivory.* SEM images obtained from the bead in figure 1 at various magnifications show some interesting features. First, the structure of modern ivory appears compact and has a laminar structure generally composed of platy layers parallel to each other, forming a step-like pattern (figure 7, left and center). Another notable feature is that the layers forming the ivory body also display a platy structure at high magnification (figure 7, right).

Fossil Ivory. The intensely weathered black layer of fossil ivory sample M1 showed the following characteristics.

Broken and crushed splintery cracks were often observed on the rupture surface (figure 8). Although there were cracks in both kinds of ivory (figure 7, left; figure 8, left), their formation was different. Because modern ivories contain a high proportion of organic materials, external mechanical forces usually cause cracks to occur straight through the surface. But because the organic materials in fossil ivories reduce gradually due to weathering, the cracks tend to form gradually into splinters. Under long-term weathering (figure 8), the structure of the fossil ivory is probably
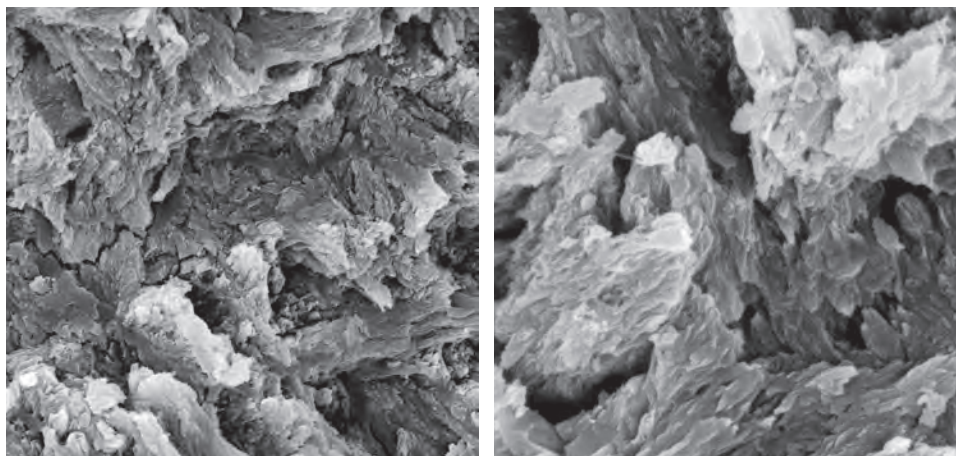
Figure 8. Splintery cracks in the black layer of fossil ivory M1 are visible at 3000× magnification (left). The cracks could be caused by rearrangement of hydroxyapatite crystals due to the loss of organic materials and the reduced binding force. With so many cracks between the hydroxyapatite crystals, the structure of the black layer appears broken and disordered at 10,000× magnification (right). Photos by Qinfeng Luo.

loosened by the lack of organic materials, which reduces the binding force to arrange hydroxyapatite (Qi et al., 2010).

Many long, narrow channels and small holes were found in the intensely weathered layer of fossil ivory M1. These cylindrical channels were common in SEM images of mammoth ivory samples from this study. They oriented themselves along the length of the ivory. Previous studies (Su et al., 1999; Ge et al., 2006) concluded that in prehistoric bones and ivories, hydroxyapatite exists on the nanoscale (10^{-9} m) with a laminar structure and its c-axis oriented along the length of collagen fibers. Müller et al. (2011) pointed out that in all ivories the collagen fiber bundles are organized around the pulp cavity in the center of the tusk. The black surface layers experienced the most rapid loss of organic substance. Based on the orientation and shape of these channels and holes, we deduce that they were caused by the loss of collagen fibers.

Some obvious and irregular grooves lie perpendicular to the crystal stacking layers in the black layer of fossil ivory. The grooves can be individual or overlapping (figure 10). They are different from the channels in figure 9, with a nearly vitreous luster. Existing research and observation with the polarizing microscope suggests that the grooves are related to collagen fibers and the growth mechanism of the Schreger lines (Su et al., 1999).

Magnification at 1500–6000× shows that the structure of the weakly weathered white layer of fossil ivory M1 is nearly as compact as the structure of mod-
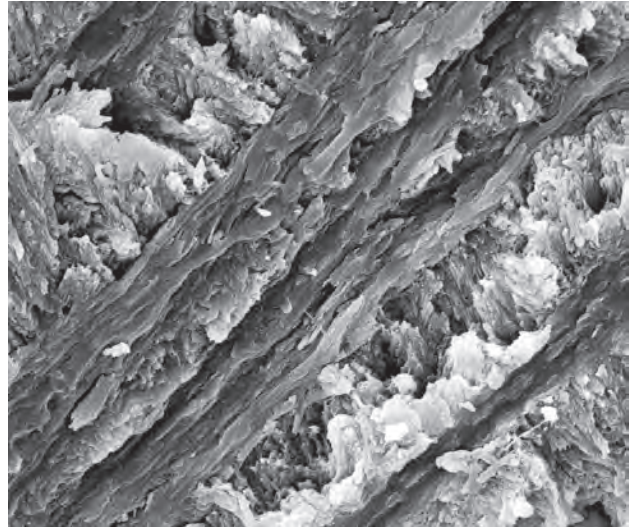
Figure 10. The black layer of mammoth ivory sample M1 contained these continuous grooves interspersed among the hydroxyapatite crystals. The grooves are apparently lower than the surface of the laminar structure. Photo by Qinfeng Luo; magnified 2500×.

ern ivory (figure 11). There are some tiny holes in the white layer, but they are less abundant and less obvious than those of the black layer (figure 9, left). Similarly, we deduce that the holes were likely formed due to the loss of organic materials by weathering.

Chemical Analysis. *Infrared Spectroscopy.* Dan et al. (2006) showed that ivory is composed of biogenic hy-

Figure 9. At 1000× magnification (left), fine parallel channels are visible within the black layer of fossil ivory sample M1. There are up to 20–30 channels per cm². At 5000× magnification (center), the channels appear cylindrical and at close intervals. 10,000× magnification (right) shows that many of the crystals are stacked. The channels and holes are perpendicular to the stacking layers. Photos by Qinfeng Luo.
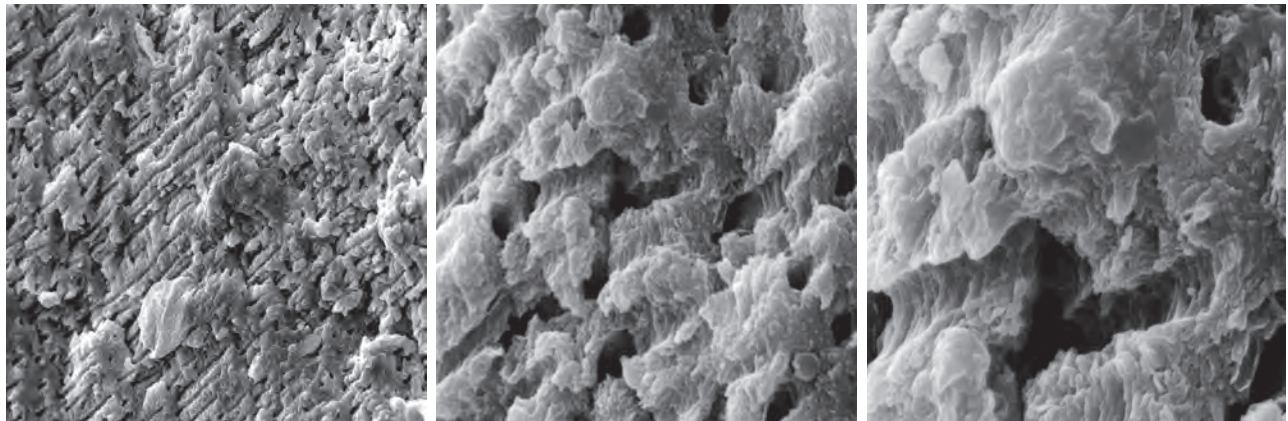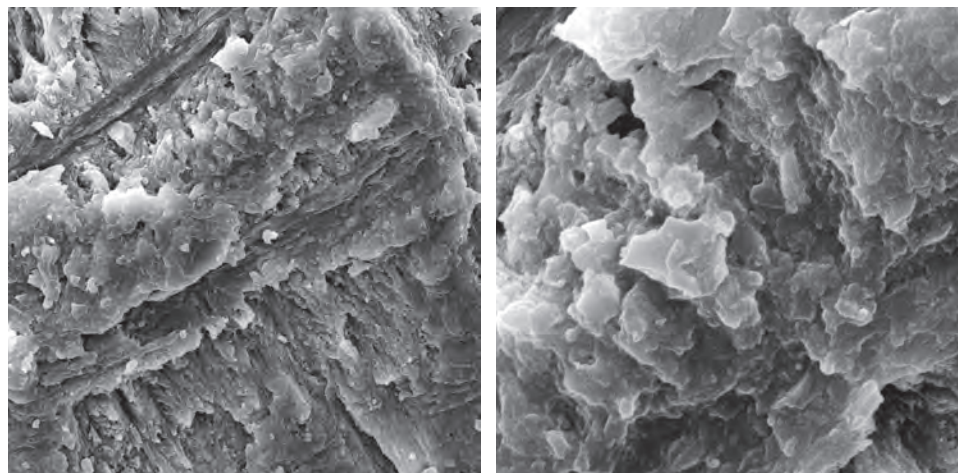
Figure 11. Long grooves can still be seen in white layers of fossil ivory sample M1 (left, magnified 1500×). Tiny holes can also be observed, though the black layer of sample M1 contain more of them (compare with figure 9, left). The structure of the white layer still appears compact under 6000× magnification compared with figure 8 of the black layer. Photos by Qinfeng Luo.

droxyapatites and collagen. Living creatures' hydroxyapatites are slightly crystallized. Upon burial, noncrystalline hydroxyapatite will start to crystallize due to diagenesis. Comparison of modern and the least weathered fossil ivories' FTIR spectra (figure 12) showed the following results:

1. 4000–3000 cm^{-1}: Modern ivory has a broad IR absorption band around the 3320 cm^{-1} peak. In the least weathered layer of fossil ivory, some sharp bands are found between 3300 and 3500 cm^{-1}. Dan et al. (2006) demonstrated that the IR absorption bands between 3400 and 3500 cm^{-1} are caused by hydroxyl stretching vibration, which indicates that fossil ivory has a much lower water content than modern ivory.

2. 3000–2000 cm^{-1}: The IR absorption peaks of modern ivory at 2927 and 2855 cm^{-1} result from collagen (Qi et al., 2005). Because the samples were handled with gloves and wiped with alcohol and dried in the air, contamination can be ruled out. Modern ivory's absorption peak at 2927.60 cm^{-1} is caused by asymmetric stretching vibration of the CO_3^{2-} group, and the 2855.51 cm^{-1} peak is caused by symmetric stretching vibration of CO_3^{2-} groups (Farmo, 1982). The IR absorption spectra of fossil ivory have a weak absorption peak near 3000 cm^{-1}, indicating a significant loss of collagen after burial for tens of thousands of years (Qi et al., 2005).

3. 2000–1000 cm^{-1}: The IR spectra of modern elephant ivory feature two strong absorption peaks at 1660.79 and 1557.66 cm^{-1}, caused by bending vibration of coordinated water, or twisting of H-O-H. Fossil ivory spectra show only a weak absorption peak at 1642.22 cm^{-1}, indicating much lower water content (Zhou et al., 1999). Both kinds of ivory have a strong absorption band at about 1038.90 cm^{-1}, caused

Figure 12. The FTIR spectrum of modern elephant ivory (A) has a broad band at 3320 cm^{-1}, while the spectrum of fossil ivory (B) contains wide and sharp absorption bands between 3300 and 3500 cm^{-1}.
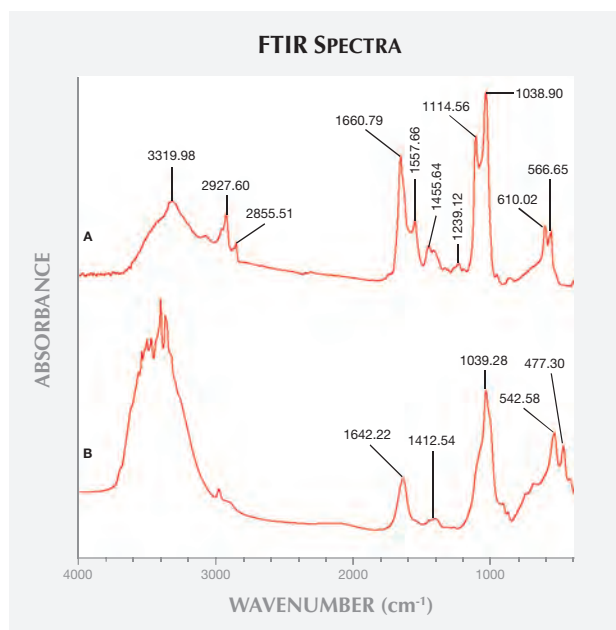
	Major elements	Trace elements
Elephant ivory	P, Ca, Na, Mg, H, C, N, O	Sr, Ba, Hg, Cr, Si
Fossil ivory (white layer)	P, Ca, Na, Mg, H, C, N, O	Sr, Ba, Fe, Mn, Ti, Al
Fossil ivory (brown layer)	P, Ca, Na, Mg, H, C, N, O	Sr, Ba, Fe
Fossil ivory (black layer)	P, Ca, Na, Mg, H, C, N, O	Sr, Ba, Fe, Mn, Si

Refers to the LIBS results of this study and Dan et al. (2006), Huang et al. (2007), and Müller et al. (2011).

by asymmetric stretching vibration of the PO_4^{3-} group, because their major constituent is hydroxyapatite. The biogenic hydroxyapatites have three absorption peaks at 1541–1548, 1455, and 1417 cm^{-1} (Huang et al., 2007).

4. 1000–400 cm^{-1}: Both kinds of ivory have two peaks and exhibit no obvious differences here.

LIBS Analysis. Ivory is composed of 70% hydroxyapatite (some of the calcium having been replaced by magnesium) and 30% organic substance (collagen fibers). Thus the major elements of both ivories are the same: Ca, Na, Mg, P, H, C, N, and O, with higher concentrations of Ca, Na, and Mg (figures 13–16) (Müller et al., 2011; Huang et al., 2007; Dan et al., 2006).

Comparing the LIBS data of modern ivory and the three layers of fossil ivory (table 1), we found that:

1. Besides the major elements consistent in both kinds of ivory, modern ivory has Hg, Cr, and Si; the white layer of fossil ivory contains Fe, Ti, Mn, and Al.

2. The Al and Ti in the white layer of fossil ivory are absent in the brown and black layers.

3. The black surface layer of fossil ivory contains some Si, which is absent in the white and brown layers.

As noted by Wilson and Pollard (2002), chemical changes achieve thermodynamic equilibrium between the archaeological material and the surrounding environment. According to this principle, all bone materials should tend to have an identical chemical composition under similar environmental conditions. We inferred that Sr and Ba are common replacements for Ca in the apatite of both ivory types. Due to the different living environments of mammoth and modern elephants, Fe, Mn, Ti, and Al replaced Ca in mammoth ivory; Hg, Cr, and Si replaced Ca in modern elephant ivory.

Singh et al. (2006) found higher concentrations of
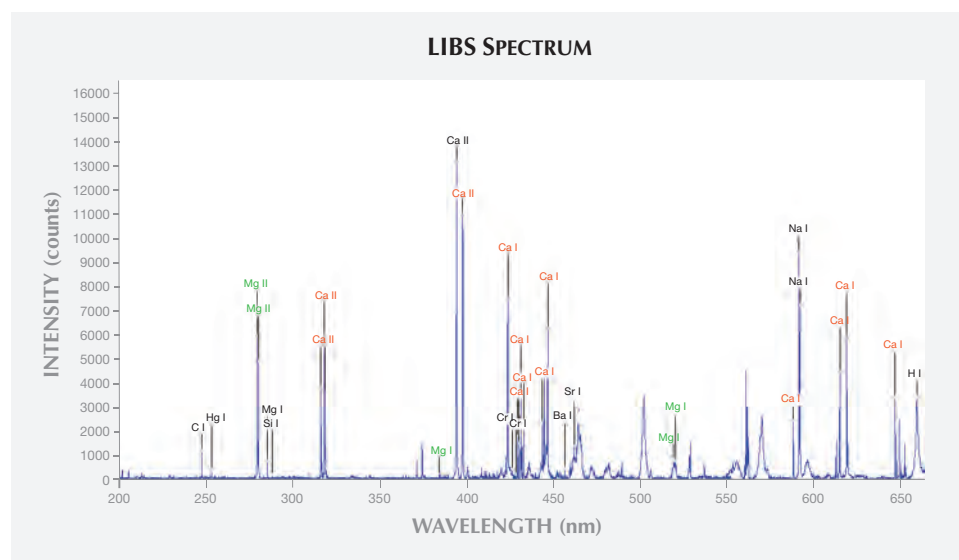
Figure 13. This LIBS spectrum of modern elephant ivory (200–650 nm) shows the elements Ca, Hg, Cr, Na, Mg, Si, Sr, and Ba. Due to space limitations, we cannot enlarge the spectrum to label every detected element.
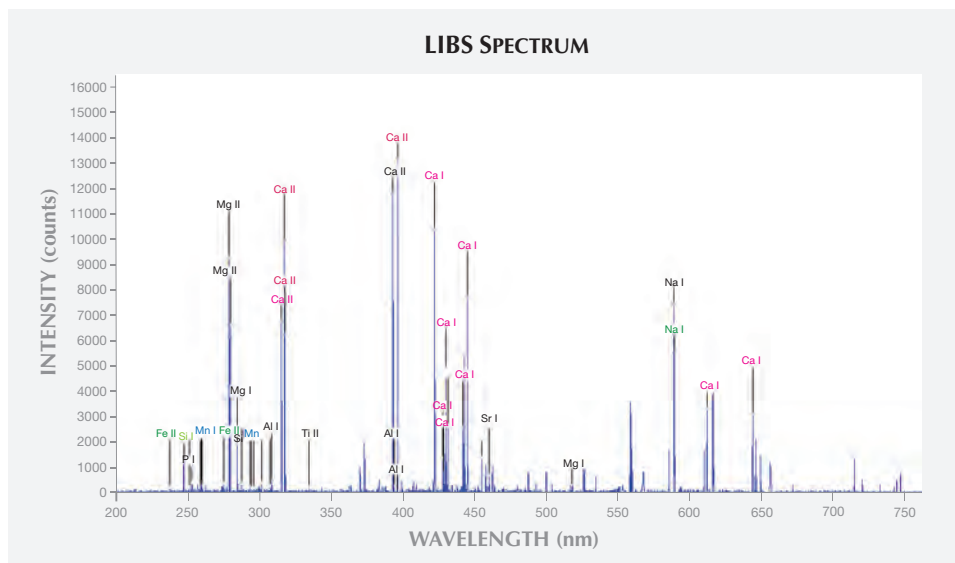
Figure 14. The LIBS spectrum of the white layer from fossil ivory sample M1 (200–750 nm) shows Fe, Mn, Mg, Al, Ca, Ti, Ba, Sr, Na, and Ca, with higher concentrations of Na and Mg.
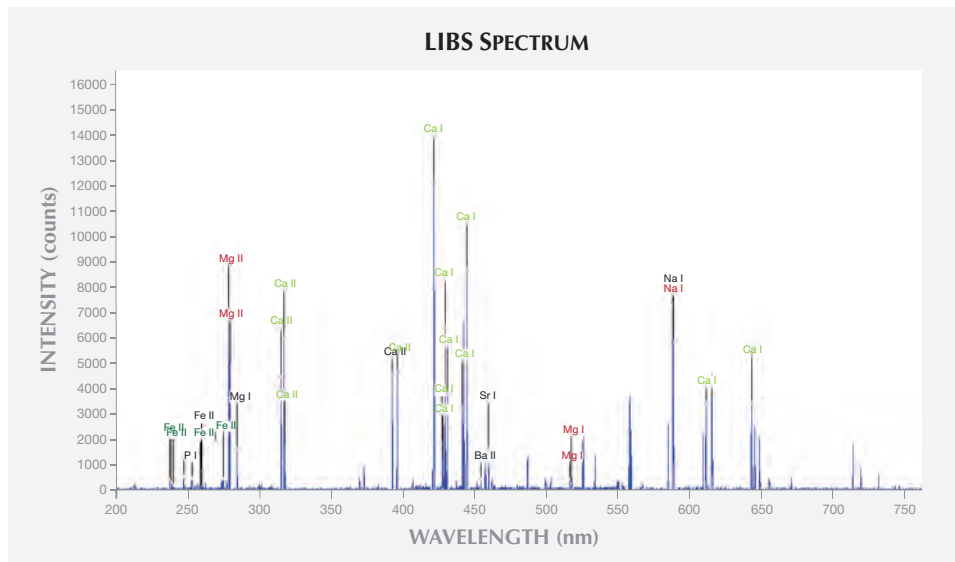
Figure 15. This LIBS spectrum of the semi-weathered layer from fossil ivory sample M1 (200–750 nm) shows the elements Fe, Mg, Ca, Ba, Sr, and Na.
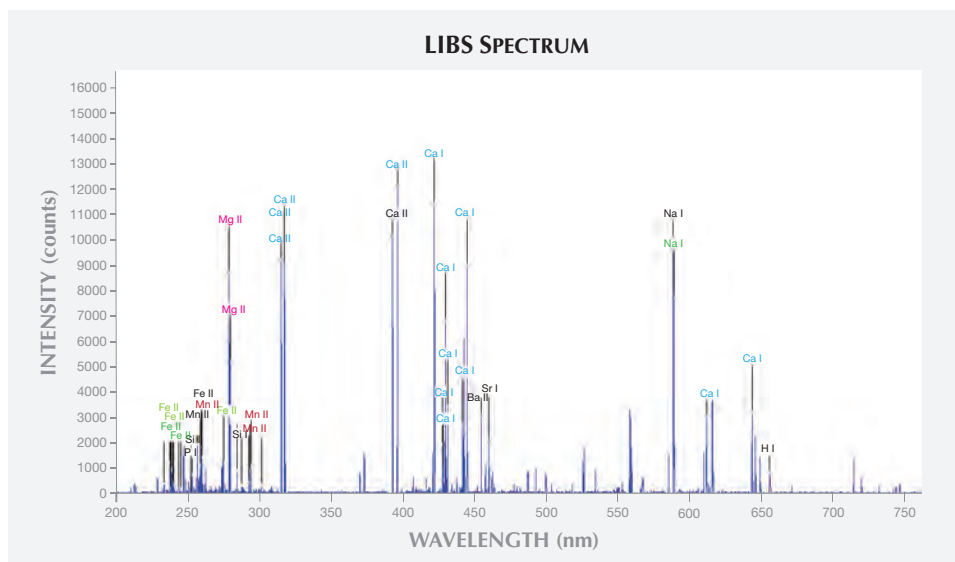
Figure 16. This LIBS spectrum of the black surface layer of fossil ivory sample M1 (200–750 nm) shows Fe, Si, Mg, Mn, Ca, Ba, Sr, and Na.

P, Mg, and Cr in Asian elephant ivory than in the African species. Thus it is possible to distinguish fossil and modern ivories by analyzing their trace element concentrations. Although our current research did reveal some differences between the two types of ivory, many more samples are needed for a conclusive discrimination.

CONCLUSION

This comparison of fossil and modern ivories suggests multiple ways to distinguish them. Schreger angles are often used to identify different types of ivories, but these are not definitive. The observed Schreger angle can vary depending on the layer of a tusk and the cutting angle relative to the length of the tusk. Microscopic examination of fossil ivory samples revealed broken lines, cracks, long channels, and grooves that were not seen in the modern ivory samples. The infrared spectrum of modern elephant ivory showed distinct absorption peaks related to collagen, while fossil ivory did not show these peaks. Similarly, absorption peaks related to coordinated water are pronounced in modern elephant ivory's spectrum and weak in that of mammoth ivory. FTIR testing proved effective in identifying the two kinds of ivories. LIBS analysis showed that besides the major elements consistent to both kinds of ivory, white fossil ivory contains Fe, Ti, Mn, and Al, while modern ivory has Hg, Cr, and Si. The difference in trace element concentrations can potentially assist in the identification of fossil and modern ivories.

ABOUT THE AUTHORS
Dr. Yin is a professor (yinzuowei1025@163.com), Dr. Chen (chenquanli_0302@163.com, corresponding author) and Dr. Zhang are lecturers, and Ms. Zheng is a graduate student at the Gemological Institute, China University of Geosciences in Wuhan. Ms. Luo is an engineer at Sichuan Provincial Gem & Precious Metal Testing Centre in Chengdu. Ms. Li is an engineer at the Hebei Provincial Gem & Precious Metal Testing Centre in Shijiazhuang.

REFERENCES

Basilyan A.E., Anisimov M.A., Nikolskiy P.A., Pitulko V.V. (2011) Wooly mammoth mass accumulation next to the Paleolithic Yana RHS site, Arctic Siberia: Its geology, age, and relation to past human activity. *Journal of Archaeological Science*, Vol. 38, No. 9, pp. 2461–2474.

Dan H., Wang L., Ye Q.M., Deng M., Fan H., Sun J., Yang Y.D. (2006) Study on the environment of preserving the ancient ivory unearthed from Chengdu Jinsha Site, China. *Journal of Chengdu University of Technology (Sciences & Technology Edition)*, Vol. 33, No. 5, pp. 541–545.

Edwards H.G.M., Farwell D.W. (1995) Ivory and simulated ivory artefacts: Fourier transform Raman diagnostic study. *Spcctrochimica Acta Part A*, Vol. 51, No. 12, pp. 2073–2081, http://dx.doi.org/10.1016/0584-8539(95)01455-3.

Edwards H.G.M., Farwell D.W., Holder J.M., Lawson E.E. (1997) Fourier-transform Raman spectra of ivory III: Identification of mammalian specimens. *Spectrochimica Acta Part A*, Vol. 53, No. 13, pp. 2403–2409, http://dx.doi.org/10.1016/S1386-1425(97)00180-7.

Edwards H.G.M., Brody R.H., Hassan N.F.N., Farwell D.W., O'-Connor S. (2006) Identification of archaeological ivories using FT-Raman spectroscopy. *Analytica Chimica Acta*, Vol. 559, No. 1, pp. 64–72, http://dx.doi.org/10.1016/j.aca.2005.11.067.

Fan H., Wang L., Deng M. (2006) Phases and crystalline characteristics in ancient ivory unearthed from Shanxi and Jinsha. *Journal of the Chinese Ceramic Society*, Vol. 33, No. 6, pp. 744–748.

Farmo V.C. (1982) *Infrared Spectrum of Minerals*. Beijing: Science Press, pp. 309–311 (in Chinese).

Fisher D.C., Trapani J., Shoshani J., Woodford M.S. (1998) Schreger angles in mammoth and mastodon tusk dentin. *Current Research in the Pleistocene*, Vol. 15, pp. 105–106.

Ge Jun, Cui Fu-zhai, JI Ning, Yan Jian-xin (2006) New observations of hierarchical structure of human enamel. *Chinese Journal of Conservative Dentistry*, No.2, pp. 61–66.

Huang C.M., Zhang Q., Song P., (2007) FTIR and XRD analysis of hydroxyapatite from fossil human and animal ivories in Jinsha Relict, Chengdu. *Spectroscopy and Spectral Analyses*, Vol. 27, No. 12, pp. 2448–2252.

Iacumin P., Davanzo S., Nikolaev V. (2005) Short-term climatic changes recorded by mammoth hair in the Arctic environment. *Palaeogeography, Palaeoclimatology, Palaeoecology*, Vol. 218, No. 3-4, pp. 317–324.

Lasheras R.J., Bello-Gálvez C., Rodríguez-Celis E.M., Anzano J. (2011) Discrimination of organic solid materials by LIBS using methods of correlation and normalized coordinates. *Journal of Hazardous Materials*, Vol. 192, No. 2, pp. 704–713.

Müller K., Reiche I. (2011) Differentiation of archaeological ivory and bone materials by micro-PIXE/PIGE with emphasis on two Upper Palaeolithic key sites: Abri Pataud and Isturitz, France. *Journal of Archaeological Science*, Vol. 38, No. 12, pp. 3234–3243, http://dx.doi.org/10.1016/j.jas.2011.06.029.

Palombo M.R., Ferretti M.P., Pillola G.L., Chiappini L. (2012) A reappraisal of the dwarfed mammoth *Mammuthus lamarmorai* (Major, 1883) from Gonnesa (south-western Sardinia, Italy). *Quaternary International*, Vol. 255, pp. 158–170.

Pasquini C., Cortez J., Silva L.M.C., Gonzaga F.B. (2007) Laser induced breakdown spectroscopy. *Journal of the Brazilian Chemical Society*, Vol. 18, No. 3, pp. 463–512, http://dx.doi.org/10.1590/S0103-50532007000300002.

Qi L.J., Yuan X.Q., Cao S.M. (2005) Representation and application of infrared reflection spectra of gems. *Journal of Gems & Gemmology*, Vol. 7, No. 4, pp. 21–25.

Qi L.J., Zhou Z.Y., Liao G.L., Lin S.S. (2010) Differences on growth microstructure and FTIR absorption spectra between mammoth teeth and ivory. *Journal of Gems & Gemmology*, Vol. 12, No. 4, pp. 1–5.

Raubenheimer E.J., Bosman M.C., Vorster R., Noffke C.E. (1998) Histogenesis of the chequered pattern of the African elephant. *Archives of Oral Biology*, Vol. 43, pp. 969–977, http://dx.doi.org/10.1016/S0003-9969(98)00077-6.

Reiche I., Vignaud C., Champagnon B., Panczer G., Brouder C., Morin G., Solé V.A., Charlet L., Menu M. (2001) From mastodon ivory to gemstone: The origin of the turquoise color in odontolite. *American Mineralogist*, Vol. 86, pp. 1519–1524.

Sakae T., Oinuma H., Higa M., Kozawa Y. (2005) X-ray diffraction and FTIR study on heating effects of dentin from mammoth tusk. *Journal of Oral Biosciences*, Vol. 47, No. 1, pp. 83–88, http://dx.doi.org/10.1016/S1349-0079(05)80013-1.

Singh R.R., Goyal S.P., Khanna P.P., Mukherjee P.K., Sukumar R. (2006) Using morphometric and analytical techniques to characterize elephant ivory. *Forensic Science International*, Vol. 162, No. 1-3, pp.144–151

Su X.W., Cui F.Z. (1999) Hierarchical structure of ivory: From nanometer to centimeter. *Materials Science and Engineering C*, Vol. 7, No. 1, pp. 19–29, http://dx.doi.org/10.1016/S0928-4931(98)00067-8.

Trapani J., Fisher D.C. (2003) Discriminating proboscidean taxa using features of the Schreger pattern in tusk dentin. *Journal of Archaeological Science*, Vol. 30, pp. 429–438.

Wang P.F., Lu Q.W. (2004) Synthetic and structural characteristics of hydroxyapatite. *Function Material*, Vol. 35, pp. 2411–2413.

Wilson L., Pollard M. (2002) Here today, gone tomorrow? Integrated experimentation and geochemical modelling in studies of archaeological diagenetic changes. *Accounts of Chemical Research*, No. 35, pp. 644–651.

Zhou L.D., Liu Y.K., Zhou G.F. (1999) A study on modern biological apatite and fossil apatite. *Acta Mineralogica Sinica*, No. 1, pp. 41–47.

For online access to all issues of GEMS & GEMOLOGY, visit:

gia.edu/gems-gemology

INFRARED SPECTROSCOPIC STUDY OF FILLED MOONSTONE

Jianjun Li, Xiaofan Weng, Xiaoyan Yu, Xiaowei Liu, Zhenyu Chen, and Guihua Li

The laboratory of the National Gold & Diamond Testing Center (NGDTC) encountered some plagioclase (moonstone) beads with blue adularescence. Fifteen of the 22 moonstones fluoresced moderate to strong bluish white to long-wave UV, with the fluorescence visible in fissures. Electron microprobe analysis of one bead and micro-infrared reflectance spectra of all 22 samples indicated a composition nearly identical to albite. The specimens with strong fluorescence exhibited 3053 and 3038 cm^{-1} peaks in their direct transmission infrared spectra, confirming impregnation by a material with benzene structure. This treatment can be detected with a standard gemological microscope by observing characteristics such as relief lines.

In identifying gemstones from the Chinese market over the last five years, the National Gold & Diamond Testing Center (NGDTC) found that some treatments usually applied to top-grade colored stones such as emerald (Johnson et al., 1999) or jadeite jade (Fritsch et al., 1992) had also been used to enhance other materials. Impregnated aquamarine, tourmaline, and kyanite have all been encountered. Li et al. (2008) examined the characteristics and identifying features of filled aquamarine. Wang and Yang (2008) reported on a filling technology applied to carvings, beads, and faceted gems from the jewelry market of Guangdong Province. They also researched the identification of these filled gemstones.

A few months ago, the NGDTC laboratory received from a client six bracelets of plagioclase (moonstone) beads with blue adularescence. The

bracelets were reportedly from Donghai County in Jiangsu Province, the trading center for crystal quartz. They displayed moderate to strong bluish white fluorescence in an irregular curvilinear pattern, which caused suspicion. Observing the beads from different directions showed that the fluorescence was confined to the fractures, and the authors deduced the presence of some foreign material. In addition to determining the mineral composition of the samples, we collected infrared spectra to confirm the existence of the filling material and examine its composition.

MATERIALS AND METHODS

The samples came from a strand of 22 moonstone beads (table 1) that showed beautiful blue adularescence (figure 1). We examined the samples' standard gemological properties using an Abbe refractometer, an ultraviolet fluorescence lamp, and a microscope.

The chemical composition of sample 1 was first determined by electron microprobe analysis at the Chinese Academy of Geological Sciences (CAGS). The sample was removed from the strand, and a flat surface was polished oblique to the lamellae of polysynthetic twinning. After the electron microprobe analysis we could still see the strongest adularescence of this sample and collect its infrared spectra for further tests. CAGS used a JXA-8230 electron microprobe with an accelerating voltage of 15 kV, a beam current of 20 nA, and a beam diameter of 5 μm. Jadeite was used as the Na standard, and Na was run before the other elements to avoid undercounting sodium. The standard materials for this test were natural minerals and synthetic oxides, and the detection limit was about 100 ppm.

The 22 samples, including sample 1, were also tested at NGDTC with a Nicolet Nexus 470 Fourier transfer infrared spectrometer. To collect the microscopic reflective infrared spectra, we used an MCT/B detector. A total of 32 sample scans were taken at a resolution of 8.0 cm^{-1} and a background gain of 4.0. The Omnic 6.1a software recommends a scanning wavenumber range of 4000–650 cm^{-1}, and the infrared
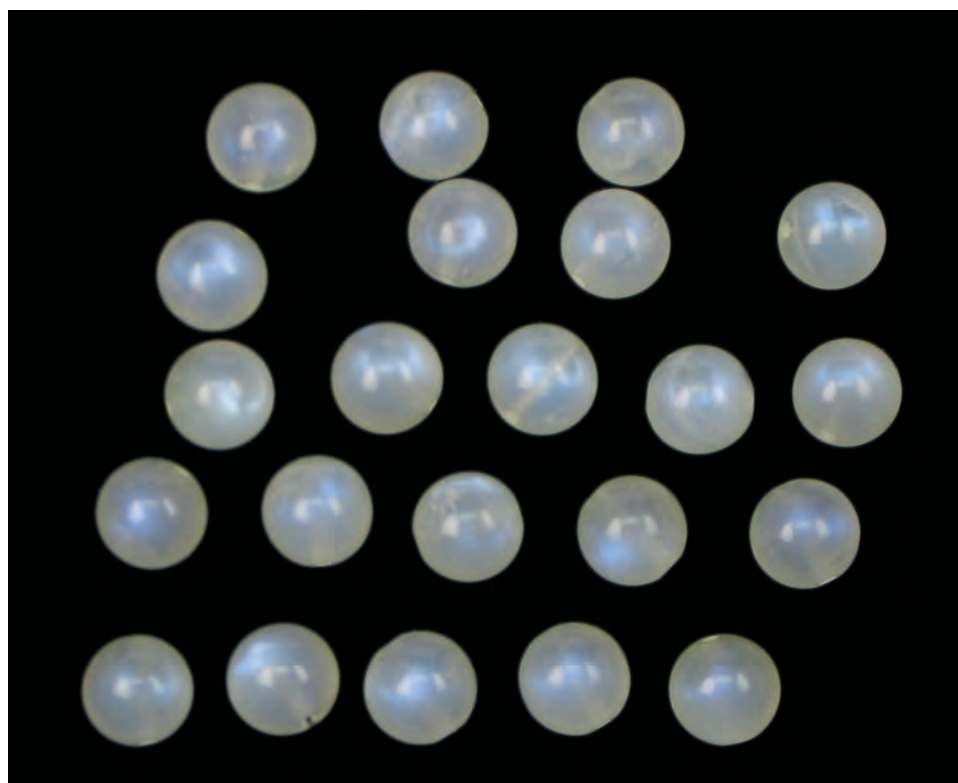
Figure 1. These 22 moonstone beads (4.01–4.31 ct) show blue adularescence. Testing showed that they were impregnated by a material with benzene structure. Photo by Jianjun Li.

spectrometer extended that range to 7800–400 cm⁻¹. Given the test requirements of the functional group (4000–2000 cm⁻¹) and the fingerprint region of silicate minerals in reflective infrared spectroscopy, the scanning wavenumber range was set at 1300–500 cm⁻¹.

Thompson and Wadsworth (1957) used infrared spectroscopy to determine albite and anorthite proportions in plagioclase. Li Jianjun et al. (2007) showed

In Brief

- A strand of 22 moonstone beads with blue adularescence displayed an irregular pattern of bluish white fluorescence, arousing suspicion of treatment.
- A combination of standard gemological testing and infrared spectral analysis showed that the moonstone had been impregnated by a material with benzene structure.
- While UV fluorescence can indicate the possibility of impregnation, infrared spectroscopy provides more conclusive evidence.

that the infrared spectra will vary when the samples are tested in different orientations. Thus the authors sought to obtain infrared spectra from a consistent crystal orientation to determine whether the samples

had the same composition. We used a simple orientation method: With the light source directed from the viewpoint, we looked for the area where the blue adularescence was the strongest and recorded the micro-infrared reflective spectra of each sample from the same orientation. Because the chemical composition of sample 1 was determined by both EPMA and microscopic reflective infrared spectroscopy, comparing the spectra of all other samples to that of sample 1 allowed us to determine whether they had the same composition.

Direct transmission was then applied to each whole bead to test the existence of the filling material using a DTGS KBr detector. A total of 32 sample scans were taken at a resolution of 8.0 cm⁻¹, a background gain of 1.0, and a scanning range of 7000–400 cm⁻¹. With air as the background, we collected the spectra of infrared rays through each whole bead.

RESULTS AND DISCUSSION

Gemological Properties. The samples' spot refractive index (RI) was approximately 1.53. The RI of the polished surface on sample 1 was 1.530–1.535. Because each sample contained a hole for stringing, specific gravity was not measured due to the possible complication caused by the holes. Most samples fluoresced weak to moderate blue-white to long-wave UV (table

Sample number	Weight (ct)	Diameter (mm)	Long-wave UV reaction
1	4.21	8.55	Moderate
2–6			Moderate
7			Weak
8			Strong
9			Moderate
10, 11			Very weak
12			Moderate
13	4.01–4.31	8.41–8.63	Inert
14			Moderate
15			Weak
16			Strong
17, 18, 19			Moderate
20, 21			Very weak
22			Strong
1 (polished section)	3.75	8.55 x 6.36	Moderate

Figure 3. Brightfield illumination revealed fine, closely woven needle-shaped and schistose inclusions in this 4.18 ct moonstone. Photomicrograph by Jianjun Li; magnified 70×.

1; figure 2 left). Only one sample was inert to long-wave, while three displayed strong fluorescence. Under short-wave UV their fluorescence was weaker or inert (figure 2, right). Because the fluorescence was visible along the fissures, we deduced that there might be some foreign material within them. Large fissures would contain more foreign substance, producing stronger fluorescence while the beads with no fissures were inert under UV fluorescence lamp.

Microscopic observation with brightfield illumination revealed a fine, closely woven needle-shaped schistose structure (or inclusions) in all samples (figure 3), while parallel twin layers were visible from certain directions (figure 4). There was a clear relationship between twinning planes and adularescence intensity: Adularescence was the strongest when the lighting and viewing directions were approximately perpendicular to the twinning planes. To keep a constant viewing direction, we collected micro-infrared reflectance spectra of all samples with the incident infrared rays perpendicular to the twinning planes.

Figure 2. Most of the moonstones fluoresced moderate to strong blue-white to long-wave UV, with the fluorescence visible in the fissures (left). Under short-wave UV (right), most of them either fluoresced weak bluish white (seen in the fissures) or were inert. Photo by Jianjun Li.
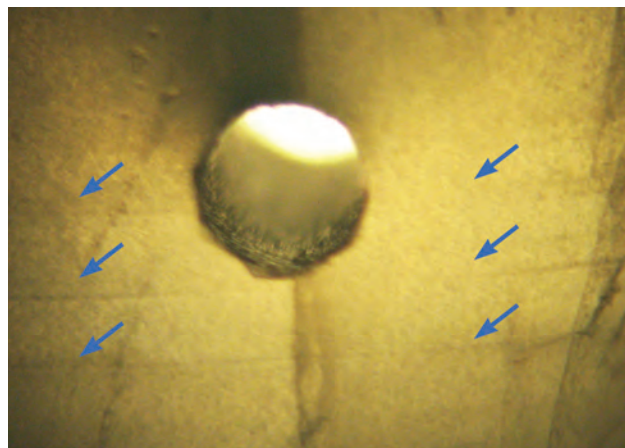
Figure 4. Fine internal parallel layers (polysynthetic twins) were observed with brightfield illumination. The circular feature near the center is a hole for stringing. Photomicrograph by Jianjun Li; magnified 30×.
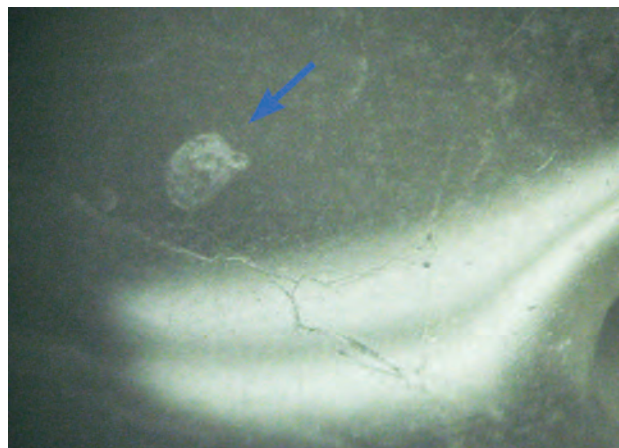
Figure 5. Veins were observed on the surface of the moonstones. Only one sample displayed residual flat, high-relief areas (holes or gas bubbles, indicated by the blue arrow). Photomicrograph by Jianjun Li; magnified 40×.

Observing these samples under the microscope with overhead illumination, we saw many veins on their surfaces, which appeared similar to the relief lines on filled aquamarine described by Li et al. (2009). Nevertheless, it was difficult to find the fractured reflective surfaces we would expect to accompany such veins; cracks were visible on the surface but barely penetrated the moonstone (figure 5). Meanwhile, an unusual residual flat high-relief area (again, see figure 5) was observed in sample 2, but not in any other moonstone. Similar high-relief areas are common microscopic features in filled aquamarine (Li et al., 2008) and thought to be products of incomplete filling. In other words, they were holes or gas bubbles.

Electron Microprobe Analysis. Complete electron microprobe data from six analytical points on sample 1 are listed in table 2. Based on the calculation method of Brandelik (2009), the three components of sample 1 are albite (Ab), orthoclase (Or), and anorthosite (An). The calculated composition of sample 1 was $Ab_{91.01}Or_{1.92}An_{7.07}$.

Infrared Spectroscopy Analysis. As figure 6 demonstrates, the 22 samples had very similar micro-infrared reflection spectra when they were collected at the strongest iridescence area (perpendicular to the polysynthetic twinning plane). This means the samples had identical mineral composition.

TABLE 2. Electron microprobe data of sample 1, calculated as $Ab_{91.01}Or_{1.92}An_{7.07}$.

No.	SiO_2	TiO_2	Al_2O_3	Cr_2O_3	FeO	MnO	CaO	MgO	NiO	K_2O	Na_2O	P_2O_5	SO_3	Total
LJJ-1-1	66.796	0.008	20.704	0.008	0.044	0.011	1.513	0.008	nd	0.358	10.559	nd	nd	100.009
LJJ-1-2	66.572	nd	20.771	0.002	0.056	nd	1.472	nd	0.003	0.357	10.376	0.022	nd	99.631
LJJ-1-3	66.524	0.025	20.844	0.015	0.066	0.002	1.501	nd	nd	0.344	10.497	0.003	nd	99.821
LJJ-1-4	66.609	0.005	20.68	0.023	0.075	nd	1.46	nd	nd	0.312	10.567	nd	nd	99.731
LJJ-1-5	66.772	0.014	20.752	0.011	0.059	nd	1.521	nd	0.009	0.351	10.84	nd	nd	100.329
LJJ-1-6	66.573	nd	20.747	0.015	0.036	0.02	1.474	0.021	nd	0.317	10.749	nd	nd	99.952

nd = Not detected

MICRO-INFRARED REFLECTANCE SPECTRA
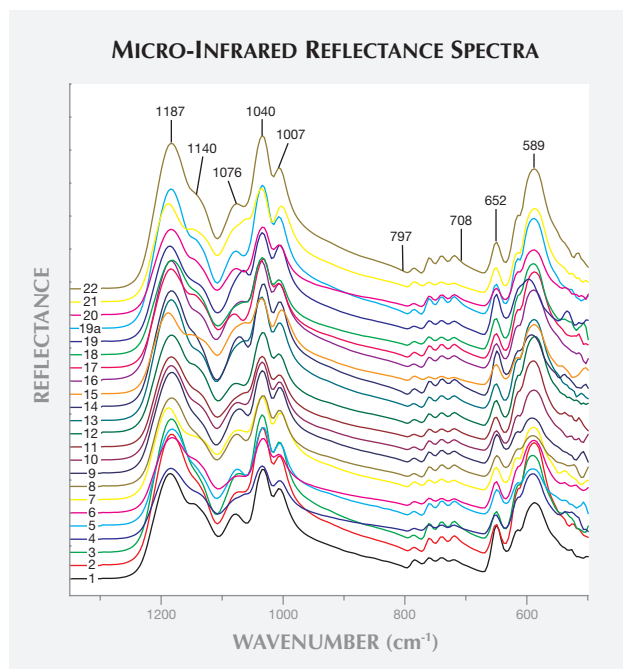
Figure 6. Micro-infrared reflectance spectra of the moonstone samples were collected at the area of strongest adularescence (with incident infrared rays perpendicular to the polysynthetic twinning plane). The similar patterns indicate a nearly identical composition.

1200–900 cm⁻¹: This region shows the Si-O stretching vibration bands in SiO_4 tetrahedral polymers (Zhang et al., 1986). The 22 samples generally shared the same peaks or shoulders: 1187, 1040, and 1007 cm⁻¹ peaks; a 1140 cm⁻¹ shoulder; and a shoulder developing to a peak in the 1076 cm⁻¹ region.

800–700 cm⁻¹: This region shows the Si-O bending vibration bands in SiO_4 tetrahedral polymers, as well as the Al-O stretching vibration bands in polyhedral polymers (Zhang et al., 1986). There were four peaks in all 22 samples.

Below 700 cm⁻¹: These are the stretching vibration bands of Al-O (and/or Si-O) and the bending vibration bands of O-Si-O (and/or O-Al-O), producing sharp peaks at 652 and 589 cm⁻¹ and the shoulders between them (Zhang et al., 1986).

As figure 7 shows, the direct transmission infrared spectra of the beads with moderate or strong fluorescence collected from three orthogonal directions presented absorption peaks at 3053 and 3038 cm⁻¹, which is due to the cumulative frequency involved in the stretching vibration of C-H in benzene

and the bending vibration of the benzene ring (Johnson et al., 1999a,b). The 4344 cm⁻¹ peak was due to the combined frequencies of the stretching and bending vibrations of C-H in CH_3 and CH_2 (Zhang et al., 1999), but the peak at about 4065 cm⁻¹ was associated with the combined frequencies of the stretching vibrations of C-H and C-C bands from organic material. Interestingly, an earlier study of filled jadeite jade found a 4060 cm⁻¹ absorption peak, confirming the filler material as epoxy or a similar substance (Zhang et al., 1999). Meanwhile, the infrared spectra of untreated moonstones from NGDTC's database

Figure 7. These direct transmission infrared spectra are from a filled moonstone with moderate fluorescence (sample 12) and untreated moonstones from NGDTC's database (a, b, and c). Top: The spectra of two white moonstones (a and b) and an orange moonstone (c) do not present peaks at 4344, 4065, 3053, and 3038 cm⁻¹. Bottom: The spectra of the filled moonstone, collected from three orthogonal directions, do show these four peaks. The 4344 cm⁻¹ peak is from the combined frequency related to the stretching and bending vibration of C-H in the structure of CH_2, and the 4065 cm⁻¹ peak is due to the combined frequencies of the C-H and C-C stretching vibrations. The 3053 and 3038 cm⁻¹ peaks are associated with the combined frequencies of the C-H stretching vibration and the bending vibration of the benzene ring.
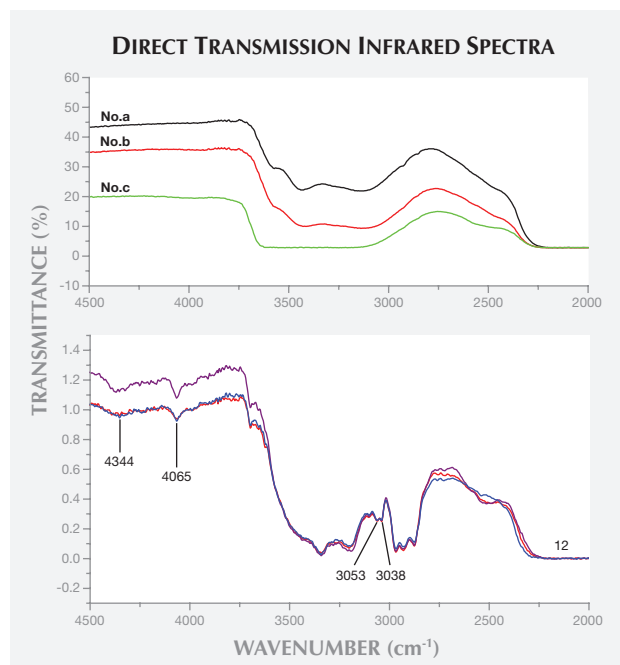
showed no peaks at 4344, 4065, 3053, or 3038 cm⁻¹ (again, see figure 7).

Most of the beads showed absorption peaks at 2969, 2927, and 2869 cm⁻¹, associated with the stretching vibration of CH_2. Three strong absorption peaks at 2962, 2926, and 2872 cm⁻¹ were frequently found by Johnson et al. (1999a) in a study of emerald filled by epoxy. The untreated moonstones did not present these three peaks (again, see figure 7).

From the above tests, we confirmed that all the beads were filled by a material with the structure of benzene.

There was a clear difference in the 2927–2869 cm⁻¹ range between the strongly and weakly fluorescent samples. The strongly fluorescent moonstone had a strong absorption band, and the weakly fluorescent samples showed weak absorption (figure 8). This suggests that samples with stronger fluorescence contain more filling.

CONCLUSION

From standard gemological testing, electron microprobe analysis, and infrared spectral analysis of the fluorescent moonstone samples, we reached several conclusions. The sample tested by electron microprobe had a composition of $Ab_{91.01}Or_{1.92}An_{7.07}$, or albite. Micro-infrared reflectance spectroscopy showed that all 22 samples had a nearly identical composition. Microscopic examination revealed curved veins without the fractured, reflective surfaces expected to accompany them. These surface features plus the patterned fluorescence indicated that the samples were filled. 3053 and 3038 cm⁻¹ peaks in their direct transmission infrared spectra confirmed that the beads were impregnated by a material with benzene structure. In terms of identification, UV fluorescence

could indicate the need for further testing, while the infrared spectra could provide more conclusive evidence of impregnation.

DIRECT TRANSMISSION INFRARED SPECTRA
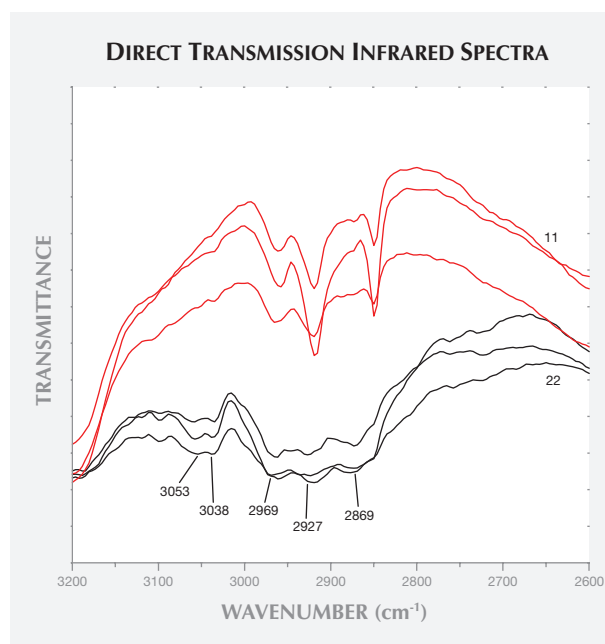
Figure 8. Direct transmission infrared spectra are shown for samples with very weak fluorescence (sample 11) and strong fluorescence (sample 22). Each sample was examined from three orthogonal directions. The difference between the strongly fluorescent and weakly fluorescent samples at 3053, 3038, 2969, 2927, and 2869 cm⁻¹ is associated with CH_2. Strong fluorescence is associated with a strong absorption band, and weak fluorescence with weak absorption.

ABOUT THE AUTHORS

Mr. Li (geoli@vip.sina.com) is the technical supervisor on gemology at the National Gold & Diamond Testing Center (NGDTC) and the senior engineer at the Shandong Provincial Key Laboratory of Metrology and Measurement, Shandong Institute of Metrology. Ms. Weng is a graduate student and Dr. Yu is a professor at the School of Gemology, China University of Geosciences. Liu Xiaowei is the director of NGDTC. Dr. Chen is a senior geochemical engineer at the Institute of Mineral Resources, Chinese Academy of Geological Sciences. Dr. Li is NGDTC's chemical engineer.

REFERENCES

Brandelik A. (2009) CALCMIN—An EXCELTM Visual Basic application for calculating mineral structural formulae from electron microprobe analyses. *Computers & Geosciences*, No. 35, pp. 1540–1551.

Fritsch E., Wu S.-T, Moses T., McClure S.F., Moon M. (1992) Identification of bleached and polymer-impregnated jadeite. *G&G*, Vol. 28, No. 3, pp. 176–187, http://dx.doi.org/10.5741/GEMS.28.3.176.

Johnson M.L., Elen S., Muhlmeister S. (1999a) On the identification of various emerald filling substances. *G&G*, Vol. 35, No. 2, pp. 82–107, http://dx.doi.org/10.5741/GEMS.35.2.82.

——— (1999b) Characterization of some emerald filling substances. *G&G*, Vol. 35, No. 3, pp. 149–151.

Li J.J., Luo Y.P., Chen Zh., Meng L.J. (2007) Usefulness and limitations of using routine FTIR spectra for identifying gemstones compared with the use of classical FTIR spectra using KBr pellets. *Australian Gemmologist*, Vol. 23, No. 2, pp. 64–70.

Li J.J., Liu X.W., Chen Y.F. et al. (2008) Characteristics and identity of filled aquamarine. *China Gems*, Vol. 17, No. 1, pp. 187–189 (in Chinese).

Li J.J., Sun Y., Hao W.J., Luo H., Cheng Y.F., Liu H.F., Liu Y., Ye H., Fan Ch. X. (2009) Polymer-filled aquamarine. *G&G*, Vol. 45, No. 3, pp. 197–199.

Li J.J., Liu X.W., Li G.H. (2011) Methods for identifying the polymer-filled peristerite. *Journal of Gems and Gemmology*, Vol. 13, No. 4, pp. 43–46 (Chinese article with English abstract).

Thompson C.S., Wadsworth M.E. (1957) Determination of the composition of plagioclase feldspars by means of infrared spectroscopy. *American Mineralogist*, Vol. 42, Nos. 5–6, pp. 334–341.

Wang P., Pan Zh.L., Weng L.B. (1984) *Systematic Mineralogy* (in Chinese). Publishing House of Geoscience, pp. 402–403.

Wang Y.M., Yang M.X. (2008) The filling treatment of semi-precious gemstones. *Journal of Gems and Gemmology*, Vol. 10, No. 4, pp. 23–27 (Chinese article with English abstract).

Zhang B.L., Gao Y. (1999) Identification of B jade by FTIR spectrometer with near-IR fibre-optic probe accessory. *Journal of Gems and Gemmology*, Vol. 1, No. 2, pp. 25–28 (Chinese article with English abstract).

Zhang B.M., Yuan Y.M., Shen Sh.Y. (1986) The variation of infrared spectra of plagioclases from basic-ultrabasic intrusions in Yanbian and Panzhihua, Sichuan Province. *Earth Science*, Vol. 11, No. 6, pp. 616–623 (Chinese article with English abstract).

For online access to all issues of GEMS & GEMOLOGY, visit:

gia.edu/gems-gemology

The
Dr. Edward J. Gübelin
Most Valuable Article
AWARD

First Place

CVD SYNTHETIC DIAMONDS FROM GEMESIS CORP.

Wuyi Wang, Ulrika D'Haenens-Johansson, Paul Johnson, Kyaw Soe Moe, Erica Emerson, Mark Newton, Thomas Moses

Wuyi Wang, director of research and development at GIA's New York laboratory, has spent 20 years studying diamond geochemistry and gem treatments. He holds a bachelor's degree in geology from Beijing University and a doctorate in geology from the University of Tsukuba. **Ulrika D'Haenens-Johansson** is a research scientist at GIA in New York, focusing on diamond defects and methods for identifying synthetic and treated diamonds. She holds master's and PhD degrees in physics from the University of Warwick, UK. **Paul Johnson** is supervisor of advanced diamond testing at GIA in New York, specializing in color origin. Mr. Johnson has a bachlor's degree from the University of Southampton, UK. **Kyaw Soe Moe** is a research associate at GIA in New York. He has a bachelor's degree in geology from Yangon University. **Erica Emerson**, a former GIA research assistant in New York, recently completed her master's degree at Syracuse University. **Mark Newton** is a reader in experimental physics at the University of Warwick, where he received a doctor of sciences degree. Dr. Newton specializes in spectroscopic and microscopic techniques, with an emphasis on diamond defects and impurities. **Thomas Moses** is senior vice president of GIA laboratory and research in New York.

Wuyi Wang

Second Place

GEMSTONES FROM VIETNAM: AN UPDATE

Le Thi-Thu Huong, Tobias Häger, Wolfgang Hofmeister, Christoph Hauzenberger, Dietmar Schwarz, Pham Van Long, Ursula Wehmeister, Nguyen Ngoc Khoi, Nguy Tuyet Nhung

Le Thi-Thu Huong is a lecturer in mineralogy at Vietnam National University in Hanoi, where her work involves characterization of Vietnamese pearls and gemstones. She holds a PhD in mineralogy from the University of Mainz, Germany. **Tobias Häger** is a lecturer in mineralogy at the University of Applied Sciences in Idar-Oberstein, as well as managing director of the Centre for Gemstone Research at Johannes Gutenberg University in Mainz and its branch, the Institute of Gemstone Research Idar-Oberstein. Dr. Häger holds a PhD in mineralogy. **Wolfgang Hofmeister** is head of gemstone and geomaterials research at the Institute of Gemstone Research Idar-Oberstein at Johannes Gutenberg University, where he is dean of faculty for chemistry, pharmaceutical science, and geoscience. Dr. Hofmeister is also director of the Konrad Weidemann Centre for Mineralogical Archaeoscience. **Christoph Hauzenberger** is associate professor of mineralogy and petrology at the Institute of Earth Sciences at the University of Graz, Austria. His research focuses on the genesis of gem deposits, and trace elements in rock-forming minerals. **Dietmar Schwarz** is head of research at the Gübelin Gem Lab in Lucerne, Switzerland. As a member of the International Gemmological Conference, he has written dozens of articles for scientific journals. **Pham Van Long** is a gemologist at the Center for Gem and Gold Research and Identification in Hanoi. He has a PhD in mineralogy from Vietnam National University. **Ursula Wehrmeister** is supervisor of pearl identification at the Centre of Gemstone Research at Johannes Gutenberg University, where she received a PhD in mineralogy. Dr. Wehrmeister is involved in characterizing Asian pearls. **Nguyen Ngoc Khoi** is an associate professor and **Nguy Tuyet Nhung** is a retired associate professor of geology at Vietnam National University. Their research interest is the characterization of Vietnamese gems.

Le Thi-Thu Huong

Third Place

EMERALDS FROM THE FAZENDA BONFIM REGION, RIO GRANDE DO NORTE, BRAZIL

J. C. (Hanco) Zwaan, Dorrit E. Jacob, Tobias Häger, Mário T. O. Cavalcanti Neto, Jan Kanis

Hanco Zwaan is curator at the National Museum of Natural History (Naturalis) and director of the Netherlands Gemmological Laboratory in Leiden. Dr. Zwaan has a PhD in geology from the Free University in Amsterdam. **Dorrit Jacob** holds the Future Fellowship and associate professor position at the Department of Earth and Planetary Sciences at Macquarie University in Sydney, Australia. She received a PhD at the University of Goettingen for her work on the geochemistry and radiogenic isotopes of mantle eclogites. **Tobias Häger** was profiled in the second-place entry. **Mário T. O. Cavalcanti Neto** is a geologist at the Federal Institute for Education, Science, and Technology of Rio Grande do Norte in Brazil. **Jan Kanis**, a consulting geologist specializing in gem exploration, has vast experience as a mine owner and partner in southern Africa. Dr. Kanis is one of the cofounders of the International Colored Gemstone Association.

J. C. (Hanco) Zwaan

We extend our thanks to all the readers who participated. And congratulations to **Ruediger Hein** of Henderson, Nevada, whose ballot was drawn from the entries to win a one-year subscription to *G&G*, plus a flash drive containing the 2002–2012 back issues.

Most Valuable Article

GEMOLOGICAL CHARACTERISTICS OF SALTWATER CULTURED PEARLS PRODUCED AFTER XENOTRANSPLANTATION

Stefanos Karampelas and Aurore Lombard

Experimental saltwater cultured pearls produced after xenotransplantation between *P. margaritifera* and *P. maxima* were studied using UV-Vis-NIR and PL spectroscopy as well as radiography. The results further demonstrate that the graft (*saibo*) largely determines the coloration and nacre thickness of the cultured pearl.

The value of beaded saltwater cultured pearls (SWCPs) depends on five main factors: shape, size (diameter and nacre thickness), color (bodycolor and overtone), luster, and surface condition (Taylor and Strack, 2008; Tayale et al., 2012). Statistics have shown that only 5% of all SWCPs are top quality, yet these account for about 95% of a pearl farm's income (Haws, 2002). To increase the percentage of top-quality SWCPs, several authors have experimented with variables such as environmental factors and the choice of donor and acceptor mollusks (see examples in Lucas, 2008; Southgate, 2008; and Mamangkey, 2009).

Most saltwater pearls are cultivated after transplantation of a piece of mantle tissue. This graft, also known by the Japanese term *saibo*, is cut from a bivalve mollusk donor. A bead, usually from the inner shell of a freshwater mollusk belonging to the Unionidae family, is simultaneously implanted into the gonad of a bivalve mollusk acceptor or host. When the donor and the acceptor bivalves belong to the same species, as is generally the case, the process is

known as *allotransplantation*. Allotransplanted mollusks of *Pinctada maxima* typically produce white to light gray, silver, cream, and yellow to golden SWCPs. Allotransplanted mollusks of *Pinctada margaritifera* commonly yield dark gray to black as well as light gray to white SWCPs. Various other natural-color SWCPs can be also found in both bivalves (see Karampelas et al., 2011 and 2012, and references therein).

McGinty et al. (2010 and 2011) presented the results of their genetic studies involving successful xenotransplantation between two different species (*P. margaritifera and P. maxima*) and the influence on the aforementioned SWCP quality factors. This study investigated experimental SWCPs, using methods different from those presented by McGinty et al., to further confirm the effect of the *saibo* from the donor mollusk.

MATERIALS AND METHODS

This study was carried out on 10 successfully cultivated experimental SWCPs (selected from McGinty et al., 2010) with various colors and sizes (see figure 1 and table 1). Seven samples (nos. 1–7) were cultivated in *P. maxima* after transplantation of a *P. margaritifera* tissue graft, while the other three (nos. 8–10) were cultivated in *P. margaritifera* after transplantation of a *P. maxima* graft. All samples were cultivated for 14 months on a farm belonging to Cendanda Indopearls on the Indonesian island of Bali; more on the exact conditions of cultivation can be found in McGinty et al. (2010). None of them had been subjected to any treatment. All but sample 9 were round or near-round, with good to very good surface condition and mostly good luster; see Gübelin Gem Lab (2012) for more information about the grading system used. SWCPs cultivated in *P. maxima* mollusks with *P. margaritifera* grafts had more gray-

Figure 1. Ten xenografted saltwater cultured pearls were chosen for this study. Seven samples (nos. 1–7) were cultivated in P. maxima *with transplanted* P. margaritifera *tissue graft, while the other three (nos. 8–10) were cultivated in* P. margaritifera *with transplanted* P. maxima *graft. Composite photo by S. Karampelas (samples not to scale).*

ish color than those cultivated in *P. margaritifera* mollusks with *P. maxima* grafts (again, see table 1).

The samples' UV fluorescence reaction was observed with a 6W long- and short-wave (365 and 254 nm, respectively) UV lamp. Their UV-Vis-NIR spectra were obtained for the 250–1600 nm range using a Cary 5000 spectrometer fitted with a Varian diffuse reflectance accessory. Only the 250–900 nm range, which contains the color-related absorption bands, is presented here. The data sampling interval and spectral bandwidth of each measurement were set at 0.7 nm and the scan rate at 60 nm/minute. Matte black sample holders were used for a more intense signal. Photoluminescence (PL) spectra were acquired using

a Renishaw Raman 1000 spectrometer coupled with a Leica DMLM optical microscope at 50× magnification, with an excitation wavelength of 514 nm emitted by an argon-ion laser (Ar⁺), a power of 10 mW, a 10-second acquisition time, and a resolution of about 0.1 nm. Digital radiography was performed at the Gübelin Gem Lab with a Comet X-ray unit and a Kodak 6120 digital sensor. Parameters were adjusted to the sample size, with voltage from 60 to 65 kV and current from 5 to 7 mA.

RESULTS AND DISCUSSION

Figures 2–4 show the diffuse reflectance UV-Vis-NIR spectra for six xenotransplanted samples. The spectra

TABLE 1. Characteristics of xenografted SWCP samples.

| Sample	Host mollusk	Donor mollusk (*saibo* species)	Size (mm)	Color	Average nacre thickness (mm)
GGL-ATL001	*P. maxima*	*P. margaritifera*	10.65–10.80	Very light gray	1.6
GGL-ATL002	*P. maxima*	*P. margaritifera*	8.10–8.30	Dark gray	0.8
GGL-ATL003	*P. maxima*	*P. margaritifera*	8.60–9.20	Dark gray	0.9
GGL-ATL004	*P. maxima*	*P. margaritifera*	8.80–9.00	Gray	0.7
GGL-ATL005	*P. maxima*	*P. margaritifera*	8.60–8.70	Dark gray	0.6
GGL-ATL006	*P. maxima*	*P. margaritifera*	8.40–8.50	Light gray yellow	0.5
GGL-ATL007	*P. maxima*	*P. margaritifera*	9.50–9.90	Very light gray	1.7
GGL-ATL008	*P. margaritifera*	*P. maxima*	10.10–10.20	Very light gray	1.9
GGL-ATL009	*P. margaritifera*	*P. maxima*	9.10 × 8.90	White	1.6
GGL-ATL010	*P. margaritifera*	*P. maxima*	16.50–16.60	Light yellow	4.4

UV-VIS-NIR REFLECTANCE SPECTRA
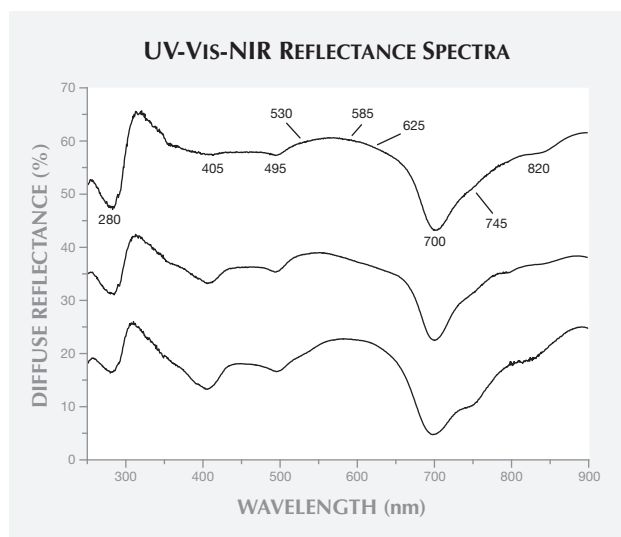
Figure 2. These diffuse-reflectance spectra of a black allografted P. margaritifera *SWCP (bottom) and two gray xenografted samples from a* P. maxima *host and* P. margaritifera *donor (GGL-ATL002 and GGL-ATL004) show absorptions at 280 nm, from 330 to 460 nm (with apparent maxima at 330–385 nm and 385–460 nm), and at 405, 495, and 700 nm. Also observed is a weak continuous absorption with a maximum at 820 nm, plus some less-intense features at 530, 585, 625, and 745 nm. For clarity, the spectrum of GGL-ATL004 is shifted up 5% and that of the black natural-color SWCP is shifted down 5%.*

present an absorption (a decrease in diffuse reflectance) at around 280 nm. Figure 2 shows two natural-color samples cultivated after xenotransplantation into *P. maxima* mollusks with *P. margaritifera* grafts, GGL-ATL002 (dark gray) and GGL-ATL004 (gray), as well as one black natural-color SWCP from *P. margaritifera* after allotransplantation (bottom spectrum). All three spectra contain six main absorption bands: from 330 to 460 nm, with maxima at 330–385 nm and 385–460 nm, and at 405, 495, 700, and 745 nm (plus a continuous band extending through the visible range with a maximum in the near infrared at around 820 nm). Also observed are three less-intense bands at around 530, 585, and 625 nm, which are common in allotransplanted *P. margaritifera* SWCPs (Elen 2002; Karampelas et al., 2011). Differences in the spectra patterns are due to the different relative intensities of these bands. The 700 nm band is currently known only from allotransplanted *P. margaritifera* SWCPs (Elen, 2002). Moreover, the 405 nm band has not been observed in natural-color allotransplanted *P. maxima* SWCPs (Karampelas, 2012). These results are in accordance with those found experimentally by McGinty

et al. (2010 and 2011), as well as other authors (e.g., Wada and Komaru, 1996). In other words, the *saibo*—in this case, *P. margaritifera* tissue—is mainly responsible for the coloration of the SWCPs. None of these bands is linked to a specific pigment, except for the one at approximately 405 nm, which is attributed to a kind of porphyrin (Iwahashi and Akamatsu, 1994).

Figure 3 shows the UV-Vis-NIR spectra of two light yellow samples, cultivated after xenotransplantation. Sample GGL-ATL006, cultivated in a *P. maxima* mollusk with a *P. margaritifera* graft, is a bit grayish. Sample GGL-ATL010 is cultivated in a *P. margaritifera* mollusk with a *P. maxima* graft. Both spectra contain the characteristic absorption feature from 330 to 460 nm observed in yellow to golden natural-color allotransplanted SWCPs from *P. margari-*

Figure 3. The light yellow xenografted sample GGL-ATL010 (second spectrum from the top; P. margaritifera *host and* P. maxima *donor) shows a weak absorption feature from 330 to 460 nm (with weak bands at 330–385 nm and 385–460 nm), as well as other bands at 495 nm and in the near-infrared region. Similar bands are observed to analogous natural-color (light brownish yellow) allografted sample from* P. maxima *(top spectrum), with different relative intensities of the same bands. The light gray yellow xenografted sample GGL-ATL006 (second spectrum from the bottom;* P. maxima *host and* P. margaritifera *donor) presents similar absorptions, as well as two additional bands at around 405 and 700 nm. Similar bands are observed in the natural-color allografted sample from* P. margaritifera *(bottom spectrum). The spectrum for GGL-ATL006 is shifted down 10% for clarity.*
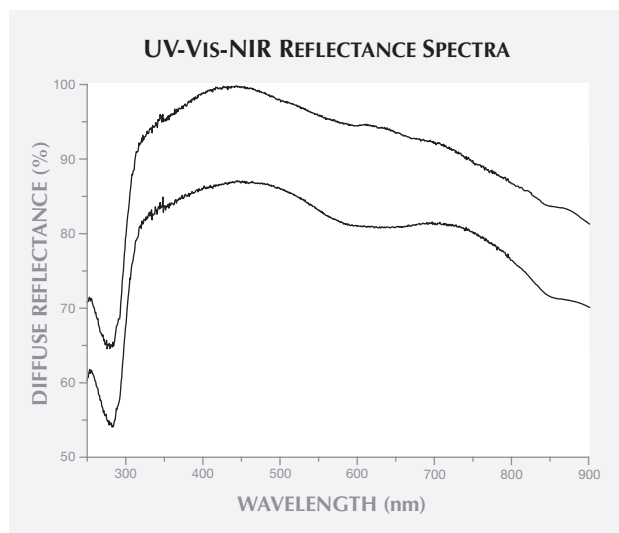

UV-VIS-NIR REFLECTANCE SPECTRA

UV-VIS-NIR REFLECTANCE SPECTRA
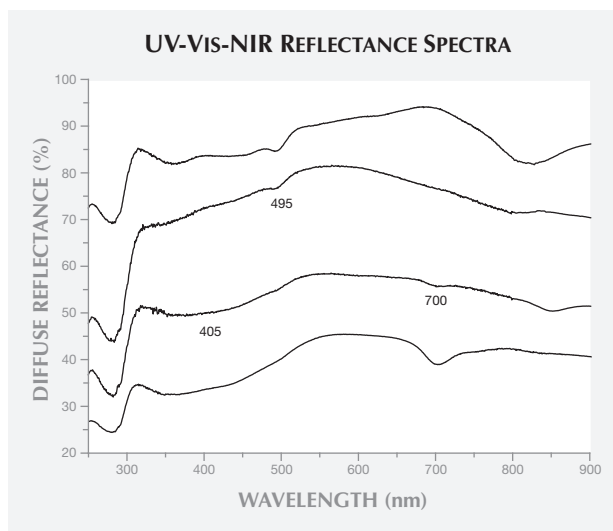
Figure 4. Two very light gray ("white-silver") SWCPs were cultivated after xenografting: GGL-ATL007 (P. maxima "host" and P. margaritifera donor) and GGL-008 (P. margaritifera "host" and P. maxima donor). These display only weak absorptions in the visible region that are not characteristic of either bivalve species. The samples' very light gray coloration is due to a weak continuous absorption through the visible region, with a maximum in the near-infrared region. The spectrum for GGL-ATL007 is shifted up 10% for clarity.

tifera and *P. maxima* (Elen, 2002). Both spectra also have a weak band at around 495 nm, similar to yellowish allotransplanted SWCPs of both mollusks (Karampelas, 2012). A weak band at around 700 nm and a shoulder at about 405 nm are also observed in the spectrum of sample GGL-ATL006. These absorption bands, present in allotransplanted SWCPs in *P. margaritifera* and absent from those cultivated in *P.*

In Brief

- Ten saltwater cultured pearls (SWCPs) cultivated after xenotransplantation between *P. maxima* and *P. margaritifera* mollusks were studied using UV-Vis-NIR and PL spectroscopy as well as X-ray microradiography.

- In xenotransplantation, the graft (*saibo*) from the donor mollusk largely determines the coloration and nacre thickness of the cultured pearl.

- Through spectroscopy studies, gemological laboratories can identify (with the exception of some light-colored SWCPs) the species of the donor (e.g., the 700 nm absorption band characteristic of graft from *P. margaritifera*) but not that of the host.

maxima (again, see figure 3), spectroscopically confirm the genetic results from McGinty et al. (2010 and 2011).

Figure 4 presents two samples of very light gray or "white-silver" color from the xenotransplantation of GGL-ATL007 and GGL-ATL008. The two spectra look similar; virtually the entire visible region is transmitted. A weak continuous absorption through the visible range with a maximum in the near-infrared region was responsible for the samples' light gray color. Very similar spectra can be observed in some white as well as other light-colored (white-silver and light yellow) allografted samples from *P. maxima* and *P. margaritifera*. The absorption band at around 700 nm is present in all of the colored samples (allografted or xenografted) cultivated using *saibo* from *P. margaritifera*, but was absent from the two light-colored samples (GGL-AUT001 and 007). The 700 nm absorption was absent, or sometimes present as a shoulder, in white to light-colored allotranplanted samples from *P. margaritifera* (Elen, 2002; Karampelas et al., 2012). Thus, the absence of the 700 nm band from a light-colored SWCP does not preclude the possibility that it was cultivated using *saibo* from *P. margaritifera*.

Figure 5. The photoluminescence spectrum of xenografted sample GGL-ATL005 (with saibo from P. margaritifera) shows bands at around 620, 650, and 680 nm. The sharp bands in the 520–550 nm region are due to the Raman effect. The light colored samples (GGL-ATL007 and GGL-ATL008) present less intense bands with a broad apparent maximum around 630 nm. All spectra intensities are adjusted to the main Raman band and shifted for clarity.

PHOTOLUMINESCENCE SPECTRA
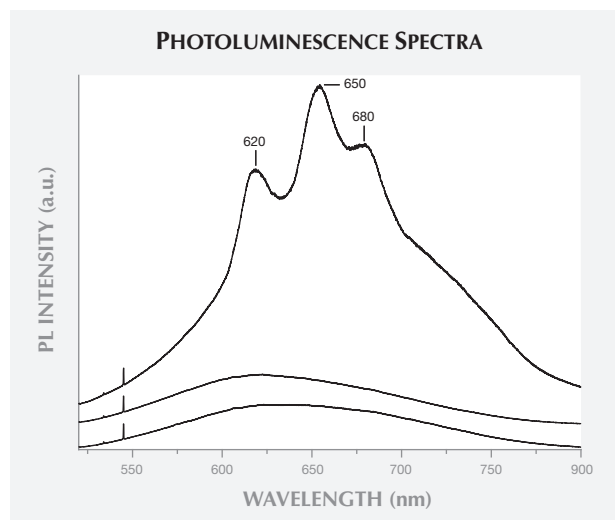
PL spectra of the dark-colored xenografted samples using *saibo* from *P. margaritifera* displayed bands in the orange to red region at about 620, 650, and 680 nm with green excitation (figure 5), similar to those in allografted *P. margaritifera* samples (Miyoshi et al., 1987). The light-colored xenografted samples—cultivated with both grafts—showed less-intense bands (again, see figure 5); similar results were found in allografted samples from both mollusks. Moreover, like allotransplanted SWCPs from the same mollusks, the light-colored samples were inert to short- and long-wave UV radiation (GGL-AUT001 and GGL-AUT006–010), while the others showed a weak greenish yellow and weak yellow reaction, respectively.

From the X-radiographs, the samples cultivated with a *P. maxima* donor and a *P. margaritifera* host generally contained thicker nacre (approximately 1.6–4.4 mm) than those cultivated using a *P. margaritifera* donor and a *P. maxima* host (0.5–1.8 mm; see also table 1). Allografted SWCPs from *P. maxima* had thicker nacre (as well as nacre weight) than allografted *P. margaritifera* SWCPs after cultivation for the same period of time in the same farm and under similar conditions; see examples in McGinty et al. (2010). This was probably due to the different growth rate (directly related to the nacre deposition rate) of *P. maxima* and *P. margaritifera* bivalves; *P. maxima* have a higher growth rate than their *P. margaritifera* counterparts (Yukihira et al., 2006; Saucedo and Southgate, 2008). Nevertheless, the growth rate of *P. maxima* and *P. margaritifera* can vary with environmental conditions such as salinity and water temperature (Gervis and Sims, 1992; Yukihira et al., 2006; Saucedo and Southgate, 2008). The radiography results here do confirm that the *saibo* plays an important role in nacre deposition (McGinty et al., 2010 and 2011).

CONCLUSION

Xenotransplantation between *P. margaritifera* and *P. maxima* can yield gem-quality SWCPs, as documented by McGinty et al. (2010 and 2011). This study using UV-Vis-NIR spectroscopy as well as radiography confirmed the histological and genetic findings by various researchers (e.g., Arnaud-Haond et al., 2007; McGinty et al., 2010) that the *saibo* from the donor mollusk is mainly responsible for the color as well as the nacre thickness. Using spectroscopic means, gemological laboratories can identify (with the exception of some light-colored SWCPs) the mollusk species of the donor (e.g., the 700 nm absorption band characteristic of *saibo* from *P. margaritifera*) but not the host. The host mollusk probably plays some role in the nacre deposition. For instance, xenotransplanted SWCPs with a *P. margaritifera* host and *saibo* from *P. maxima* have slightly thicker nacre than the allotransplanted SWCPs from *P. maxima* (McGinty et al., 2010). Additional research is needed to shed light on this.

Moreover, several studies have shown that selecting the best-secreting *saibo* for transplantation into a healthy host mollusk is the key to SWCP quality (e.g., Acosta-Salmón et al., 2004; Southgate, 2008). Further research is also needed on all five quality factors in xenografted SWCPs, including comparison with allografted SWCPs from the same mollusk species under identical conditions, after careful selection of donor and host mollusks. These investigations would clearly show if quality can be improved through xenografting. Another meaningful experiment, suggested by various authors, would be to see if xenografting between other Pinctada species (e.g., *P. fucata*) or even related species (e.g., *Pteria sp.*) can yield high-quality SWCPs.

ABOUT THE AUTHORS
Dr. Karampelas (s.karampelas@gubelingemlab.ch) is a research scientist at the Gübelin Gem Lab in Lucerne, Switzerland. Dr.

Lombard is a technical manager at Cendanda Indopearls (Atlas South Sea Pearls) in Denpasar, Bali, Indonesia.

REFERENCES

Acosta-Salmón H., Martínez-Fernández E., Southgate P.C. (2004) A new approach to pearl oyster broodstock selection: Can saibo donors be used as future broodstock? *Aquaculture*, Vol. 231, No. 1-4, pp. 205–214, http://dx.doi.org/10.1016/j.aquaculture.2003.08.022.

Arnaud-Haond S., Goyard E., Vonau V., Herbaut C., Prou J., Saulnier D. (2007) Pearl formation: persistence of the graft during the entire process of biomineralization. *Marine Biotechnology*, Vol. 9, No. 1, pp. 113–116 http://dx.doi.org/10.1007/s10126-006-6033-5.

Elen S. (2002) Identification of yellow cultured pearls from the black-lipped oyster *Pinctada margaritifera*. *G&G*, Vol. 38, No. 1, pp. 66–72, http://dx.doi.org/10.5741/GEMS.38.1.66.

Gervis M.N., Sims N.A. (1992) The biology and culture of pearl oysters (Bivalvia: Pteriidae). *International Center for Living Aquatic Resources Management Studies and Reviews*, Vol. 21, 49 pp.

Gübelin Gem Lab (2012) *The Pearl*, http://www.gubelingemlab.ch/PDF/GGL_Pearlbooklet_en.pdf [date accessed: Feb. 22, 2013]

Haws M. (2002) *The Basic Methods of Pearl Farming: A Layman's Manual*. Center for Tropical and Subtropical Aquaculture Publication No. 127, 79 pp., www.ctsa.org/files/publications/CTSA_1276316728619239483681.pdf [date accessed: Nov. 12, 2012].

Iwahashi Y., Akamatsu S. (1994) Porphyrin pigment in black-lip pearls and its application to pearl identification. *Fisheries Science*, Vol. 60, No. 1, pp. 69–71.

Karampelas S. (2012) Spectral characteristics of natural-color saltwater cultured pearls from *Pinctada maxima*. *G&G*, Vol. 48, No. 3, pp. 193–197, http://dx.doi.org/10.5741/GEMS.48.3.193.

Karampelas S., Fritsch E., Gauthier J-P., Hainschwang T. (2011) UV-Vis-NIR reflectance spectroscopy of natural-color saltwater pearls from *Pinctada margaritifera*. *G&G*, Vol. 47, No. 1, pp. 31–35, http://dx.doi.org/10.5741/GEMS.47.1.31.

Lucas J.S. (2008) Environmental influences. In P.C. Southgate and J.S. Lucas, Eds., *The Pearl Oyster*. Elsevier, Amsterdam, pp. 187–222.

Mamangkey N. (2009) Improving the quality of pearls from *Pinctada maxima*. PhD thesis, James Cook University (Australia), 167 pp.

McGinty E.L., Evans B.S., Taylor J.U.U., Jerry D.R. (2010) Xenografts and pearl production in two pearl oyster species, *P. maxima* and *P. margaritifera*: Effect on pearl quality and a key to understanding genetic contribution. *Aquaculture*, Vol. 302, No. 3-4, pp. 175–181, http://dx.doi.org/10.1016/j.aquaculture.2010.02.023.

McGinty E.L., Zenger K.R., Taylor J.U.U., Evans B.S., Jerry D.R. (2011) Diagnostic genetic markers unravel the interplay between host and donor oyster contribution in cultured pearl formation. *Aquaculture*, Vol. 316, No. 1-4, pp. 20–24, http://dx.doi.org/10.1016/j.aquaculture.2011.02.020.

Miyoshi T., Matsuda Y., Komatsu H. (1987) Fluorescence from pearls and shells of black-lip oyster, *Pinctada margaritifera*, and its contribution to the distinction of mother oysters used in pearl culture. *Japanese Journal of Applied Physics*, Vol. 26, No. 7, pp. 1069–1072, http://dx.doi.org/10.1143/jjap.26.1069.

Saucedo P.E., Southgate P.C. (2008) Reproduction, development and growth. In P.C. Southgate and J.S. Lucas, Eds., *The Pearl Oyster*. Elsevier, Amsterdam, pp. 137–186.

Southgate P.C. (2008) Pearl oyster culture. In P.C. Southgate and J.S. Lucas, Eds., *The Pearl Oyster*. Elsevier, Amsterdam, pp. 231–272.

Tayale A., Gueguen Y., Treguier C., Le Grand J., Cochennec-Laureau N., Montagnani C., Ky C-L. (2012) Evidence of donor effect on cultured pearl quality from a duplicated grafting experiment on *Pinctada margaritifera* using wild donors. *Aquatic Living Resources*, Vol. 25, No. 3, pp. 269–280, http://dx.doi.org/10.1051/alr/2012034.

Taylor J.J.U., Strack E. (2008) Pearl production. In P.C. Southgate and J.S. Lucas, Eds., *The Pearl Oyster*. Elsevier, Amsterdam, pp. 273–302.

Wada K., Komaru A. (1996) Color and weight of pearls produced by grafting the mantle tissue from a selected population for white shell color of the Japanese pearl oyster *Pinctada fucata* martensii (Dunker). *Aquaculture*, Vol. 142, No. 1–2, pp. 25–32, http://dx.doi.org/10.1016/0044-8486(95)01242-7

Yukihira H., Lucas J.S., Klumpp D.W. (2006) The pearl oysters, *Pinctada maxima* and *P. margaritifera*, respond in different ways to culture in dissimilar environments. *Aquaculture*, Vol. 252, No. 2-4, pp. 208–224, http://dx.doi.org/10.1016/j.aquaculture.2005.06.032.

CHALLENGE

The following 25 questions are from the Spring, Summer, Fall, and Winter 2012 issues of *Gems & Gemology*. Refer to the articles in those issues to find the **single best answer** for each question.

Mark your choice on the response card provided in this issue or visit gia.edu/gems-gemology to take the Challenge online. Entries must be received no later than **Thursday, August 1, 2013**. All entries will be acknowledged with an email, so please remember to include your name and email address (and write clearly).

Score 75% or better, and you will receive a certificate of completion (PDF file). Earn a perfect score, and your name also will be listed in the Fall 2013 issue of *Gems & Gemology*.
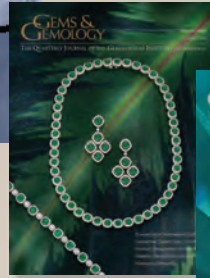
1. CVD synthetic diamonds commonly display _____ fluorescence.
   A. blue
   B. green
   C. weak yellow
   D. orange-red

2. Emeralds from the Fazenda Bonfim region of Brazil can be distinguished from other emeralds found in schist deposits by their _____.
   A. lack of amphibole inclusions
   B. lower potassium content
   C. slightly lower RI
   D. higher lithium content

3. Which of these techniques provides the most definitive answer as to whether a "golden" cultured pearl is dyed?
   A. UV-Vis reflectance spectroscopy
   B. UV fluorescence
   C. FTIR spectroscopy
   D. inspection of the surface for dye concentrations

4. Which gemstone is *not* mined in Vietnam?
   A. green facet-grade orthoclase
   B. star ruby
   C. untreated heliodor
   D. Melo pearls

5. What unique piece of jewelry was found in the tomb of a young Roman woman from the time of Marcus Aurelius?
   A. ruby earrings
   B. an emerald necklace
   C. a diamond solitaire ring
   D. a sapphire and spinel brooch

6. Sapphires recently discovered in southeastern Sri Lanka differ from typical Sri Lankan sapphires in what way?
   A. They lack rutile needles.
   B. They display strong dichroism.
   C. The as-found crystals have sharp edges.
   D. There is quartz in the rocks at the deposit.

7. The Beer-Lambert Law allows the calculation of what aspect of a chromophore?
   A. absorption cross section
   B. wavelength of absorption
   C. chromophore identity
   D. chromophore cation charge

8. Which of the following is *not* true about turquoise from Zhushan County in China's Hubei Province?

A. In the mines, it is often associated with clay minerals.
B. It generally contains white blebs and brownish black veinlets/patches.
C. The predominant color is medium bluish green.
D. It is always treated, as it has a less compact structure.

9. Which technique from the semiconductor industry has been used to treat the surface of diamond simulants?
   A. dry etching
   B. thin-film coating deposition
   C. lithography
   D. rapid thermal annealing

10. In the Australian natural pearl industry, what does "snide" refer to?
    A. pearl meat
    B. a secure box used for storing recovered pearls on the pearling vessels
    C. pearls smuggled from the pearling vessels
    D. the gonad of *Pinctada maxima*

11. Which of these companies produces both HPHT and CVD

synthetic diamonds for the gem trade?

A. Apollo Diamond, Inc.
B. Gemesis Corporation
C. Element Six
D. LifeGem

12. Which property is unique to nano-polycrystalline diamond (NPD) and not found in natural diamonds or synthetic diamonds grown using CVD or HPHT techniques?

A. luster
B. uniform hardness at the macro scale
C. specific gravity
D. color outside of the previously observed range for diamonds

13. Growing the cultured pearl industry in the Federated States of Micronesia will require _____.

A. a focus on high-volume, inexpensive pearl production
B. increasing the number of donor-funded projects
C. a strategy for marketing differentiation
D. switching to dark-colored brood stock

14. Natural diamonds may contain magnetic minerals, the most common of which is _____.

A. chromite
B. pyrrhotite
C. hematite
D. chrome pyrope garnet

15. Tsavorite garnets from _____ have the highest iron content.

A. Itrafo, Madagascar
B. Arusha, Tanzania
C. Tsavo region, Kenya
D. Gogogo, Madagascar

16. Which type of pearl does not clearly fit the definition of "cultured"?

A. pearl formed with an inserted bead in a technician-created sac in a wild mollusk
B. pearl formed with an inserted bead in a technician-created sac in a hatchery mollusk
C. pearl formed in a natural sac in a hatchery mollusk

D. pearl formed with an inserted natural shell in a technician-created sac in a hatchery mollusk

17. Which of the following is *not* true about the two-circle reflecting goniometer?

A. They are more precise than non-contact optical scanners.
B. They are better suited than non-contact optical scanners for creating reference stones for measuring inter-facet angles.
C. Fancy cuts are more difficult to measure using them.
D. They are commonly found in gemological laboratories.

18. The aquamarine found in the Ambatofotsikely area of central Madagascar can be described as _____.

A. almost exclusively suitable for faceting
B. containing reddish brown, black, and gray inclusions of striking prominence
C. almost pure blue in color
D. possessing unusually high specific gravity

19. Which radioactive impurity is sometimes found in natural, untreated gems?

A. iron
B. thorium
C. cesium
D. zinc

20. Spectroscopic splitting factors, also known as *g-factors*, are determined with electron spin resonance (ESR) spectroscopy to identify _____.

A. the type and amount of radiation used to treat a pearl or gemstone
B. whether a pearl is cultured and the origin of its color
C. the presence of specific paramagnetic molecules, defects, and free radicals
D. the electron spin of unpaired electrons in irradiated pearls or gemstones

21. High-pressure, high-temperature (HPHT) treatment is commonly used to increase the value of diamonds by reducing their _____.

A. brown coloration
B. pinpoint inclusions
C. yellow coloration
D. impurity doping

22. An absorption feature at 700 nm is observed using _____ for natural-color saltwater pearls originating from the _____ mollusk.

A. UV-Vis-NIR diffuse reflectance spectroscopy, *Pinctada margaritifera*
B. UV-Vis-NIR diffuse reflectance spectroscopy, *Pteria sterna*
C. Photoluminescence spectroscopy, *Pinctada maxima*
D. Photoluminescence spectroscopy, *Pinctada margaritifera*

23. Sustainable pearl farming does not _____.

A. enhance local fish stocks
B. greatly impact the local environment
C. generate income for local communities
D. lead to low stocking densities

24. Lavender jadeite's color is attributed to the presence of the chromophore manganese, based upon _____.

A. its ability to form a charge-transfer pair with iron
B. electron microprobe analysis and spectroscopic techniques, including UV-visible spectroscopy
C. its strong blue-green fluorescent reaction to short-wave UV radiation
D. chromophore effectiveness analysis paired with LA-ICP-MS and UV-visible spectroscopy

25. Which of the following is true about Diamantine diamond simulants?

A. They are produced in Asia.
B. They contain nitrogen.
C. Their treatment can be partially removed with adhesive tape.
D. They are a product of HPHT treatment.

G&G Lab Notes

Editors

Thomas M. Moses | Shane F. McClure

DIAMOND

Buff-Top Round

The modern round brilliant diamond is getting a "new old" look with the use of Japanese laser technology. Diamond's high refractive index and adamantine luster make it ideal for faceting to produce dramatic scintillation, brilliance, and fire. One of the oldest and simplest cuts is the cabochon, with its smooth convex dome. A popular cut among colored stones, the cabochon is rarely if ever used in diamonds due to the gem's extreme hardness and the difficulty in polishing it into a smooth, rounded surface. The New York lab recently examined several diamonds with an interesting variation on the cabochon.

About 30 buff-top round diamonds ranging from 0.25 to 1.50 ct, originally submitted to GIA's Japanese lab, were received for grading. The buff-top cut has a low cabochon dome with a faceted pavilion (figure 1). These diamonds were cut with four short main pavilion facets (figure 2). This rare cut posed a challenge for the grading staff, as the smooth dome and faceted pavilion combined to produce internal reflections that made it very difficult to see clearly into the stone. Although diamonds can be cut with lasers, the polishing process with the use of diamond abrasives into a smooth

Figure 1. A profile view of this buff-top round diamond shows its low polished dome.

rounded surface is both laborious and time consuming. The unfaceted dome was likely created using the same technology that produced the first synthetic nano-polycrystalline diamond sphere in Japan in 2011. One Japanese study (T. Okuchi et al., "Micromachining and surface processing of the super-hard nano-polycrystalline diamond by three types of pulsed lasers," *Applied Physics A: Materials Science & Processing*, Vol. 96, No. 4, 2009, pp. 833–842) found that pulsed lasers most efficiently produce a smooth, undamaged surface for fine finishing diamonds. A combination of three lasers was used: a near-infrared laser for the rough shaping, and ultraviolet and femtosecond lasers for fine finishing (E. Skalwold, "Nano-polycrystalline diamond sphere: A gemologist's perspective," Summer 2012 *G&G*, pp. 128–131).

This advancement in diamond finishing offers new possibilities for a variety of interesting shapes and forms that could not be achieved with previous methods of polishing and faceting alone. Diamond cabochons, completely smooth spherical beads, and sugarloaf cuts could emerge next.

Siau Fung Yeung

Large HPHT-Treated Fancy Pink

These days, high-pressure, high-temperature (HPHT) treatment is very commonly applied to change diamond color. Most of the HPHT-treated pink diamonds submitted to GIA range from 1 to 2 ct, and sizes over 10 ct are extremely rare. We previously reported on a 21.73 ct HPHT-annealed Light pink diamond (see Fall 2011 Lab Notes, p. 227). We have encountered another large HPHT-treated diamond that showed stronger pink coloration.

Figure 2. Viewed face-up, the buff-top diamond shows an arrangement of four main pavilion facets.

Figure 3. This 20.32 ct pear-shaped diamond was color graded as Fancy pink. Advanced testing suggested that its strong pink color was enhanced by HPHT treatment.

The 20.32 ct pear-shaped brilliant submitted to the New York laboratory (figure 3) was color graded as Fancy pink. We applied FTIR, UV-visible, and PL spectroscopy to examine the color origin for this diamond. The mid-infrared spectrum confirmed it was a type IIa diamond. The UV-visible spectrum showed a broad band at approximately 550 nm, a typical cause of pink coloration in diamond. But the PL spectra suggested that the pink color was improved by HPHT treatment. Most HPHT-treated pink diamonds have a secondary color component in addition to "pure" pink, either brownish or purplish. Interestingly, this sample had no secondary color component. Such HPHT-treated pure pink is extremely rare. Some HPHT-treated diamonds may contain graphitized inclusions and/or pitted surfaces on the girdle, but this one was microscopically "clean," both internally and on the surface. It also showed the typical tatami strain of a type II diamond when viewed in cross-polarized light, along with the high interference colors often associated with HPHT treatment (figure 4).

This sample demonstrated the improvement of HPHT treatment techniques in achieving more intense pink coloration in large diamonds. This was one of the largest HPHT-treated pink

diamonds tested in GIA's New York laboratory. It is very difficult to detect such treated pink color using traditional gemological instrumentation, especially with stones that are free of inclusions, and advanced gemological testing is critical for this purpose.

Kyaw Soe Moe

Orange, with Unusual Color Origin

Orange bodycolor in diamond is usually caused by an absorption band centered at approximately 480 nm or by a high concentration of isolated nitrogen. Meanwhile, it is well known that the 550 nm absorption band often introduces pink to red colors. Physical models of these two optical centers have not been resolved yet. The New York laboratory recently examined an orange diamond whose color was attributed mainly to the 550 nm absorption band.

This 1.53 ct heart-shaped diamond (6.84 × 7.76 × 3.88 mm) was color graded as Fancy Intense pinkish orange (figure 5). Color was distributed evenly throughout the stone, which was very clean and showed no internal features under the microscope. The absorption spectrum in the infrared region revealed that it was a regular type IIa diamond, with no nitrogen- or hydrogen-related absorptions. The UV-Vis region showed a

Figure 4. The typical tatami strain of type II diamond was observed by viewing the sample under crossed polarizers. It also showed high interference colors, which are often observed in HPHT-treated diamonds. Magnified 30×.
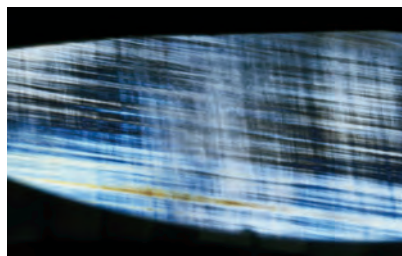

Figure 5. This 1.53 ct diamond was color graded as Fancy Intense pinkish orange. Spectroscopic analysis revealed it was type IIa and dominated by an approximately 550 nm band absorption, which usually introduces a pink-red color in natural diamonds rather than orange.

broad absorption band centered at ~550 nm and its corresponding band at ~390 nm, absorption features typical of natural type IIa pink diamonds. From the optical centers detected, we would not expect this diamond to show a dominant orange bodycolor.

The reason for this discrepancy is not fully understood. Our finding from this stone demonstrates the complexity of diamond color origin.

Wuyi Wang and Ren Lu

Pseudo-Synthetic Growth Structure Observed in Natural Diamond

Synthetic diamonds created using the traditional HPHT (high-pressure, high-temperature) process ordinarily grow as cuboctahedra. Temperature dictates the crystal form, as cubic growth is predominant at the relatively low temperatures of synthesis. At the higher temperatures of natural formation environments, diamonds typically grow as octahedrons. While small cuboctahedral diamonds are found in nature, these are very rare.

Recently submitted to the GIA laboratory in Israel was a near-colorless 0.70 ct round brilliant (figure 6).

Figure 6. This 0.70 ct, D-color natural round brilliant displayed the cuboctahedral growth structure of an HPHT-grown synthetic diamond.
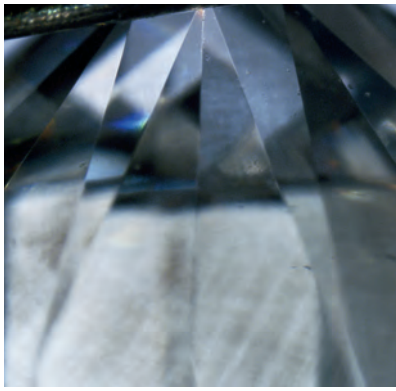

Figure 8. A tatami strain pattern, observed under crossed-polarized light, indicated natural growth. Magnified 40×.
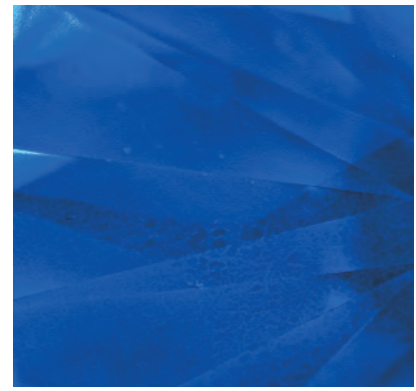

Figure 9. DiamondView imaging showed a micro-dislocation network on pavilion facets, conclusive proof of natural crystal growth.

Found to be a type IIa diamond with no detectable nitrogen impurity, it was examined further for possible treatments and to verify the origin of color.

In the short-wave UV radiation of the DiamondView, a subtle cuboctahedral growth structure (figure 7) was observed on the pavilion facets. This type of structure usually indicates an HPHT-grown synthetic diamond.

The diamond possessed D color and high clarity, with no internal inclusions to help indicate whether it was in fact natural. Shallow surface-reaching fractures were observed, and a few extra facets close to the pavilion contained these natural-looking fractures.

Figure 7. DiamondView imaging of the pavilion facets revealed a subtle growth structure. The inset shows the growth structure of a type IIb synthetic diamond.
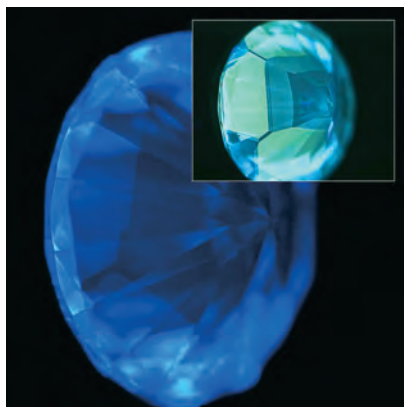
Microscopic observation with cross-polarized light showed relatively strong tatami strain pattern (figure 8), a feature indicative of natural growth. Further examination at higher magnification revealed small polygonal dislocation networks on the pavilion. These provided conclusive evidence that the stone was a natural diamond crystal (figure 9).

This stone was a good example of a very rare natural diamond exhibiting synthetic growth characteristics. It exemplifies the challenges posed to gemological laboratories in separating natural from undisclosed gem-quality synthetic diamonds in today's jewelry market. We concluded that the diamond had a natural color origin.

Paul Johnson

Green, Treated with Radioactive Salt

Recently submitted to the East Coast Laboratory was a 3.17 ct round brilliant cut diamond, color graded as Fancy Deep green (figure 10). Natural diamonds of this color are very rare and desirable.

Examination with a gemological microscope revealed a very unusual surface coloration. The surface had a mottled pattern created by very shallow green staining, likely from exposure to radiation (figure 11). This unusual feature is rarely observed on natural diamond surfaces or facets.

Natural radiation staining on the surface of a diamond crystal would be mostly removed during faceting.

The stone owes all of its green color to these shallow radiation stains. Today, most artificially irradiated diamonds are treated with a low-energy electron beam. This often results in shallow color zoning that penetrates into the stone and aligns with the facet shape. In this case, the shallow staining was created using the older method of exposing the diamond to radioactive salts for an extended period of time. Mainly used on polished stones, this method leaves surface contamination. Stones irradiated in this fashion can have residual radiation, so we

Figure 10. This 3.17 ct round brilliant cut diamond owed its Fancy Deep green color to irradiation with radioactive salts.
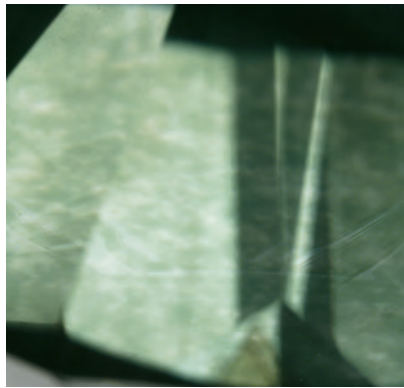
Figure 11. Observed at 35× magnification, the diamond shows a mottled effect created by shallow green radiation stains.
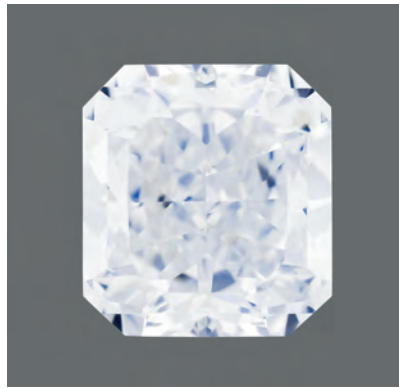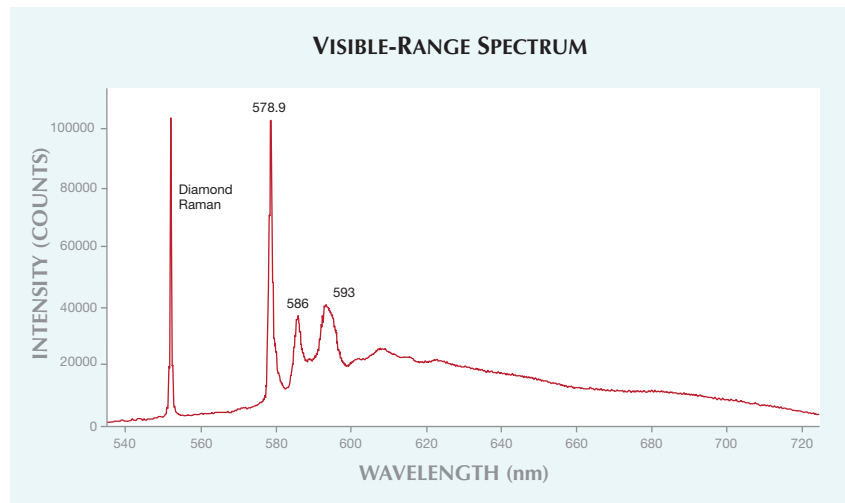

Figure 12. This 4.72 ct Light blue type IIb diamond displayed some of the strongest dislocations ever observed in natural diamonds by GIA. This resulted in a hazy impression and a lower transparency than other type IIb diamonds.

tested this stone using a Geiger counter. Only background radiation was detected, indicating that the treatment likely occurred decades earlier. Thus, this diamond posed no radiation hazards. Sir William Crookes first discovered radiation's effects on diamond color by conducting a series of experiments using radium salts in 1904. Although rarely encountered today, these types of treated diamonds still show up in the trade. A careful inspection of the surface in diffused lighting is the most effective means of revealing the diagnostic surface coloration.

Marzena Nazz and Paul Johnson

With Extremely Strong 578.9 nm Emission Center

Photoluminescence analysis at liquid-nitrogen temperatures and varying laser excitations has become increasingly important in diamond color origin testing. The 578.9 nm emission normally occurs with many other emission lines, and it is usually weak in natural type IIa and IIb diamonds. Meanwhile, the physical model of this optical center is unclear. The New York laboratory tested a very rare diamond that showed extremely strong 578.9 nm emission.

This 4.72 ct rectangular diamond (9.75 × 8.90 × 5.92 mm) had a color grade of Light blue and an even color distribution (figure 12). Infrared absorp-

tion spectroscopy analysis identified it as a type IIb diamond with a boron concentration of about 16 ppb. This stone showed very strong dislocations, resulting in a hazy impression and a lower degree of transparency than most type IIb diamonds. Microscopic observation revealed very strong linear graining and related high interference colors. The intensity of the dislocations was among the strongest ever ob-

served in natural diamonds at a GIA laboratory.

The outstanding feature of this diamond was the extremely strong emission at 578.9 nm, with possible side bands at 586 and 593 nm (figure 13). No other emission line was detected in the visible light region, which is very unusual for a natural type IIa or IIb diamond. This feature was confirmed with 457 and 488 nm laser excitations. The exclusive occurrence of the 578.9 nm emission and the very strong lattice dislocations suggested that this emission was a dislocation-related optical center.

Wuyi Wang

SYNTHETIC DIAMOND

CVD-Grown, with Aggregated Nitrogen Impurities

Synthetic diamonds grown by the chemical vapor deposition (CVD) method have become a key topic in the jewelry industry over the past few years. These products, which can be grown at low pressures and moderately high temperatures (approximately 800–900°C), are seeing more widespread use in jewelry. CVD synthetics

Figure 13. The diamond showed extremely strong emission at 578.9 nm and its possible side bands at 586 and 593 nm. The exclusive occurrence of the 578.9 nm emission and the very strong lattice dislocations in this diamond suggested that the emission was a dislocation-related optical center.
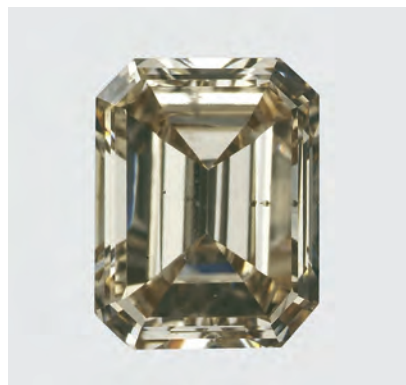
Figure 14. Unusual 0.94 ct yellow-brown CVD synthetic diamond.

Figure 15. A cloud of needle-like inclusions was observed in the synthetic diamond (left, magnified 50×). The side view clearly showed that the cloud was confined to a plane (center; magnified 45×). With cross-polarized light, the mottled and crosshatched strain pattern was visible (right; magnified 15×).

are almost always brown or colorless type IIa specimens with little to no FTIR-measurable nitrogen or boron impurities. A few of these synthetics have been doped with nitrogen or boron to produce rare type Ib or IIb colored samples.

Recently, an unusual 0.94 ct Fancy yellow-brown emerald cut (figure 14) was submitted to GIA for a synthetic diamond grading report. It contained a cloud of black needle-like inclusions occurring along a plane (figure 15, left
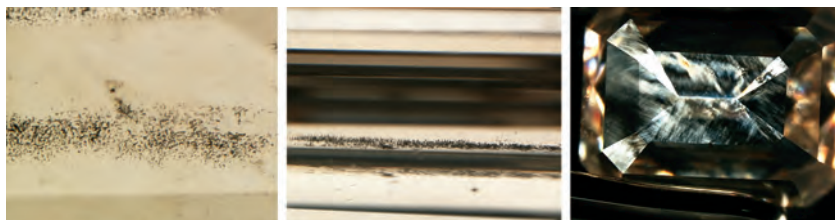
and center) and showed weak green transmission with fiber-optic illumination. Under cross-polarized light, the synthetic diamond displayed a black and white mottled strain pattern, somewhat similar in appearance to the crosshatched "tatami" pattern usually seen in natural type IIa diamonds (figure 15, right). FTIR spectroscopy revealed that it was type IaA, with approximately 10 ppm of aggregated nitrogen atom pairs in the lattice (figure 16). DiamondView imaging showed red fluorescence and planar growth patterns that are common in CVD synthetic diamonds (figure 17).

Photoluminescence spectroscopy detected silicon-vacancy defects introduced during the CVD growth process (not shown), and further examination of the FTIR spectrum revealed a very weak peak at 3123 cm^{-1} (again, see figure 16), confirming this was an as-grown CVD synthetic diamond (P.M. Martineau et al., "Identification of synthetic diamond grown using chemical vapor deposition [CVD]," Spring 2004 G&G, pp. 2–25).

This marked GIA's first examination of a CVD synthetic diamond with aggregated nitrogen impurities. During HPHT treatment, nitrogen atoms typically start to aggregate as pairs at temperatures above 2000°C. Although some CVD synthetics are HPHT-treated to remove brown coloration, spectroscopic evidence indicates that this sample had not undergone such treatment. It is un-

Figure 16. FTIR spectroscopy revealed that the CVD synthetic diamond was type IaA with aggregated nitrogen atom pairs, the first CVD synthetic diamond GIA has seen with this configuration of nitrogen impurities. The 3123 cm^{-1} peak confirms this is an as-grown CVD diamond.
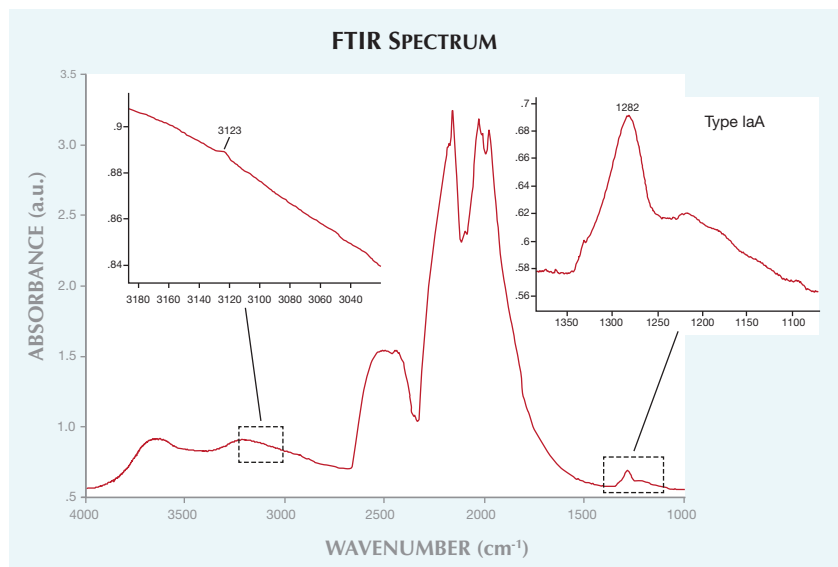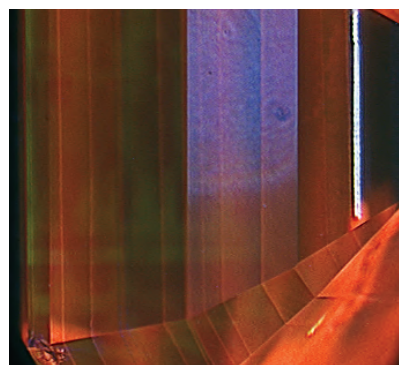

Figure 17. DiamondView imaging showed banded red fluorescence with a striated pattern, typical of CVD synthetic diamonds.

clear how the nitrogen impurities came to be in their aggregated state. It is possible that a type IaA natural diamond was used as a seed crystal for multi-stage CVD growth and remains within the current gemstone, thereby producing the FTIR results. However, no clear evidence of this scenario was uncovered. More research is currently under way to understand this unusual CVD synthetic diamond with aggregated nitrogen impurities.

*Troy Ardon, Tara Allen, and
Christopher M. Breeding*

Three CVD Synthetic Diamonds Submitted to Mumbai Laboratory

CVD-grown synthetic diamonds continue to become more abundant in the gem market, as evidenced by several reports from major diamond-grading laboratories during the past year (e.g., C. Even-Zohar, "Synthetics specifically 'made to defraud,'" *Diamond Intelligence Briefs*, Vol. 27, No. 709, 2012, pp. 7281–7283). In December 2012, three CVD synthetic diamonds were submitted to GIA's Mumbai laboratory. In keeping with the evolving technology of the CVD process, the gemological and spectroscopic characteristics of these type IIa synthetic diamonds suggested that they experienced different growth and/or treatment histories.

One sample was a 0.93 ct very light brown (O to P range) rectangular step cut with a VVS_2 clarity grade due to the presence of pinpoint inclusions and graining. Viewed under crossed-polarizers it showed heavy strain, with high-order birefringence colors. The photoluminescence (PL) spectra acquired at liquid-nitrogen temperatures using various laser excitations were dominated by the emission of $[N-V]^0$ and $[N-V]^-$ centers (with zero-phonon lines at 575 and 637 nm, respectively). These ZPLs are widened by high levels of strain and have been previously studied in CVD synthetic diamonds (W. Wang et al., "CVD synthetic diamonds from Gemesis Corp.," Summer 2012 *G&G*, pp. 80–97). The $[N-V]^{0/-}$ peaks for this sample

had full-widths at half-maximum (FWHM) of 0.43 nm and 0.35 nm, respectively. These are relatively broad compared to colorless diamonds, but consistent with the high strain observed under crossed polarizers. The 596.5/597.2 nm doublet commonly observed in "as-grown" CVD synthetic diamonds was weak, as was the 736.5/736.9 nm doublet attributed to $[Si-V]^-$. Notably, the $[Si-V]^-$ emission was too weak to detect with the 514.5 nm laser excitation. Infrared laser excitation at 830 nm resulted in many emission peaks in the 850–880 nm region, dominated by a sharp peak at 878.5 nm whose origin has not been conclusively identified. The Dia-

mondView fluorescence was primarily red due to the strong [N-V] centers. Although CVD-characteristic violet-blue dislocation patterns were observed, growth striations could not be discerned (figure 18A). The sample did not phosphoresce. The PL features observed, the $[N-V]^{0/-}$ widths, and the DiamondView behavior were similar to those reported for near-colorless CVD synthetics produced by Apollo, Inc. (e.g., W. Wang et al., "Latest-generation CVD-grown synthetic diamonds from Apollo Diamond Inc.," Winter 2007 *G&G*, pp. 294–312).

The other two samples were round brilliants weighing 0.52 and 0.57 ct. Both received G color and VS_1 clarity

Figure 18. DiamondView fluorescence images show distinct colors and patterns that helped identify these as CVD synthetic diamonds. Red fluorescence with purple mottling appears in the putative "as-grown" O-P color rectangular step cut (A). The greenish blue striations in the 0.52 ct sample are more typical patterns (B). The 0.57 ct CVD synthetic demonstrates a unique combination of fluorescence features—dominant [N-V] center–related fluorescence, with minor areas showing some violet-blue dislocations and greenish blue striations (C–D).
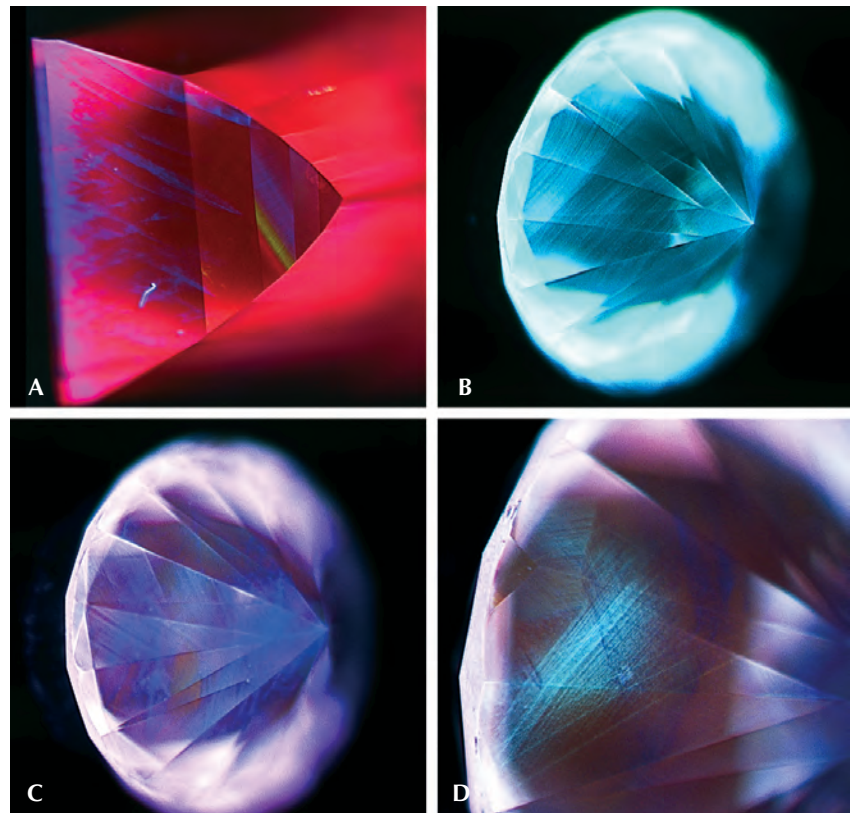
grades. The clarity grades were affected by pinpoint inclusions and small fractures. Both round brilliants were weakly strained, revealing low-order (gray and brown) interference colors. They shared several PL spectroscopic traits, including emissions from $[N-V]^{0/-}$, $[Si-V]^-$, H3 (503.2 nm), and weak N3 (415.2 nm) centers. The 596.5/597.2 nm doublet was not observed in either specimen. The absence of this feature, combined with the presence of multi-nitrogen defects such as H3 and N3, suggests that they had undergone post-growth high-temperature annealing to remove the as-grown brown coloration (again, see W. Wang et al., 2012). The FWHMs for the $[N-V]^0$ and $[N-V]^-$ centers were 0.21 nm and 0.16 nm, respectively, for the 0.52 ct round, and 0.23 nm and 0.22 nm for the 0.57 ct sample. These were comparable to the narrowest widths reported for natural diamonds and newer-generation HPHT-treated CVD synthetics produced by Gemesis Corp., and consistent with the low levels of strain detected.

The round brilliants exhibited distinct behavior when examined using the DiamondView instrument (see figure 18, B–D). The 0.52 ct sample showed greenish blue fluorescence and clear growth striations, as well as strong green-blue phosphorescence. These observations were akin to those for HPHT-treated CVD synthetic diamonds produced by Gemesis (again, see W. Wang et al., 2012). Although green-blue phosphorescence was also observed for the 0.57 ct sample, its DiamondView fluorescence images were primarily purplish pink, with violet-blue dislocation bundles and a patch of greenish blue fluorescence. This fluorescence combination in a CVD synthetic diamond had never been observed at a GIA laboratory. The purplish pink fluorescence color was attributed to $[N-V]$ centers. Comparison of the Raman-normalized PL intensities of the peaks revealed that the $[N-V]^0$ and $[N-V]^-$ peaks were approximately 57% and 68% more intense in the 0.57 ct round than in the 0.52 ct sample. This may explain the difference in the Di-

amondView fluorescence responses of these synthetic diamonds. It is possible that the 0.57 ct round was HPHT-annealed at a lower temperature.

The gemological and spectroscopic observations for these three samples emphasize the variations that might be possible through different growth procedures and subsequent treatment for near-colorless to lightl brown CVD synthetic diamonds. Nevertheless, the specimens could be readily identified as synthetic by careful analysis of data from a combination of laboratory techniques.

Ulrika D'Haenens-Johansson, Sally Eaton-Magaña, Manisha Bhoir, and Yogesh Shinde

Very Large CVD-Grown

In the last decade, we have witnessed rapid improvement in the quality and size of lab-grown CVD synthetic diamonds. The New York laboratory recently tested a 2.16 ct CVD synthetic from Scio Diamond Technology Corp. (figure 19), the largest specimen GIA has seen so far.

This marquise, which measured 13.42 × 6.73 × 3.94 mm, was more than twice the size of a 1.05 ct pear shape examined in 2010, previously the largest CVD synthetic tested by GIA (see Summer 2010 *G&G* Lab Notes, pp. 143–144). It had J/K color with a brownish tint, and microscopic observation revealed small fractures, pinpoints, and non-diamond-carbon black inclusions, resulting in an SI_2 clarity grade.

The mid-infrared absorption spectrum revealed that the diamond could be classified as type IIa. It was very pure in the infrared region, with no nitrogen- or hydrogen-related absorption features. Photoluminescence analysis at liquid-nitrogen temperature with varying laser excitations displayed typical CVD features: very strong emissions from N-V centers, moderate emission lines at 736.6/736.9 nm from the $[Si-V]^-$ center, and the CVD-specific 596/597 nm pair (figure 20). Also detected was weak emission from the H3 defect with a

Figure 19. This 2.16 ct marquise (13.42 × 6.73 × 3.94 mm) is the largest CVD synthetic diamond tested by GIA. It had J/K color, with a brownish tint.

zero-phonon line at 503.1 nm, making for an interesting combination of optical centers. Under the short-wave UV radiation of the DiamondView, the table and crown facets showed pure blue fluorescence while the pavilion displayed banded orange fluorescence with irregular blue fluorescence regions. Very strong internal stress with irregular patterns was confirmed under the microscope using cross-polarized light.

Testing of this large, gem-quality CVD synthetic underscored the rapid improvement of lab-grown diamond technology. It is foreseeable that more of these products will continue to reach the jewelry industry.

Wuyi Wang, Kyaw Soe Moe, Siau Fung Yeung, and Ulrika D'Haenens-Johansson

Yellow SYNTHETIC SAPPHIRE Colored by Trapped-Hole Mechanism

Natural sapphires with pale or lemon yellow color and no orange hue are traditionally associated with the chromophore Fe^{3+}, which substitutes for aluminum in corundum. The New York laboratory recently received a 2.58 ct yellow emerald-cut stone (figure 21, inset), identified as sapphire by its RI and SG. But the desk-model spectroscope showed broadband absorption below ~500 nm without any of the Fe^{3+}-related absorption features associated with yellow coloration
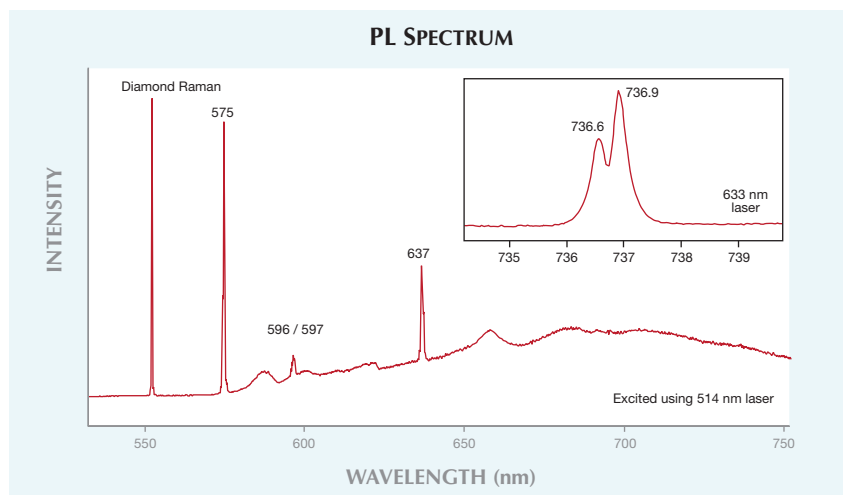
PL Spectrum

Figure 20. The 2.16 ct synthetic diamond showed typical photoluminescence features of CVD growth, including strong emissions from N-V centers at 575 and 637 nm, moderate CVD-specific emissions at 596/597 nm, and 736.6 and 736.9 nm emissions from the [Si-V]⁻ center.

(e.g., at 450 nm). Microscopic observation showed an exceptionally clean interior with only a small cluster of tiny particles that resembled gas bubbles from synthetic materials. The stone fluoresced medium orange to long-wave UV radiation and inert to short-wave UV.

The suspicious inclusion scene and the absence of diagnostic spectral features warranted additional testing. A standard immersion image failed to show any zoning or features. By contrast, a DiamondView image clearly revealed parallel curved bands characteristic of synthetic origin. Quantitative UV-visible spectra exhibited strong broadband absorptions in the blue and green regions and created a transmission window in the yellow

Figure 21. The UV-visible spectrum of this yellow sapphire shows broadband absorption features below ~500 nm, originating from trapped holes associated with Mg and Cr. The DiamondView image clearly displays curved bands (sub-parallel to the long direction of the stone under the table), indicating a synthetic origin. These curved bands are not seen with standard immersion, demonstrating the DiamondView's effectiveness (the red color is due to the fluorescence of chromium). The stone's CIE L*a*b* color coordinates are reproduced from the measured UV-visible spectrum.

UV-Vis Spectrum

$L^*a^*b^* = 93, -8, 34$
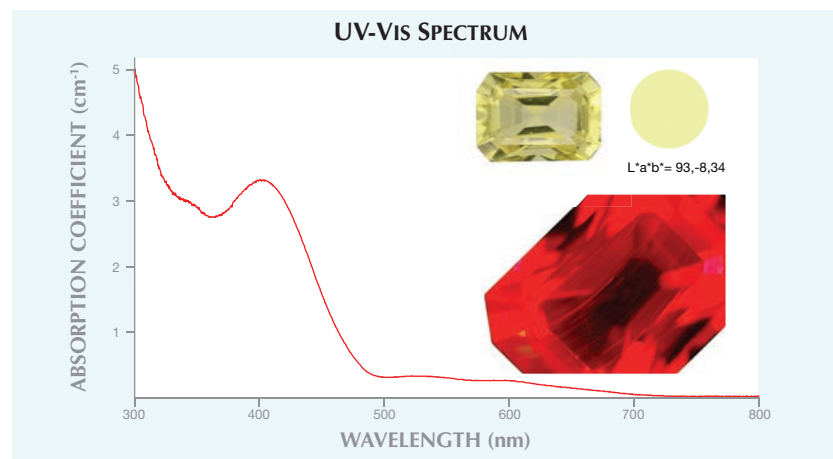
spectral region (figure 21). Detailed chemical analysis via LA-ICP-MS was performed to identify chromophores and color origin. The elements Mg, Cr, and Ni were detected at trace levels (a few ppma). Naturally occurring elements such as Ga were not detected, further indicating synthetic origin. Trace Cr was confirmed both by red fluorescence and by laser photoluminescence spectra with 514 nm excitation, exhibiting a doublet at 692/694 nm and side bands.

A combination of trace-element analysis and UV-visible spectroscopy clearly indicated that the yellow color originated from the much more effective chromophore known as "trapped holes," associated with the trace amount of Mg and Cr in this stone (J.L. Emmett et al., "Beryllium diffusion of ruby and sapphire, Summer 2003 G&G, pp. 84–134). By comparison, a sapphire colored by Fe^{3+} would only display a pale yellow coloration with a concentration above 500 ppma. This synthetic sapphire, however, showed no iron above the detection limit (< 1 ppma). The contribution of trace amounts of Ni is not well known.

Natural and synthetic sapphires colored by a trapped-hole mechanism often possess an orange or reddish orangy hue. This synthetic sapphire exhibited a yellow coloration much like those of samples colored by Fe^{3+}. This example demonstrates that a clear understanding of chromophore contribution and the application of relevant advanced testing can reliably identify the cause of color as well as natural or synthetic origin. In this instance, the prominent curved growth supported the identification, but even without this feature a thorough understanding of the cause of color in sapphire can provide helpful identification clues.

Ren Lu

TUCSON 2013

COLORED STONE AND ORGANIC MATERIALS

Blue cat's-eye apatite. Apatite is a group of minerals belonging to the hexagonal crystal system with the chemical formula of $Ca_5(PO_4)_3(F,Cl,OH)$. It has a variety of colors and is usually transparent to translucent. The most common apatite is the fluorine-rich type, known as fluorapatite. Blue apatite is particularly rare and popular. Previous research indicates that due to the similarity between the optical absorption and emission spectra of natural blue apatite and synthetic compounds containing MnO_4^{3-}, the blue color results from the substitution of PO_4^{3-} with MnO_4^{3-} (P.D. Johnson et al., "Apatite: Origin of blue color," Science, Vol. 141, No. 3586, pp.1179–1180). Chatoyancy is a very common phenomenon in apatite crystals with green or yellow bodycolors. Deep blue apatite with a cat's-eye effect, however, is very rare.

At this year's GJX show in Tucson, Duarte & Bastos Ltd. from Teófilo Otoni, Brazil, exhibited a 12.50 ct intense blue cat's-eye apatite cabochon (figure 1). The stone was said to be from Brazil. It had a neon blue bodycolor and a very sharp eye seen with a spot light source. Further research is needed to verify the color origin of this stone.

Tao Hsu
GIA, Carlsbad

Figure 1. This 12.50 ct neon blue cat's-eye apatite is fromBrazil. Courtesy of Duarte & Bastos Ltd. Photo by Eric Welch.

Figure 2. This piece of stingray jewelry is placed on a backdrop of stingray skin. Courtesy of the Ferraccia Jewelry Collection. Photo by Eric Welch.

Exotic stingray skin jewelry. Leather has long been used in jewelry, combined with precious metals and gemstones to add a special flavor. The variety of textures from different animal skins offers a highly versatile component for designers.

The Ferraccia Jewelry Collection exhibited a huge variety of stingray leather goods at the AGTA show, including bracelets (figure 2), necklaces, earrings, rings, belts, purses, and mobile phone cases. Stingray is not considered an endangered species. They are harvested as a delicacy in Asia and some Eastern European countries. The leather used in this collection comes only from the top of the stingray. This part of the skin, which serves as the animal's armor and backbone, rarely exceeds 10 inches wide and 17 inches long (figure 3). The polished stingray skin displays a unique texture resembling hundreds of sparkling pearl-like spots under proper lighting. This pattern is tactile as well as visual. Considerable effort went into the tanning and finishing process
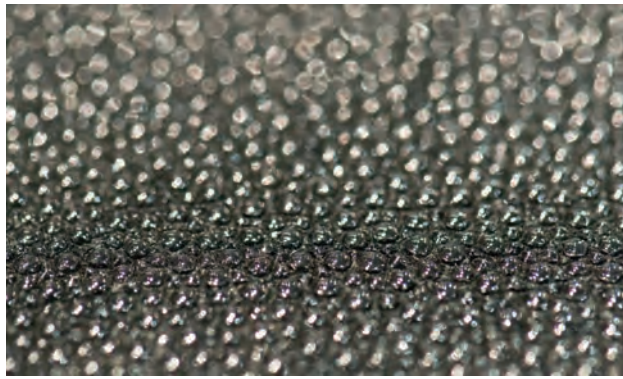
Figure 3. A close-up view of the processed stingray skin shows numerous shiny pearl-like spots. Courtesy of the Ferraccia Jewelry Collection. Photo by Eric Welch.

Figure 4. These rare double-trapiche emerald slices, about 1.77 ct each, are from Muzo, Columbia. Courtesy of Equatorian Imports Inc. Photo by Eric Welch.

to obtain the deep color and durability. Thirty custom dyed colors were created, and each skin has its own pattern, adding to the uniqueness and exotic appeal.

Stingray leather is also very durable because the tiny grains are all rooted in the underside of the skin. With proper care, it should last more than a lifetime. A damp cloth, air drying, clear leather polish, and mild soap are used to remove any remnants between the individual grains.

Tao Hsu

Rare double-trapiche emerald. The term "trapiche," named after the Spanish word for the spoked wheel used to grind sugar cane, describes a very special growth phenomenon. Basic components usually include a six-ray star, a clear or dark hexagonal core at the center, and a transition between the core and the outer sectored crystal. It is commonly associated with emerald, but trapiche corundum, tourmaline, quartz, and andalusite are also found (T. Hainschwang et al., "Trapiche tourmaline from Zambia," Spring 2007 G&G, pp. 36–46). For the past 40 years, gemologists have tried to interpret this phenomenon, proposing theories that involve different growth rates and growth conditions.

At the AGTA show, Equatorian Imports exhibited two pieces of emerald with a very rare double-trapiche pattern. They weighed about 1.77 ct each and are reportedly from Muzo, Columbia. Instead of a six-ray star, twelve arms radiated from the center (figure 4). There was no core at the center. The twelve-ray star appeared to be composed of two six-ray stars shifted slightly from each other. The rays had a dendritic appearance, with some of them intertwined. Unlike previously reported trapiches, these two specimens displayed at least three growth sectors. The formation of this double-trapiche pattern was most unusual.

Tao Hsu

Rock buttons from the United States. At the AGTA show, Columbia Gem House (Vancouver, Washington) introduced its American rock button collection. The rocks were collected from about 25 different states, then processed and finished in the company's own cutting facilities. The rocks are

sliced and shaped into round buttons and drilled through along different directions. Each button is about 3–4 mm thick and 1–3 cm in diameter. Some are polished, while others have a dull finish. Natural gemstones are mounted in some of the rock buttons, bringing out the colors of both.

The collection features a wide variety of rocks (figure 5). Blue veil quartz, a combination of quartz matrix with blue azurite veins, was discovered in Washington state. Perhaps the most interesting item is copper-bearing brick from a Michigan copper smelter. For years, melted copper dropped on the floor and sealed the fractures in the bricks, giving them a unique look after polishing. Green serpentine, the California state rock, is a metamorphic rock composed of

Figure 5. These rock buttons were seen in Tucson. Bottom row, left to right: blue veil quartz from Washington, rhodonite from Colorado, amazonite from Virginia, serpentine from California, black jasper from Oregon, copper-infused brick from Michigan, jasper from Idaho, oligoclase from Nevada, fossilized coral from Alaska, polka-dot agate from Oregon, and lemon chrysoprase from Australia. Top row: glacier stone from Idaho, bertrandite from Utah, and black jasper from Oregon. Courtesy of Columbia Gem House. Photo by Eric Welch.

magnesium-rich silicate minerals. Amazonite from Virginia is the beautiful bluish green variety of microcline. With some minor albite stripes, it displays an alternating blue and white pattern. From Utah comes bertrandite, a beryllium source composed of many different minerals. Bertrandite is just one mineral component of the rock, which is quite rare; most are destroyed in ore crushers before they can reach the jewelry market. Other interesting specimens included rhodonite from Colorado, black jasper and polkadot agate from Oregon, oligoclase from Nevada, coral from Alaska, and glacier stone from Idaho.

These rock buttons are sold individually. Designers or consumers can use them in any combination to create their own custom looks. The buttons can be strung on metal, leather, or other materials to form individualized necklaces and bracelets.

Tao Hsu

MISCELLANEOUS

Colored stones cut with high precision. At the AGTA and GJX shows, China Stone (Bangkok) marketed a selection of tiny, precisely cut natural gemstones. Sold as parcels, the stones ranged from 0.03 to 3.0 mm in diameter. Despite their small size, they were impressively saturated with a full spectrum of colors (figure 6).

The stones are natural and purchased directly from the source suppliers, then cut and polished in the company's Chinese factories. With computer-controlled automation, the stones are digitally calibrated and precisely cut to be set into commercial jewelry. The company's products include ruby, blue and fancy-color sapphire, amethyst, chrome tourmaline, and tsavorite. The matched stones can be used in graphic designs or as accent stones in fine jewelry.

Clients of China Stone's high-precision cut stones include watch manufacturers, fine jewelers, and designers.

Figure 6. Tiny but precisely cut and highly saturated stones were offered at Tucson. Photo by Eric Welch.

The company developed its own inventory grading, stock management, and order processing systems to maintain the strictest standards of shape, size, color, and quality. For each type of gemstone, color grades are assigned with several different color codes. Customers can easily combine their favorite colors and sizes of a certain stone type and see whether the goods are in stock or need to be ordered. With the development of automated cutting technology, small rough can be easily handled and cut with very high precision, giving jewelry designers creative flexibility.

Tao Hsu

GNI REGULAR FEATURES

COLORED STONES AND ORGANIC MATERIALS

Musgravite from Myanmar. Two small, near-colorless stones reportedly from Myanmar (0.11 and 0.24 ct; figure 7) were recently loaned to GIA for examination by Brad Payne (The Gem Trader, Surprise, Arizona). Both samples had a refractive index of 1.718–1.723 and a specific gravity of 3.66 (calculated from optical measurements using a Sarin device, due to the small size of the samples). Both showed a very weak orange fluorescence to long-wave UV radiation and luminesced weak red to short-wave UV.

These properties are within the established ranges for musgravite and taaffeite, which have similar chemical composition and structure. Distinguishing between the two minerals requires Raman spectroscopy or X-ray diffraction. Conclusive identification of these samples as musgravite was accomplished by Raman spectroscopy (see L. Kiefert and K. Schmetzer, "Distinction of taaffeite and musgravite," *Journal of Gemmology*, Vol. 26, No. 3, 1998, pp. 165–167). Even though several stones have been submitted to GIA's laboratory over the years as musgravite, rarely have they been confirmed as such (see Summer 1997 Gem News, pp. 145–147; Spring 2001 Lab Notes, pp. 60–61).

Microscopic observation revealed a heavily roiled growth structure and small colorless needles and particulates scattered throughout. Also present were numerous black opaque hexagonal platelets, identified by Raman analysis as graphite (figure 8). Interestingly, the graphite

Figure 7. These two musgravites (0.11 and 0.24 ct) are reportedly from Myanmar. Photo by Brad Payne.
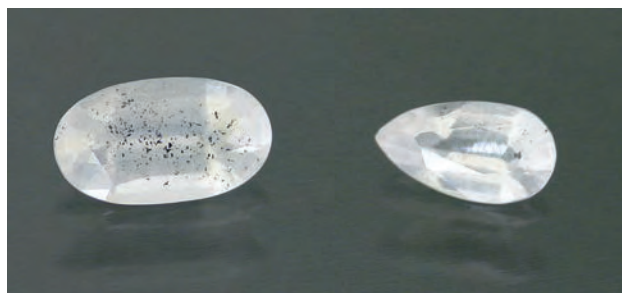
Figure 8. Hexagonal graphite platelets were the most conspicuous inclusion in the 0.24 ct musgravite. Photomicrograph by N. Renfro; field of view is 1.08 mm.

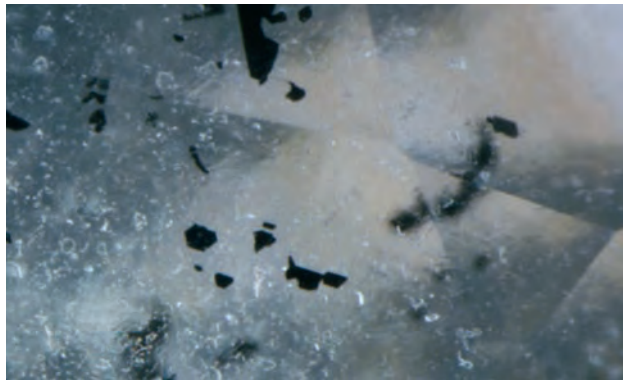*Figure 9. This 8.54 ct cabochon was a composite of brown opal and white calcite. Photo by G. Choudhary.*

platelets all appeared to be crystallographically aligned within the host musgravite.

According to Mr. Payne's supplier, Burmese "taaffeite" (which includes a small percentage of musgravite) comes from Chaunggyi, a few kilometers northwest of Mogok. Although production is quite limited, more musgravite may appear as miners become aware of this rare gem's existence. Due to the overlap of physical properties between musgravite and taaffeite, stones suspected of being the rarer musgravite should be submitted to a qualified gemological laboratory for confirmation.

Nathan Renfro (nrenfro@gia.edu)
GIA, Carlsbad

An opal-calcite composite. Composites assembled from opaque to translucent gem materials such as turquoise, chalcedony, and chrysocolla have become quite popular in recent years, as evidenced by the number of samples received for identification at the Gem Testing Laboratory in Jaipur, India. We recently examined a white-brown, translucent to opaque oval cabochon (figure 9) that turned out to be a composite featuring an unusual combination of gem materials.

The specimen weighed 8.54 ct and measured 18.03 × 13.12 × 4.63 mm. At first glance, it appeared to be a rock consisting of some brown and white mineral, but the presence of golden veins ruled out such a possibility, suggesting instead a manmade product. Closer inspection of the cabochon from all sides revealed four distinct areas—a colorless polymer, golden veins and patches, a brown mineral, and a white mineral—all showing a different surface luster (figure 10, left). At the base of the cabochon, individual grains of a white mineral were embedded in the colorless polymer, as well as golden areas comprised of fine flakes, composed of zinc (figure 10, right). These features were consistent with those observed in a composite material (e.g., G. Choudhary, "A new type of composite turquoise," Summer 2010 *G&G*, pp. 106–113).

Although the cabochon was recognized as a composite, its components had yet to be identified. Spot RIs of 1.56 and 1.45 were obtained from the white and brown portions, respectively. The white portion also displayed a large birefringence blink, typically associated with carbonate minerals
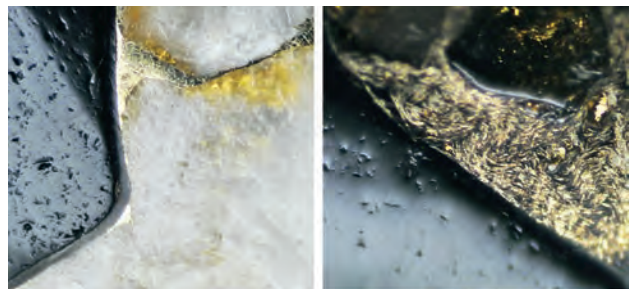
such as calcite, while no blink was observed on the brown portion. Under long- and short-wave UV radiation, the cabochon remained largely inert, except for a weak whitish glow observed on the white portions. Furthermore, magnification of the white portion revealed cleavage planes, liquid films, white cloudy inclusions, and doubling, while the brown portion was milky with fine flaky inclusions.

Spot RIs and magnification identified the white portion as calcite and the brown portion as opal, but these tests were not sufficient to prove their identity. Raman spectroscopy of the white portion in the 200–2000 cm^{-1} range (using 532 nm laser) displayed many sharp peaks at 281, 482, 712, 1086 (the strongest), 1435, and 1749 cm^{-1}; these peaks are associated with calcite. Raman spectra of the brown portion displayed broad absorptions at around 400–500, 800, and 1000 cm^{-1}; these did not display sharp absorption features other than a peak at 487 cm^{-1}. These absorptions are associated with amorphous materials such as opal (opal-A), and the 487 cm^{-1} peak is associated with Si-O vibrations (e.g., C.J. Brinker et al., "NMR confirmation of strained 'defects' in amorphous silica," *Journal of Non-Crystalline Solids*, Vol. 99, 1988, pp. 418–428).

Figure 10. Under reflected light, the cabochon's luster varied across four distinct portions (left). Note the polymer vein at the center of the image and the parallel planes and cloudy inclusions at the top of the white portion. Some of the golden areas were comprised of fine flakes embedded in polymer (right). Photomicrographs by G. Choudhary; magnified 24× (left) and 48× (right).

Figure 11. A map of the Ilakaka-Sakaraha mining areas of southern Madagascar.

Identification of this cabochon as a composite was straightforward, but the components were more difficult to detect. Although Raman spectroscopy identified the materials present, the use of these two substances for making a composite remains unclear.

Gagan Choudhary (gagan@gjepcindia.com)
Gem Testing Laboratory, Jaipur, India

Update on sapphire mining in Ilakaka-Sakaraha, Madagascar. In July-August 2010 and August 2012, this contributor visited southern Madagascar to collect reference samples from the Ilakaka-Sakaraha deposit, probably the world's largest sapphire producer over the past 13 years. This update presents a map of the mining areas (figure 11). Note that all the sapphire-producing localities are associated with sandstone areas.

The first discovery happened in 1998, near Ilakaka Be. Because the village was near Route Nationale 7 (RN7), the main road linking the capital city Antananarivo to the port of Toliara, the locals quickly found a thriving market with Thai and Malagasy merchants. Within months, miners from around the island settled near the bridge on the Ilakaka River, and a boomtown was born. Ilakaka is a much quieter place today. Tourists regularly stop there, while Sri Lankan, Thai, and Malagasy gem traders still conduct business.

Many gemologists and traders are surprised by the extent of the deposit. Discoveries occurred beyond the Ilakaka area on the Malio and Fiherenana River basins in the north and on the Benahy, Taheza, Imaloto, and Onilahy River basins to the south and west of Ilakaka (basins are separated by yellow dots on the map). As the map shows, the deposit extends about 120 km east from Anena (on the Onilahy River)

to Anakondro (on the Imaloto), and nearly 100 km north from Anena to Antaralava (on the Fiherenana) and Anakondro to Ankaboka Malio (on the Malio).

While sapphires were also reported north of Antaralava near Fotilovo and Murarano and in the Malio Valley north of Ankaboka Malio, this contributor has not explored these remote areas.

Ilakaka River Basin: The discovery near Ilakaka Be fell short of its early promise, and within months activity moved upstream to Ambarazy, which was briefly an important trading center, and the famous Banque Suisse mining site, one of the largest pits ever dug by hand in Madagascar. Mining also occurred north of RN7 on the western side of the Ilakaka River, up to the village of Bepeha. Mining was not allowed on the eastern side of the river, which is part of Isalo National Park. While small groups were still active at Banque Suisse in 2012, mining had nearly stopped elsewhere in the basin. Besides a few groups working around the town, a small Thai mechanized operation is still at Amabrazy. Overall, some 300 people were still mining in the Ilakaka River basin, a fraction of the estimated 60,000 there in 1999.

Eastern Boundary and Imaloto River Basin: Very few sapphires have been found beyond the eastern limit of the sandstone-related rocks. The only exceptions are the secondary deposits along the Imaloto, near Lovokadabo, Ampasimamitaka, Sakabe, Ambotzove, and Ankondro, where sapphires were trapped in river sediments, probably transported from sandstone-covered regions by the Ilakaka and Benahy Rivers. In 2012, the area along the Imaloto seemed to be producing again after several relatively quiet years. Gems were also found in several areas closer to Sakalama. A rush occurred in 2004 at Ampasimamitaka, where the sapphire-rich Benaha River joins the Imaloto. A parcel of mostly milky blue sapphires mined there were later found to contain natural beryllium. In 2008, it was difficult to find miners anywhere except Sakabe. Returning in 2012, the contributor witnessed a rush near Sakalama, with about 200 people at two large pits. Nearby at Mahavily, another 100 were reportedly mining on the Benahy River. At Ampasimamitaka, about 50 people were mining on the Imaloto. Other groups were reportedly working upstream to Lovokadabo, but also far downstream. At Ankondro, 50 km downstream near Benenitra, about 50 people were digging for pink and blue sapphires. Another 200 were said to be near Ambotzove. In 2012, we estimated 500 to 1,000 miners on the eastern side of the region, mostly along the Imaloto.

Western Boundary, Sakaraha to Bezaha: The western boundary links Sakaraha, south of the Fiherenana River, and Bezaha, on the Onilahy River. West of that the geology is dominated by limestone-, basalt-, and gabbro-rich areas where gems are found in two areas, carried by the rivers from the sapphire-rich sandstone-covered region between Sakaraha and Ilakaka.

In the northwest near Antaralava, at the intersection with the sapphire-rich Fiherenana River, a narrow sandstone-rich area extends north to south between two regions containing limestone. Mining started in 2000, and in 2012 about 50 people were there.

In the southwest near Anena, on the Onilahy River, a minor rush occurred in 2005, and five years later about 100 miners were believed to be at the site. Anena is the only known deposit south of the Onilahy, a deep, powerful river not currently mined for gems. The discovery at Anena and the fact that the sapphire-rich Ilamoto and Taheza Rivers flow into the Onilahy suggest that this river is abundant with sapphires. Yet the area is too remote to attract the mechanized mining needed to work the deep sands.

Benahy River Basin: Mining along the Benahy started in 1999. The village of Vohimena soon became famous, and several mechanized operations were there from 2000 to 2011. In March 2005 an important discovery happened near Sakameloka, an area that became known for pink sapphires. Several other mechanized operations followed until late 2007, when prices for small pink rough in the Ilakaka market reportedly dropped 90% from the year before.

Other mining villages lower on the Benahy, such as Morafena, were too remote to explore. Visiting the area from Sakameloka down to Vohimena Mahafala in 2012, the contributor observed fewer than 500 miners along that portion of the Benahy. The mechanized operations seen there from 2005 to 2010 had ceased.

Malio and Fiherenana River Basins: In late 1999, mining started north of RN7 in the Fiherenana and Malio River basins near Ankaboka Malio, Analamahavelona, Betikely, Maromiandra, Ankaboka Ambinany, Andralanova, Bevilany, and Antaralava. Several Thai companies were operating machinery near Ankaboka Ambinany and the bridge at Bevilany. After the 2003 discovery of significant deposits near Manombo Be, Sri Lankan buyers opened offices there to intercept the sapphires before they reached the Thai buyers in Ilakaka.

By 2005, Manombo rivaled Ilakaka, but most of the evening activity now happens at nearby Sakaveero, the trading center built circa 2007. Activity north of RN7 was reportedly weak in 2010, but in August 2012 about 1,000–1,500 locals using hand tools were scattered north of the road, including areas of the Zombitze-Vohibasia National Park. About 400 miners were south of Manombo Be at Manombo Misereno and Anduharano. Near Analamahavelona, the discovery of fine blue and pink stones in May 2012 attracted some 400 miners. Near Ankaboka Ambinany, a few hundred people were working different deposits around the village north of the Bevilany Bridge, where a Thai mechanized operation used two excavators and a washing plant. Another few hundred were reportedly at Ankaboka Malio and other remote areas of the Malio River.

Taheza River Basin: Since about 2000, sapphires have been mined along the lower Taheza north of Bezaha and in the upper valley. Mining villages sprang up at Analasoa, Analalava, Mahasoa, and Ambalavihy, where tens of thou-

sands were reportedly working. Mining rights were soon acquired by large Sri Lankan companies. After attempting to mechanize, they decided to buy stones from locals instead, supporting them with food and tools. This model became very successful in the Taheza basin, and by 2008 it was probably the main sapphire region in the whole deposit. While activity in the upper basin has declined, it has increased near Antsoa, where about 5,000 people were mining and washing gravels in 2011 and 2012. In 2011 the main mining area was Mangatoka, but the next summer it was Ankaranduha, where more than 1,000 were working. In the Taheza basin the sapphire-rich gravels are usually about 30 meters deep, but some artisanal miners used a 50-meter vertical shaft to reach the gravels, which were mined by digging narrow horizontal tunnels. The gravels were extracted and taken to the river for washing. For the digger to breathe, air had to be sent underground using large plastic bags and tubes.

Due to the lack of roads, activity could not be observed on the Taheza south of Ambatomainty, where there were remnants of Sri Lankan operations. From Bezaha up to Ankilivaly, the contributor explored the lower Taheza basin in 2010 and 2012 and saw mining near Ankilitelo, Ambarinakoho, and Ankilivaly. A gem rush occurred at Ambalmasai in late 2011, and the following year about 500 people were still mining that remote area. Some activity was also reported at Sarouval, about 5 km north of Ambalmasai on the other side of the Taheza. At each site, Sri Lankan companies supplied the miners with loading trucks, tools, and food.

In 2012, most of the production from western Ilakaka-Sakaraha was along the Taheza, in the area south of Manombo, near Vohimena, and in a few spots north of RN7. Sapphire trading followed the same trend. Ilakaka was quiet except for the morning gem market and late at night when people offered the stones they were unable to sell at Sakaveero, the popular new trading spot.

Overall, mining and trading around Ilakaka is down from previous years. But with 10,000–20,000 miners and several hundred buyers, Ilakaka-Sakaraha probably still surpasses Ratnapura and Elahera in Sri Lanka as the world's main source for blue and pink sapphires. From April to July 2012, many of the buyers and miners left Ilakaka to work in the jungle near Didy and Ambatondrazaka, where fine rubies and sapphires were discovered in March 2012. Most of them returned to Ilakaka in July when the new site (located in a protected area) was closed by the authorities, and by August business was mostly back to normal.

Vincent Pardieu (vpardieu@gia.edu)
GIA Laboratory, Bangkok

Zoned scapolite from India. The Spring 2011 GNI section (p. 59) reported gem-quality yellow scapolite from Karur in the southern India state of Tamil Nadu. While visiting a local dealer, this contributor encountered parcels of rough and faceted scapolite that appeared strongly zoned to the unaided eye. They were reportedly mined from the same region as above. From the parcels, one rough and one faceted specimen


Figure 12. These strongly zoned scapolites, a 9.10 ct faceted stone and a 4.18 g rough specimen, were reportedly mined in the Karur region of Tamil Nadu in India. Note the patchy appearance of brown zones. Photos by G. Choudhary.

were obtained. The faceted stone was a 9.10 ct oval mixed cut, while the 4.18 g rough specimen was a tetragonal prism with partially broken bipyramidal terminations (figure 12). Both had a pale yellow color with strong brown zones.

Standard gemological testing on the faceted sample revealed an RI of 1.548–1.570, with a uniaxial negative optic sign and a birefringence of 0.022; its hydrostatic SG was measured at 2.66. These values are consistent with those reported for scapolite. Both samples fluoresced strong orange-pink (almost red) under short-wave UV radiation and were inert to long-wave UV. No absorptions were seen with a desk-model spectroscope. The color zones appeared patchy and showed some flaky inclusions along certain planes. This was confirmed with higher magnification (figure 13, left). Under oblique illumination these planes appeared highly iridescent, displaying bright spectral colors.

Further observation at high magnification revealed some angular features. Although the planes intersect with each other at 90°, the features within them appeared to be following the bipyramidal faces, as indicated by their angle and orientation (figure 13, right). This brown mineral was found

Figure 13. The color zones were composed of fine platelets oriented in planes along the length of crystal (left). Under oblique illumination, these planes displayed bright interference colors and angular features (right), suggesting the exsolution of some mineral. Photomicrographs by G. Choudhary; magnified 64×.
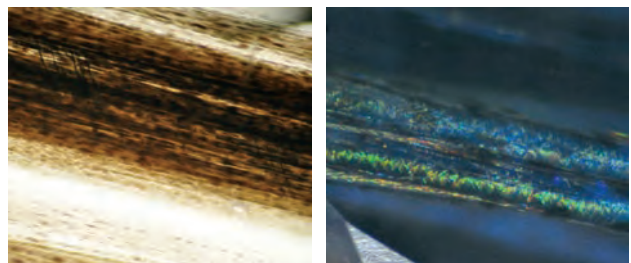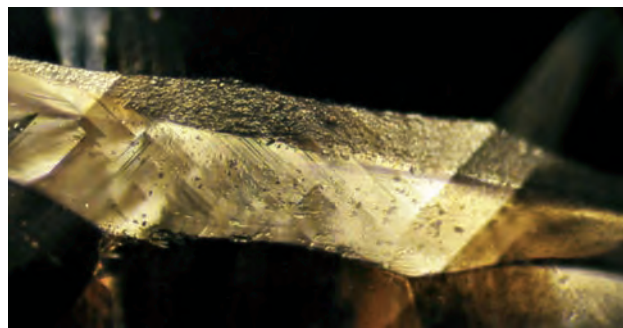
Figure 14. The planes containing a brown exsolved mineral were present in two directions and intersected at almost 90° along the prism faces, which is also the direction of cleavage in scapolite. Photomicrograph by G. Choudhary; magnified 64×.
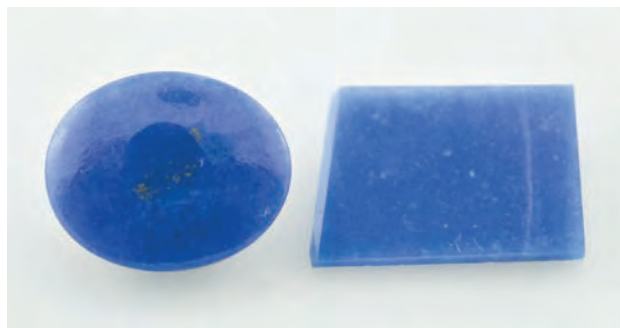

Figure 15. These 5.16 and 2.59 ct specimens, submitted as sapphire and initially thought to be dyed quartzite, were identified as dumortierite-quartz rock. Photo by G. Choudhary.

along planes in two directions intersecting at almost 90° (figure 14), which were oriented along the length of the crystal (its c-axis). Examination of the rough specimen revealed that these brownish planes were oriented along the prism faces, following the cleavage planes. Some of the brownish inclusions were also aligned along the basal pinacoid planes. The overall pattern and orientation of the zones indicated that some mineral has been exsolved along the cleavage planes, following the bipyramidal faces, as suggested by the angular features described above.

These brown platelets could not be conclusively identified, but Raman spectra indicated the presence of lepidocrocite, which has previously been reported as fillings in lath-shaped cracks of scapolite (E.J. Gübelin and J.I. Koivula, *Photoatlas of Inclusions in Gemstones*, Vol.1, ABC Edition, Zurich, 1997, pp. 368–369). While the Spring 2011 GNI entry noted the occurrence of gem-quality yellow scapolite from the same location, this production is probably more suitable as a collector's stone.

Gagan Choudhary

SYNTHETICS AND SIMULANTS

Dumortierite-quartz rock presented as sapphire. The Gem Testing Laboratory of Jaipur, India, received for identification an opaque blue specimen, submitted as sapphire. The 5.16 ct cabochon (figure 15, left) measured 12.59 × 10.28 × 4.71 mm. Examined under a fiber-optic light source, the specimen displayed an uneven blue coloration associated with dyed materials, possibly dyed quartzite.

Gemological testing gave a vague spot RI around 1.55 and a hydrostatic SG of 2.99. The stone fluoresced strong blue to short-wave UV and was inert to long-wave UV. It showed no reaction when viewed with the Chelsea color filter and no distinct absorptions using the desk-model spectroscope, reactions that would preclude the possibility of dyeing. The RI was consistent with quartz, but the SG value ruled out that possibility. Because of the curved surface and opacity of the cabochon, we asked the client to provide a

specimen with a flat polish, enabling us to properly study the material. The client also provided a thin slice of the material (figure 15, right), which allowed light to pass through easily. The properties of the slice were similar to those recorded for the cabochon. Two RI readings were obtained while slightly shifting the slice, however. Although the readings were not clear, shadow edges were seen at about 1.54 and 1.68.

Initial microscopic observations of the slice with strong transmitted light suggested blue color concentrations along the boundaries of white to colorless grains, as seen in dyed materials (figure 16, left). Yet the interstitial areas were wider than those of dyed quartzite or any other dyed substance. On further examination of the slice, inhomogeneous blue and white granular texture became evident, where some blue grains were also visible. Reflected light revealed a clear difference between the blue and whitish

Figure 16. Uneven blue and colorless areas (left) suggested color concentrations associated with a dyed specimen, but reflected light (right) revealed a clear difference between the blue and whitish portions. The sharp-edged whitish irregular grains (which appear gray in the image) seemed to be embedded in the blue matrix. The white mineral was identified as quartz and the blue mineral as dumortierite. Also note the difference in the luster of two areas, although both minerals have similar hardness. Photomicrographs by G. Choudhary; magnified 32×.
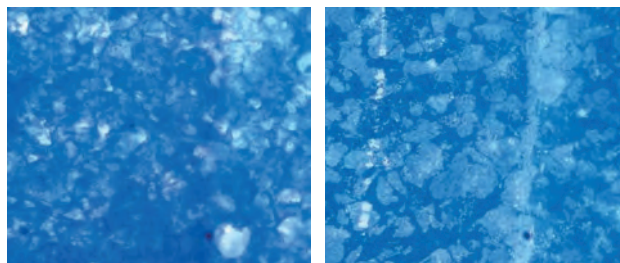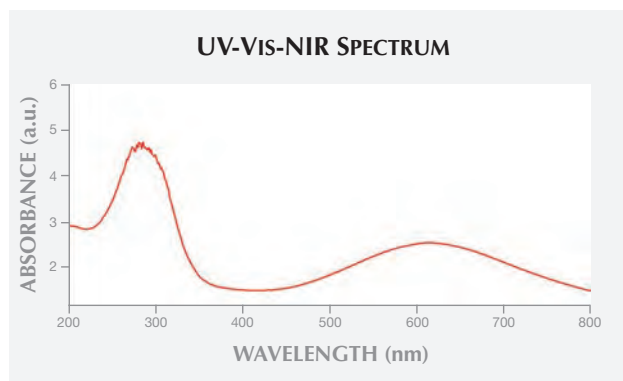
Figure 17. The slice's UV-Vis-NIR spectrum in the 200–2000 nm region showed broad absorption bands centered at ~290 and ~610 nm, which are assigned to Fe^{2+}-Ti^{4+} charge transfer and associated with dumortierite.

Figure 19. Six large CVD synthetic diamonds (1.001–1.119 ct) were submitted for grading undisclosed. Photo by H. Kitawaki.

portions (figure 16, right). The sharp-edged whitish irregular grains, which appear gray in the image, seemed to be embedded in the blue matrix. Also, the white portion had a much duller luster than the blue one. These features suggested that the blue color was indeed natural and that the uneven coloration was not the result of dyeing, but rather a mixture of white and blue materials.

UV-Vis-NIR spectroscopy of the slice in the 200–2000 nm region showed broad absorption bands (figure 17) centered at ~290 and ~610 nm, which are assigned to the Fe^{2+}-Ti^{4+} charge transfer (see Platonov et al., "Fe^{2+}-Ti^{4+} charge-transfer in dumortierite," *European Journal of Mineralogy*, Vol. 12, No. 3, pp. 521–528). This was confirmed by EDXRF analysis, which detected the presence of Fe and Ti along with Al, Si, Ca, and As. In the DiamondView, the blue portions gave strong blue reactions while the white grains remained inert (figure 18).

Raman analysis using a 532 nm laser confirmed the blue and white minerals as dumortierite and quartz, respectively. The blue durmortierite revealed major peaks in the 200–2000 cm^{-1} region at ~206, 290, 396, 446, 506, 844, 945, and 1068 cm^{-1}, while the white quartz showed major peaks at ~206, 263, 353, 464, 807, 1080, and 1157 cm^{-1}.

Figure 18. DiamondView imaging revealed strong blue fluorescence in the dumortierite portion of the slice, while the quartz grains appeared dark and remained inert.
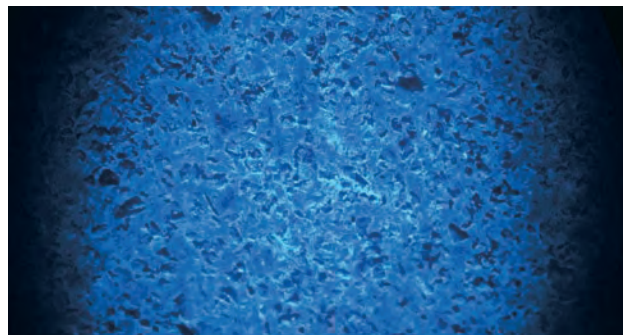

These peaks are consistent with those reported for dumortierite and quartz in the RRUFF database. Furthermore, the SG value of 2.99 suggested a composition of approximately 54.64% quartz and 45.36% dumortierite (assuming an SG of 2.65 for pure quartz and 3.40 for dumortierite, while disregarding other accessory minerals).

Identification of this specimen would have been difficult in the absence of Raman analysis, though UV reactions and a vague RI shadow edge offered some clues. For several years dumortierite has been known to occur with quartz as rock and massive forms, but it is not routinely seen in the trade, perhaps due to lack of awareness or because it is being misrepresented, as in this case. The client had no information on the origin of these specimens, which were purchased on the local market, but dumortierite in quartz has been reported from India (R. Webster, *Gems*, 5th ed., revised by P. G. Read, Butterworth-Heinemann, Oxford, UK, 1994).

Gagan Choudhary

Undisclosed samples of large CVD synthetic diamond. In mid-2012, one of the international diamond grading laboratories in Antwerp reported undisclosed CVD synthetic diamonds, causing a stir in the diamond industry (C. Even-Zohar, "Synthetics specifically 'made to defraud,'" *Diamond Intelligence Briefs*, Vol. 27, No. 709, 2012, pp. 7281–7290). Since then, reports of undisclosed CVD synthetics have also emerged from gem testing laboratories in India and China (Z. Song et al., "The identification features of undisclosed loose and mounted CVD synthetic diamonds which have appeared recently in the NGTC laboratory," *Journal of Gemmology*, Vol. 33, No. 1–4, 2012, pp. 45–48). While those samples were mostly between 0.3 and 0.5 ct, the largest colorless CVD synthetic reported by a gem laboratory so far was a 1.05 ct pear shape submitted to GIA (Summer 2010 *G&G* Lab Notes, pp. 143–144).

In December 2012, six CVD synthetics over one carat (figure 19) were submitted to the Tokyo branch of the Central Gem Laboratory for diamond grading. These were

among the largest undisclosed samples of CVD synthetic diamond ever submitted to a gem laboratory. The six round brilliants ranged from 1.001 to 1.119 ct. All had a color grade of Light yellowish gray, and their strong grayish hue made color estimation using "Cape" series master stones difficult. Four of the samples had a clarity grade of VS_1, while the other two were VS_2. Four samples had cut grades of Excellent, and two were Very Good.

Each sample contained a few pinpoint inclusions, which kept the clarity grades below VVS. The dark, irregularly shaped inclusions were presumably non-diamond carbon. Some samples showed dark graphitization on the girdle. A similar feature is seen in HPHT-treated diamond, which strongly suggests that these samples underwent post-growth treatment.

The characteristic streak pattern of anomalous double refraction due to strain (low-order black and white interference colors) was observed in every sample. The streaks run parallel with the growth direction of the crystal, which is perpendicular to the seed face. The patterns were elongated along the crystal's growth direction and presumably caused by dislocation during growth (figure 20). The samples were inert to long-wave UV radiation, while some of them displayed weak greenish yellow luminescence to short-wave UV.

After FTIR analysis, the samples were classified as type II, which do not show any distinct absorption in the nitrogen area (1500–1000 cm^{-1}) in diamond. Despite their yellow tint, the 1344 cm^{-1} absorption attributed to single substi-
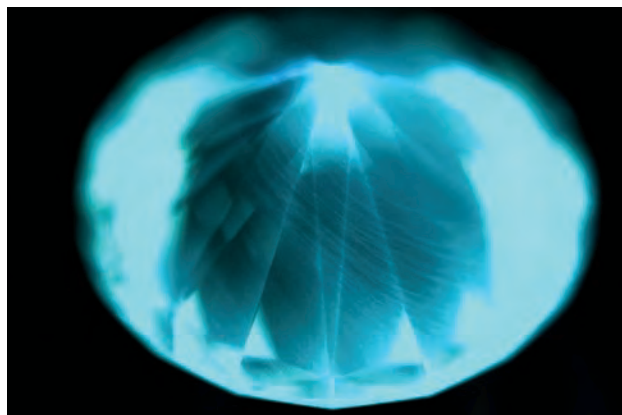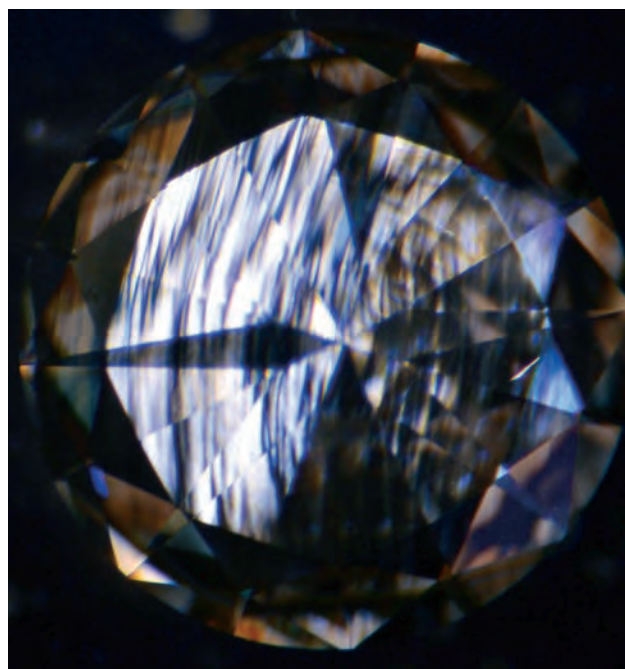
Figure 21. DiamondView fluorescence images showed a layered structure characteristic of CVD synthetic diamond. Blue phosphorescence, attributed to boron, was also observed. Photo by M. Hisanaga.

tutional nitrogen was not observed. Absorptions also originate in hydrogen at 3123 cm^{-1}, which has been reported as a characteristic of CVD-grown diamond (W. Wang et al., "Gem-quality synthetic diamonds grown by the chemical vapor deposition method," Summer 2012 *G&G*, pp. 268–283), and at 3107 cm^{-1}, which is often seen in natural diamonds, were not recognized as clear peaks.

Photoluminescence analysis at liquid-nitrogen temperatures with various excitation wavelengths revealed peaks at 637 nm (NV$^-$), 575 nm (NV^0), 503.2 nm (H3), and 737 nm (SiV$^-$; 736.4/736.8 doublet). With 488 nm laser excitation, five of the six samples displayed a 528 nm peak of unknown origin. With 325 nm excitation, 462 and 499 nm peaks with unknown origins were detected. These two peaks are not observed in natural diamonds. Two of the samples showed a very weak peak at 415.2 nm (N3).

When tested with the DiamondView, the samples showed blue phosphorescence and greenish blue-white luminescence. This luminescence is attributed to boron doping, an enhancement that makes the stone colorless (D.S. Misra, "Method for growing white color diamonds by using diborane and nitrogen in combination in a microwave plasma chemical vapor deposition system," International Patent No. 2012044251).

The samples also showed the layered structure image characteristic of CVD synthetic diamond (figure 21). These UV luminescence figures, unique to CVD synthetics, are more apparent from the pavilion than from the table. Some of them displayed straight growth lines or linear structures such as slip lines, and careful observation of the entire stone (especially from the pavilion) is imperative.

Hiroshi Kitawaki (kitawaki@cgl.co.jp),
Masahiro Yamamoto, Mio Hisanaga, Makoto Okano,
and Kentaro Emori
Central Gem Laboratory, Tokyo

Figure 20. Anomalous double refraction due to stress was observed under cross-polarized filters. Contrasting black and white low-order interference colors produced the streak pattern. Photo by H. Kitawaki.

Fabergé: A Comprehensive Reference Book

By Tatiana Fabergé, Eric-Alain Kohler, and Valentin Skurlov, 613 pp., publ. by Fondation Igor Carl Fabergé, Editions Slatkine, Geneva, 2012. Standard edition: US$200.00

Coauthored by Carl Fabergé's great granddaughter, this impressive book covers the history of the family, the firm, and the master jewelers and designers who worked with Fabergé. The authors had access to previously unobtainable Russian archives as well as unpublished family documents, allowing them to "rewrite the whole history of the House of Fabergé." Heavily illustrated with hundreds of photos—both color and black-and-white, including family portraits, hallmarks, jewelry, and art objects—this book is a worthy addition to any library.

GIA LIBRARY STAFF
Gemological Institute of America
Carlsbad, California

Apatite: The Great Pretender

By John Rakovan, Gloria A. Staebler, and Donald A. Dallaire, Eds., 124 pp., publ. by Lithographie LLC, Denver, 2013. US$35.00.

As with other titles in this series, this work is a collection of articles by several contributors. The most common phosphate mineral on earth, apatite is often confused with other minerals. Its name comes from the Greek *apate*, which means "to deceive," hence the title of this volume. Chapters cover the science, identifying characteristics, history, and localities of the mineral. The book is lavishly illustrated with color images throughout.

GIA LIBRARY STAFF

Gemstones of Peru

By Jaroslav Hyršl, 104 pp., publ. by Granit, Prague, 2012. €17.00

This supplement to the author's *Peru: Paradise of Minerals* (2010) deals with precious and ornamental stones. It is divided into three parts. The first includes archeological gemstones used in ancient Peruvian jewelry. The second and largest section covers recent ornamental stones and gemstones, which are currently being mined and used in jewelry. The third deals with rare faceted gemstones. These are listed alphabetically within each section and accompanied by photos. The book also includes a bibliography and a summary of gemological properties of several important ornamental stones.

GIA LIBRARY STAFF

Multifacets: Style Yourself with Jewelry

By Nathalie Colin, 239 pp., publ. by Abrams, New York, 2013. US$55.00

Nathalie Cohn, creative director of Swarovski, shows the various ways jewelry can be worn to suit any occasion or setting: the workplace, cocktail hour, dining out, a night out, travel, or a wedding. Playful and irreverent, the book offers practical advice on adding touches of attitude, elegance, and personality to cultivate a highly personalized look. Each accessory's color, texture, and shape can be used to achieve a "rich dialogue between jewelry, garment, and body." Numerous images featuring Swarovski pieces offer strategy and inspiration for every woman who wears contemporary jewelry.

STUART OVERLIN
Gemological Institute of America
Carlsbad, California

G&G Online
Gemological Abstracts

COLORED STONES AND ORGANIC MATERIALS

Azurite through the ages: Millennia of mining have not depleted its sources. B. Jones, *Rock & Gem*, August 2012, pp. 20–24.

Azurite, a copper carbonate mineral, is a common secondary mineral. The host is usually a volcanic rock. Collector's azurite crystals mostly came from Chessy in France (the oldest mine since mid-1800s), Morenci and Bisbee in Arizona, Tsumeb in Namibia, and Touissit in Morocco. The increasing copper price in the first decade of the 21st century lead to reopening of old known copper mines. Well-crystallized azurite specimens have been recently mined in China, Morocco and Mexico.

The quality of well-crystallized samples from a decade-old Milpillas mine in Mexico could be compared to these collector's samples. Azurite crystals (e.g., the Electric Blue from the Milpillas mine) show dark, blue color with high luster, and they are usually 1–2 inches long prisms or blocky crystals up to 4 inches long. They were gradually pseudomorphed into malachite in high oxidizing environment. Thus, malachite was found more abundant than azurite. Sometimes, thin layer of azurite can be deposited atop malachite as the final layer. The light to dark green, melachite pseudomorphs from the Milpillas mine are mostly blocky crystals, and ranged from one to ten inches in size. The Milpillas mine also produced emerald-green bronchantites, a hydrous copper sulfate, of one-two inches long needle-like crystals on a rhyolite matrix. Free copper ions of bronchantite absorb all wave lengths except green, causing bright green color.

KSM

Gemstones and minerals. S. Karampelas [s.karampelas@gubelingemlab.ch] and L. Kiefert, pp. 291–317. In H. Edwards and P. Vandenabeele, Eds., *Analytical Archaeometry*, 604 pp., 2012, Royal Society of Chemistry, Cambridge, UK.

Nestled within this huge textbook on analytical archaeometry—an interdisciplinary field representing the interface between the natural and physical sciences and professions such as archaeology, art history, and museum curatorship that uses state-of-the-art technologies to extract structural and compositional information from ancient materials—is a useful chapter for today's gem professional.

The modern gem trade's embrace of science, technology, and the information sciences is perhaps best reflected in laboratory testing. Advanced laboratory services are often necessary to detect increasingly sophisticated treatments, and new manmade materials such as CVD-grown synthetic diamonds. Lab testing is also used to detect nanotechnology films for hardness and color enhancement, some sophisticated diffusion processes, and geographic origin, to name a few.

Chapter 10, "Gemstones and Minerals," is a broad overview of several advanced spectroscopic and imaging techniques used in gemological and university laboratories to meet these modern needs. This 26-page chapter provides the gemologist, jeweler, and appraiser with succinct practical information, using numerous field examples, about advanced testing that can easily be communicated with clients.

The authors recognize that the foundational gemological methods (such as trained observation using magnification/microscopy, refractive index, specific gravity, ultraviolet indications, and optic character) often need to be augmented with advanced lab techniques, especially for conclusive determinations.

UV-visible near-infrared (UV-Vis-NIR) spectroscopy helps identify diamond treatments and determine the geographic origin of certain stones such as tourmaline and emerald. Fourier-transform infrared (FTIR) spectroscopy helps in the detect of heat treatment in corundum and organic substances used for clarity enhancement, as well as the determination of diamond type. Other applications of FTIR include the separation of natural from synthetic origin in inclusion-free stones and the determination of jade type and treatments. Raman spectroscopy is an important tool in the study of inclusions, the detection of diamond and emerald treatments, and the identification of organic pigments in gems. Energy-dispersive X-ray fluorescence (EDXRF) and laser ablation–inductively coupled plasma–mass spectrometry (LA-ICP-MS) are used in trace-element analyses, determining geographic origin, detecting beryllium treatments, and identify unknown or synthetic materials. Photoluminescence (PL) is applied to the study of natural and treated diamonds as well as pearls, spinel, rubies, and coral. X-ray imaging and radiography are widely used to evaluate cultured and natural pearls, including their treatments.   *ERB*

Petrochemical characteristics and genesic significance of Luodian jade from Guizhou. Yang Lin et al., *Journal of Mineralogy and Petrology*, Vol. 32, No. 2, 2012, pp. 12–19.

Luodian jade is a new nephrite variety discovered in 2009 at Luodian County in China's Guizhou province. The nephrite formed within the metasomatic zone between the Varisian gabbro and calc-silicate. Geochemistry and petrology studies of both the white and greenish white varieties indicate 98% and 95% tremolite, respectively. Tremolite has an ideal chemical formula of $Ca_2(Mg, Fe)_5[Si_4O11]_2(OH)_2$, with Mg and Fe substituting for each other to form a solid solution series. Al can also substitute for a small amount of Mg and Fe, while Na, K, and Mn can substitute for Ca and Mg. Chondrite-normalized REE (rare earth element) patterns of the nephrite and the host rock are very similar with enrichment of LREE (light rare earth elements). The concentration of REE is lower in the nephrite than that in the host rock. The La/Yb ratio is also much higher in nephrite, which indicates a higher differentiation of REE in nephrite. Compared to the greenish and greenish white nephrite, the white variety is more evolved. This tells us that the nephrite deposit formed in two stages. Ca/Mg is higher in the greenish and greenish white varieties, meaning they were formed when Mg was unsaturated in the fluid; the white variety formed when Ca and Mg were both saturated. The substitution of trace-element V and Cr into the crystal lattice is closely related to the saturation of Mg in fluid. V and Cr are also the chromophores of the greenish and greenish white varieties. Nephrite formation is caused by metasomatism during the interaction with thermal fluid brought by the intrusive gabbro and the limestone. Limestone provided Ca and Mg, while the fluid brought Si, K, Na, and Al.

Tao Hsu

DIAMONDS

Aviat diamonds: A window into the deep lithospheric mantle beneath the Northern Churchill Province, Melville Peninsula, Canada. J. Peats, T. Stachel, R. A. Stern, K. Muehlenbachs, and J. Armstrong, *The Canadian Mineralogist*, Vol. 50, No. 3, 2012, pp. 611–624, http://dx.doi.org/10.3749/canmin.50.3.611.

The Aviat kimberlites are located in Melville Peninsula in northeastern Nunavut. They are part of the Rae craton, which is composed of Archean granitoid rocks, supracrustal belts, and Paleoproterozoic metasedimentray rocks. The carbon isotopic composition, nitrogen concentration, and nitrogen aggregation state of 70 samples from

these kimberlites were analyzed to help understand the composition of diamond-forming fluids, paragenesis of diamond source, mantle residence history, and thermal history of the subcratonic lithospheric mantle. The colors of samples were colorless, gray, brown, and green.

FTIR analysis revealed that the majority were type IaAB, including IaA and IaB. Total nitrogen content ranged from 13 to 1467 ppma. The Aviat diamonds were relatively rich in hydrogen. Absorption bands at 3107, 2786, and 1404 cm^{-1}, caused by bending and stretching of the vinylidene group (C=CH2), were observed in most samples. An additional hydrogen-related band at 3237 cm^{-1} was also detected.

SIMS analysis revealed nitrogen content ranging from 1 to 1724 ppma. The 13C isotopic analysis suggested that these diamonds were precipitated mainly from carbonate-bearing fluids. Large variations in nitrogen content and $\delta^{13}C$ values, though they were not correlated, were observed in growth sectors, suggesting multiple events of fluid derivation from different sources, mainly ecologitic and also probably peridotitic. But the relationship between CL and carbon isotopic composition suggested that non-luminescent diamond may have been formed during one episode of growth. The Aviat diamonds were possibly formed from diamond-forming fluids or melts from several orogenic events, such as transportation of graphitized organic matter and marine carbonates into the deep mantle via subducting oceanic slabs.

Catastrophic platelet degradation was suggested by the positive correlation between platelets and B aggregates of nitrogen. This phenomenon was probably caused by transient heating events or deformation or both during mantle residence. Blue luminescence of nitrogen-rich samples may be related to intense degradation of platelets. The residence temperature of most samples was extrapolated to ~1050–1150°C, suggestive of a diamond source near the top of diamond stability field at ~150–170 km.   *KSM*

Canadian mining industry: Taking a step up with range of operations. *Israel Diamonds*, No. 241, 2012, pp. 56–58.

The expansion of various mining projects in Canada's North (Northwest Territories, Yukon, and Nunavut) is set to lead the country in economic growth over the next two years. Spinoff activity that accompanies mine-related prosperity is also expected to increase based on pending mines in the assessment phases or preproduction stages, thus further boosting employment and local economic development. The projections see productions in these areas lasting well into the coming decades. Environmental groups and local residents are also interested in the impact on the Canadian North ecosystem as well as the long-term effects on the towns and industry when the boom is over.

MK

A new defect center in type Ib diamond inducing one phonon infrared absorption: The Y center. T. Hainschwang [thomas.hainschwang@ggtl-lab.org], E. Fritsch, F. Notari, and B. Rondeau, *Diamond and Related Materials*, Vol. 21, 2012, pp. 120–126, http://dx.doi.org/10.1016/j.diamond.2011.11.002.

This paper describes the discovery of a new defect center in natural and synthetic type Ib diamonds: the Y center. Sixty-eight natural and synthetic diamonds with detectable C centers, ranging from 0.01 to 1.34 ct and representing common colors for type Ib diamonds (various hues of yellow, orange, brown, and "olive") were studied.

The other color centers traditionally responsible for one-phonon absorption (i.e., spectral absorption due to the presence of certain defects in the diamond's lattice structure) include single isolated boron, the A center (di-nitrogen), the B center (four nitrogen atoms surrounding an atomic vacancy in the diamond lattice), the C center (single-substitutional nitrogen, N^0), the X center (positively charged single-substitutional nitrogen, N^+), and the D, E, and F centers, which have not been attributed to any specific defect.

After correction and normalization of the samples' infrared spectra, and an attempt to determine the A, B, and C center nitrogen content using spectral fitting data, the researchers found that the margin of error for the C center content was at least 50%. This suggests that some absorption bands underlie the well-known single-substitutional nitrogen absorption at 1130 cm^{-1}. For this reason, all spectra are decomposed again by progressive subtraction of the A, B, C, and X center absorptions. For 38 diamonds, this resulted in a consistent residual absorption with a relatively broad apparent maximum centered at ~1145 cm^{-1}.

A large sample of type Ib diamonds confirmed that this new absorption system is not an artifact of the original spectral decomposition work. The authors propose to call it the Y center because it is clearly related to the single-substitutional nitrogen system of the last named one-phonon infrared absorption center, the X center.

ERB

Strain-induced birefringence in natural diamond: A review. D. Howell [daniel.howell@mq.edu.au], *European Journal of Mineralogy*, Vol. 24, No. 4, 2012, pp. 575–585, http://dx.doi.org/10.1127/0935-1221/2012/0024-2205.

Diamond belongs to the cubic crystal system and should therefore exhibit isotropic optical properties. But it is well documented that diamonds often show weak birefringence. This study has focused on the causes of strain-induced birefringence in natural diamonds: dislocations, lattice parameter variations, inclusions, fractures, and plastic deformation.

Strain patterns shed light on the internal stresses within the stone, which in turn reveal the growth and

transport history of the diamond. The imaging of diamonds between crossed polarizers remains a simple and rapid technique for obtaining visual information on strain patterns in diamonds. *GL*

GEM LOCALITIES

Copper-bearing minerals of Colorado. E. Raines, *Rocks & Minerals*, Vol. 87, No. 4, 2012, pp. 304–336.

Between 1868 and 1922, Colorado produced almost 260 million pounds of copper. Nearly 100 million pounds came from the Leadville district, with another 50 million pounds mined in San Juan County (Henderson 1926). During the twentieth century, the Gilman district surpassed Leadville in total copper production with more than 210 million pounds mined (Beaty, Landis, and Thompson, 1990). Total Colorado production prior to 1958 reached 585 million pounds (Del Rio 1960). In this article 106 minerals from the Colorado Mineral Belt (COMB) are listed and 39 are discussed in the text. The Eagle mine in the Gilman District is probably Colorado's most prolific producer of mineral specimens. Gilman pyrite, sphalerite, chalcopyrite, siderite, barite, and galena are found in collections all around the world. The Sweet Home mine in Buckskin Gulch, source of world-famous rodochrosite, is also well known for fine specimens of two copper-bearing minerals bornite and tetrahedrite. The Creede mining district is one of the best-studied mineral deposits and volcanic areas in the country. A detailed study of the Creede ore deposits has been made in an attempt to develop a model for epigenetic precious-metal deposits. Summitville is well known as the producer of the state's finest covellite specimens. The Good Hope mine is the type locality for four copper-bearing tellurides: rickardite ($Cu_{3-x}Te_2$); weissite ($Cu_{2-x}Te$); vulcanite (CuTe), and cameronite ($AgCu_7Te_{10}$). Turquoise was mined from the King mine deposit in Conejos County and from the Chief mine in the St. Kevin district, Lake County.

The state of Colorado has produced some significant copper-bearing mineral specimens. Most of the Colorado's copper minerals are sulfides and sulfosalts with chalcopyrite being the most common copper-bearing mineral. The authors also determine the time of crystallization of two of the pegmatites by Sm-Nd analysis on garnet, feldspar, monazite, and xenotime and by a chemical U-Th-Pb monazite age. On the basis of mineralogy, chemical composition, and crystallization ages, the evolution of the pegmatites is discussed in the framework of the geodynamic history of the Bohemian massif. The regional geology and a thorough description of the investigated pegmatites are presented. *GL*

Une découverte exceptionnelle de béryls gemmes à Chaves, District de Vila Real, Portugal [An exceptional find of gemmy beryls at Chaves, District of Vila Real, Portugal]. M. Ambroise and A. Ambroise, *Le Règne Minéral*, No. 107, September/October 2012, pp. 19–22 [in French].

The numerous pegmatites in northern Portugal are known as sources of fine mineral specimens for collectors. A passionate rockhounding couple describes how, after hard work in constant bad weather, they hit upon a pocket with gemmy aquamarines and heliodors in 2011. The crystals measured 2.1–14.2 cm (0.8–5.7 inches). Their surfaces were slightly to moderately etched. Considering the relatively few gemstone occurrences in Western Europe, this find can be regarded as outstanding. The most beautiful crystals are shown in color photos. *RT*

Gem olivine and calcite mineralization precipitated from subduction-derived fluids in the Kohistan arc-mantle (Pakistan). P. Bouilhol et al., *The Canadian Mineralogist*, Vol. 50, No. 5, 2012, pp. 1291–1304.

Geochemical data presented suggests remobilized CO_2 and H_2O from a subducted island arc helped form the calcite + olivine-bearing veins in Kohistan, Pakistan. The authors provide details on the geologic setting, mineralogy and geochemistry of the vein assemblages, which can yield gem-quality olivine (peridot). The CO_2 and H_2O from island arc magmas and carbonates mixed with mantle fluids rich in Bo (evidenced by ludwigite-vonsenite needle-like inclusions in olivine) as well as La, Ce, Ta, Cu, and Zn (from trace element analysis). Fluid origin and emplacement are discussed at length with emphasis on macro-geophysical mechanisms within the earth. Gem olivine production data and characterization of the rough was not provided. *KAM*

Perles de culture de la Mer de Cortez: Les belles inconnues [Unknown beauties: Cultured pearls from the Cortez Sea]. I. Reyjal, *Revue de l'Association Française de Gemmologie*, No. 179, March 2012, pp. 17–22 [in French].

The first part of the article gives a historical survey of pearls from the Sea of Cortez (Gulf of California), followed by an account of the actual situation. Black pearls and nacre have been known since pre-Columbian times and were much coveted in Europe after the Spanish conquest. In the 16th century, the coastal city of La Paz became the main commercial center for nacre and pearls. The most famous pearl from this source is "La Peregrina," a 203.8-grain gem last owned by Elizabeth Taylor, and John Steinbeck's story "The Pearl" also takes place there.

While nacre production was predominant in the first half of the 19th century, black pearls were very much in fashion in the middle of the century. From 1893 to 1914, José Gourieux was the first to cultivate *Pteria mazatlanica* black-lipped oysters from La Paz for their nacre. He produced about five million oysters per year, of which 10% contained natural pearls. Although these were only a by-product, they led to a sharp decline in pearl diving. In 1914, the plant farm was destroyed during the Mexican

revolution. The appearance of artificial substitutes for nacre, overfishing of the oyster banks, and a mysterious infection of the oyster larvae in 1939 finally led to the prohibition of all pearl diving a year later.

After attempts to renew pearl cultivation in the 1960s and 1970s, which failed largely because of political influences and the commercial success of black Tahitian pearls, three students of the Monterrey Institute of Technology and Superior Studies set up a small farm on the campus at Bacochicampo Bay in Guaymas. Their intent was not the industrial production of pearls but the development of environmentally sound and "oyster-friendly" methods of cultivation, which is why the oysters are implanted only once and harvests are small. The 2011 harvest consisted of 1,783 pearls, or 1.7 kg, as compared to 50 tons of Akoya pearls, 11 tons of South Sea pearls, 12 tons of Tahiti pearls, and 1,800 tons of Chinese freshwater pearls.

The other pearl-producing oyster of those waters, the rainbow-lipped *Pteria sternia*, yields black pearls with many different overtones. The young oysters are all harvested in the sea. Before the implantation of nuclei, the oysters are X-rayed. Some 3% contain natural pearls, and these oysters are not implanted. The pearls are sold as "natural," though purists would dispute this description. The oysters with nuclei are cultivated for 18–24 months. The diameter of the cultured pearls ranges from 8–12 mm (3.2–4.8 inches), the thickness of the nacre from 0.8 mm–2 mm (0.3–0.8 inches). The pearls are black and very iridescent and show various strong overtones, including red ("cranberry"). Their luster is somewhat more silky than that of the Tahitian pearls. Unlike most other cultured pearls, they are not treated in any manner, except for rinsing with water. They show a pink to red UV fluorescence, which is characteristic of pearls from the Sea of Cortez.

The future is uncertain, however. The volume of larvae has dropped significantly because of global warming effects, damage to the oyster cages from fishing boats, and the fragility and sensitivity of *Pteria sternia*.

RT

Major crocoite discoveries at the Adelaide mine, Tasmania. T.P. Moore and W.E. Wilson, *The Mineralogical Record*, Vol. 43, No. 6, 2012, pp. 651–673.
Crocoite, first discovered in the Urals in 1766, was named crocoise in 1832. Its attractive orange-red hue and adamantine to vitreous luster make it one of the most pursued mineral collector specimens. Tasmania, located southeast of mainland Australia, has long been famous for its outstanding crocoite specimens, and nearly all commercial specimens come from the Red Lead and Adelaide mines.

The mines lie within a four-square-kilometer area. Cambrian intrusions of serpentinite within the Precambrian and slightly younger metasedimentary rocks provided the Cr needed to form crocoite. During the Devonian, metal-rich granitic intrusions provided hydrothermal fluids along the extensive shear zones to alter much of the serpentinite to a peculiar rock called listwanite and precipitate pods with veins of Pb-bearing minerals. Since crocoite is more stable than other Pb-bearing minerals at low pH levels, it predominated in these mines. Crocoite was common in the gossan, but open pockets yielded the best samples.

The earliest discovery of crocoite in Tasmania dates back to 1891. Over the last 120 years, it has been mined intermittently at several localities. Until the 1970s, many of the high-quality specimens were either destroyed or used for industrial applications. In 1970, "crocoite king" Frank Mihajlowits leased the Adelaide mine and began a string of major discoveries. Among these was a watercourse discovered in 1990 that was worked on for 14 years and yielded thousands of superb specimens.

In 2004, Mihajlowits sold the mine to Adam Wright's newly established Adelaide Mining Company, which continues to work the deposit. A major new pocket of crocoite found in 2012 was of great excitement to mineral collectors. The opening of this watercourse is about one meter wide and two meters tall. Crocoite crystals of various lengths protrude at different angles to each other. This discovery is called the "Red River find," and the watercourse has been broken into from below with no end to the channel found as yet. Many of these superb specimens were exhibited at the 2012 Tucson show.

Tao Hsu

Peridot, pyroxene, and plagioclase: Mantle megacrysts from Lunar Crater volcanic field in Nevada. C. F. Brink, *Rock & Gem*, November 2012, pp. 26–30.
Megacrysts within xenoliths transported by explosive volcanic eruptions to the surface are fingerprints of the earth's upper mantle and possible collectors' items.

Lunar Crater is located in Nye County, Nevada. It is a Quaternary alkali basaltic field with lava flows, cinder cones, and maars covering more than 100 square miles of Nevada desert. At numerous alkali basaltic volcanic fields in the western United States, ultramafic mantle xenoliths of peridotite, dunite, lherzolite, and monomineralic xenocrysts are found in lunar craters. Olivine, pyroxene, plagioclase, hornblende, and magnetite ranging from a few millimeters to centimeters are common megacrysts. These megacrysts are usually ejected from the volcanic vent as the cores of volcanic bombs. Bomb morphology can vary considerably due to different viscosities of lava. While these magacrysts can provide scientific information on the upper mantle composition, the authors are interested in their possible gemological significance. Peridot, the green variety of olivine, is reported to occur in nodules up to 50 cm. But the crystals are highly fractured, making them unfit for faceting. Plagioclase crystals from the lunar crater can be clear to translucent white and show typical feldspar twinning. Pyroxene megacrysts

found in the lunar crater are usually the augite variety and apple green, bottle green, or nearly black.

Minerals in the Lunar Crater volcanic field are abundant and easily accessed. Volcanic bombs contain exotic xenocrysts of possible gem significance, making this a worthy destination for rock hunters.

Tao Hsu

INSTRUMENTS AND TECHNIQUES

Paramagnetic hole centres in natural zircon and zircon colouration. M. Klinger et al., *European Journal of Mineralogy*, Vol. 24, No. 6, 2012, pp. 1005–1016.

This article explores atomic defect centers (color centers) of natural zircon from three localities (North Carolina, the Massif Central in the south of France, and the Ural Mountains of Russia). The origin of zircon coloration is little discussed in the spectroscopic literature. This study further explores paramagnetic properties and optical absorption, and also suggests additional constraints in the nature of some of the color centers occurring in natural zircon.

Electron paramagnetic resonance (EPR, an absorption technique using magnetic fields to measure transition energies in atomic defect centers) and optical absorption spectroscopy are used on a heterogeneous sample group of eleven small untreated zircon crystals. The findings indicate an obvious correlation between colors and certain paramagnetic defect centers in the crystal structure. However, the EPR studies also show that the presence of tetragonal centers of trivalent rare-earth elements and niobium is not directly related to any specific zircon coloration.

The paper discusses the highly technical EPR spectral indications for electron and hole defect centers (e.g., angular dependencies and crystal axes; principal g-values, etc.), as well as the intricate substitutional charge patterns which reflect the isomorphism of zircon.

The optical absorption spectra in samples from the US and France (from colorless through pinkish to reddish and brownish) show one type of spectra, two broad bands, 340–350 nm and 510–515 nm. The Russian samples (from colorless through yellowish-brownish) are different, showing a more complicated spectra of three dominant bands at 320, 390, and 420 nm and a weak band at 510.

The results confirm that the subdivision of these two common color series is meaningful. *ERB*

TREATMENTS

The "glet filling": The filling of the cracks in precious stones under scrutiny. E. Vleeschdrager, *Le Bijoutier Internationnal*, No. 797, October 2012, pp. 55–57.

This short article discusses several important aspects of crack-filling in colored stones and diamonds: the differences in market values between included and filled stones, especially in high quality goods; the impact of nondisclosure within the supply chain; a brief discussion of different methods of filling and their limitations; and, finally, methods of detection.

Several similar methods of filling cracks ("glets") have been developed under such names as Yehuda and Koss (Israel) and Diascence, Genesis Enhanced, and Goldman Oved (New York). One of the filling methods discussed in more detail, the Koss system developed at least ten years ago, limits the rainbow or "flash" effect (the yellow-orange color flashing into electric blue under dark field microscopy) characteristic of many other filling methods, and useful for identifying the presence of a filler.

Regardless of method, the visual improvements achieved from filling cracks with oils or the more modern vitreous, high-RI materials is temporary; eventually the tears and cracks become visible after a few months or years. Fillers degrade with time and by environmental conditions. Some dry out to reveal noticeable residue; others deteriorate with exposures to ultrasound, ultraviolet, heat, acids, and chemical cleaners.
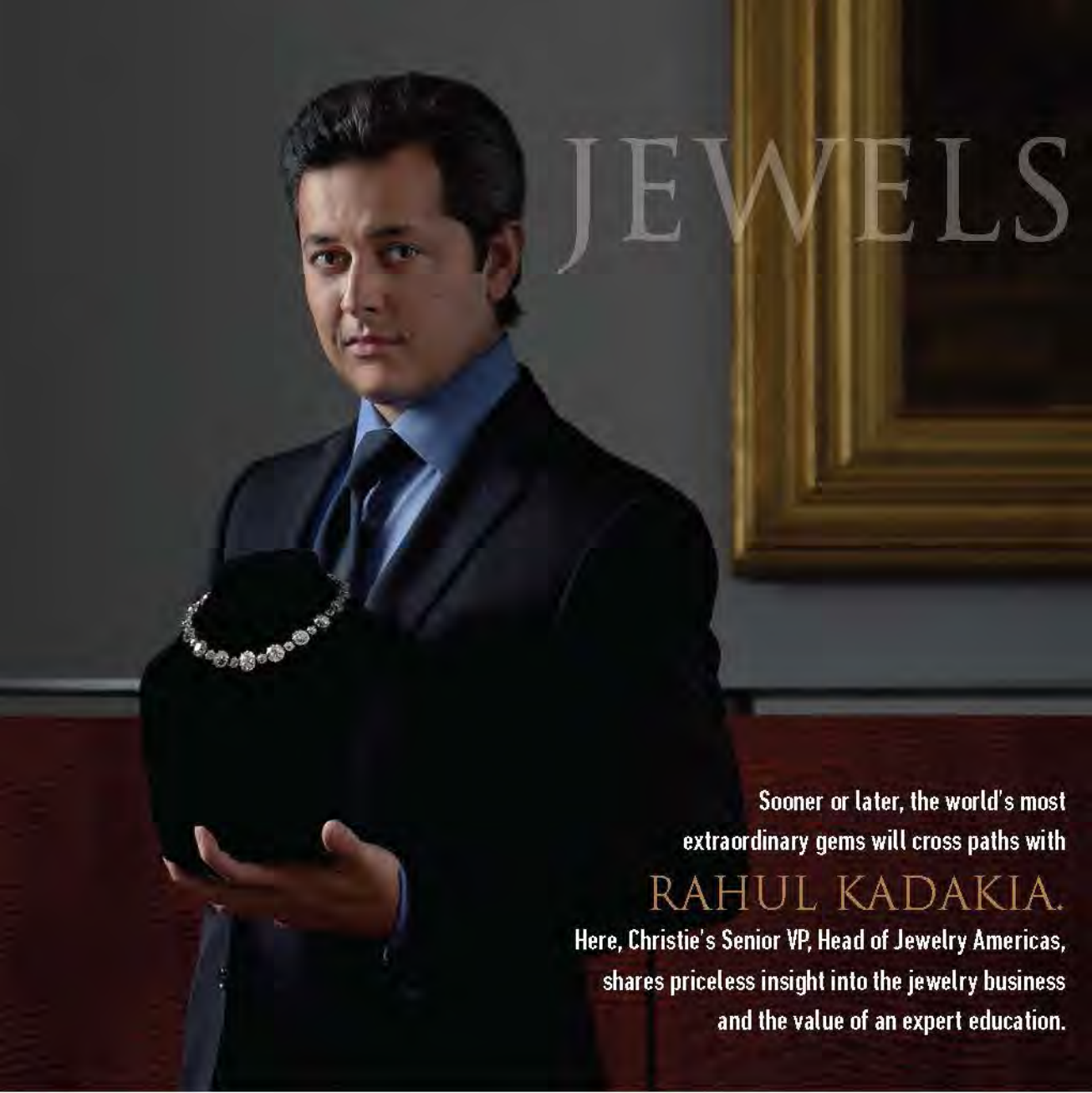
Several methods of detecting fillers are briefly mentioned. Gemologists commonly use magnification to observe bubbles, filler textures, the flash effect, and effects of deterioration. Advanced instruments such as the scanning electron microscope, X-ray fluorescence analysis, and Raman spectroscopy easily reveal the presence of filled glets. *ERB*

MISCELLANEOUS

Trade fair & play fair, says gem trade. *Israel Diamonds*, No. 242, 2012, pp. 51–53.

Consumer confidence and globalization has led to increasing public awareness of how the goods are made and where they are sourced. The article discusses how the colored gemstone industry is taking steps to create conditions that are fair and decent for miners and others involved in the industry, just as the global diamond industry has done with the Diamond Development Initiative and the Kimberley Process. The Fair Trade Gems project was launched by the Columbia Gem House firm and is the first jewelry industry company to join the Fair Trade movement. The Quality Assurance and Fair Trade Gems Protocols that were created were designed to increase the standard of living for the miners and gem cutters and also include environmental protection, fair labor practices, and health and safety standards. Protecting the quality and integrity of the product is an important feature of the Fair Trade Gems program, as it extends the protection to consumers, who deserve to know exactly what they are buying. *MK*

JEWELS OF THE TRADE

Sooner or later, the world's most extraordinary gems will cross paths with

RAHUL KADAKIA.

Here, Christie's Senior VP, Head of Jewelry Americas, shares priceless insight into the jewelry business and the value of an expert education.

A master eye for gems ... born or made? Coming from four generations of jewelers undoubtedly piqued my interest in this great business. But one needs to constantly train their eye by looking at gems – the more you learn, the better you will be at identifying and pricing gems, as well as being an effective salesperson and well-rounded businessman.

Something most people don't know about you. GIA is what brought me to Christie's. After studying in Santa Monica, I attended a GIA Career Fair where I had my first interview with the company.

Ok. Definitely a story there? I started work when I was 17 and five years into it, I thought I knew pretty much everything there was to know ... until I enrolled at GIA. The Institute's meticulous training and high standards exposed me to a whole new world of expertise.

Ultimate sales edge ... emotion or expertise? Jewelry is an emotional shopping experience, but expertise plays a decisive role. It's wonderful to show people a brilliant diamond, but it means more when you can follow up with a skillful explanation of the 4Cs exemplified in that particular gem.

Lean economy. Less jewelry? At the nexus of the downturn in late 2008, we sold the Wittelsbach Blue Diamond for $24 million, a world record price back then for any gem ever sold at auction. When you have great gems and jewels, the money makes itself available.

Any advice to the up and coming? Don't lose the passion that brought you to this business, and above all, keep learning every day.

GIA gratefully acknowledges those who, for 80 years, have used our resources to further world expertise in gems. Invest in your success at WWW.GIA.EDU

GIA®